LEVEL II

AFML-TR-78-16

TEST METHODOLOGY CORRELATION FOR FOREIGN OBJECT DAMAGE

HAMILTON STANDARD
DIVISION OF UNITED TECHNOLOGIES CORPORATION
WINDSOR LOCKS, CONNECTICUT 06096

MARCH 1978

TECHNICAL REPORT AFML-TR-78-16
For Period March 1976 – December 1977

AIR FORCE MATERIALS LABORATORY
AIR FORCE WRIGHT AERONAUTICAL LABORATORIES
AIR FORCE SYSTEMS COMMAND
WRIGHT-PATTERSON AIR FORCE BASE, OHIO 45433

NOTICE

When Government drawings, specifications, or other data are used for any purpose other than in connection with a definitely related Government procurement operation, the United States Government thereby incurs no responsibility nor any obligation whatsoever; and the fact that the government may have formulated, furnished, or in any way supplied the said drawings, specifications, or other data, is not to be regarded by implication or otherwise as in any manner licensing the holder or any other person or corporation, or conveying any rights or permission to manufacture, use, or sell any patented invention that may in any way be related thereto.

This report has been reviewed by the Information Office (OI) and is releasable to the National Technical Information Service (NTIS). At NTIS, it will be available to the general public, including foreign nations.

This technical report has been reviewed and is approved for publication.

James S Wilbeck

JAMES S. WILBECK
Metals Behavior Branch
Metals & Ceramics Division

FOR THE COMMANDER

Lawrence N. Hjelm

LAWRENCE N. HJELM
Actg Chief, Metals Behavior Branch
Metals & Ceramics Division

"If your address has changed, if you wish to be removed from our mailing list, or if the addressee is no longer employed by your organization please notify AFML/LLN ,W-PAFB, OH 45433 to help us maintain a current mailing list".

Copies of this report should not be returned unless return is required by security considerations, contractual obligations, or notice on a specific document.

AIR FORCE/56780/13 July 1978 — 300

LEVEL II

UNCLASSIFIED

SECURITY CLASSIFICATION OF THIS PAGE (When Data Entered)

REPORT DOCUMENTATION PAGE

READ INSTRUCTIONS BEFORE COMPLETING FORM

1. REPORT NUMBER: AFML-TR-78-16	2. GOVT ACCESSION NO.
3. RECIPIENT'S CATALOG NUMBER	
4. TITLE (and Subtitle): TEST METHODOLOGY CORRELATION FOR FOREIGN OBJECT DAMAGE	5. TYPE OF REPORT & PERIOD COVERED: Technical Report for Period March 1976 - December 1977
	6. PERFORMING ORG. REPORT NUMBER
7. AUTHOR(s): T. Wong, Robert W. Cornell	8. CONTRACT OR GRANT NUMBER(s): F33615-76-C-5211
9. PERFORMING ORGANIZATION NAME AND ADDRESS: Hamilton Standard Division of United Technologies Corporation, Windsor Locks, Connecticut 06096	10. PROGRAM ELEMENT, PROJECT, TASK AREA & WORK UNIT NUMBERS: 7351-06-C2, 06
11. CONTROLLING OFFICE NAME AND ADDRESS: Air Force Materials Laboratory (LLN, Air Force Systems Command, Wright-Patterson Air Force Base, Ohio 45433	12. REPORT DATE: March 1978
	13. NUMBER OF PAGES: 115
14. MONITORING AGENCY NAME & ADDRESS (if different from Controlling Office): 120 p.	15. SECURITY CLASS. (of this report): UNCLASSIFIED
	15a. DECLASSIFICATION/DOWNGRADING SCHEDULE

16. DISTRIBUTION STATEMENT (of this Report)

Approved for public release; distribution unlimited.

17. DISTRIBUTION STATEMENT (of the abstract entered in Block 20, if different from Report)

Technical Rept. Mar 76-Dec 77,

18. SUPPLEMENTARY NOTES

62102F

19. KEY WORDS (Continue on reverse side if necessary and identify by block number)

Foreign Object Damage, Fan Blades, Oblique Impacts, Composites, Computer Codes, Impact Response, Test Modeling

20. ABSTRACT (Continue on reverse side if necessary and identify by block number)

The adaptation of advanced composite materials in fan blades requires the evaluation of their resistance to damage from foreign object impacts. To construct and test full-scale blades to perform such an evaluation is prohibitive with regard to costs and time. An alternative approach to ~~this problem~~ Testing Full-scale blades is to use laboratory material coupon impact tests and complimentary analysis methods to simulate and predict ~~the~~ performance of composite materials in full-scale blades. This ~~three-phase~~ study provided an assessment

DD FORM 1 JAN 73 1473 EDITION OF 1 NOV 65 IS OBSOLETE

UNCLASSIFIED

SECURITY CLASSIFICATION OF THIS PAGE (When Data Entered)

461 400

78 08 10 052

Item 20 - Abstract (Continued)

and development of laboratory coupon tests for evaluating potential fan blade materials. Both simple and sophisticated elastic beam blade impact analyses and programs were used in this study.

In the first phase, 24 impacted cantilevered and simply-supported specimens of different materials were analyzed, and the predicted maximum stressing and time history stressing and damage results were found to compare favorably with the test results. Because the local and gross spanwise critical stressing occurs at separate places in the cantilever specimen, but at the same location in the the simply-supported specimen, and because the support action of the latter is nonlinear, the cantilever specimen was found to be the better specimen to study the gross resistance of materials to impact. The second phase consisted of evaluating six rotating blade impact cases and comparing the theoretical and test results. The correlation was good for large missile impacts but only fair for small missile impacts. The test results and theory both show there are three critically-stressed blade regions, which are stressed progressively in time. The blade chordwise response was found to be very important for small and/or high speed missiles but not for large and/or slow missiles. The parametric coupon specimen study of the third phase showed that practical cantilever impact specimens can be designed which develop approximately the same gross normal stressing, strain rate, and shear stressing as occurs in a fan blade. The study showed that the evaluation of the local blade leading edge resistance of a material requires special leading edge specimens, which should include the gross blade effect if the missile is large.

PREFACE

This report summarizes studies conducted by Hamilton Standard, Division of United Technologies Corporation, Windsor Locks, Connecticut, under U.S. Air Force Materials Laboratory, Contract No. F33615-76-C-5211. The studies were conducted by J. Marti, N. Houtz, and T. Wong. The authors of this report are T. Wong and Dr. Robert W. Cornell; the program was conducted under the direction of Dr. Robert W. Cornell.

The effort described herein was conducted in support of foreign object damage (FOD) test activity being performed at the AFML Impact Facility at Wright-Patterson Air Force Base. This test activity is concerned with the study of the behavior of homogenous and composite materials under impact loading conditions typical of jet engine fan blades subjected to foreign object impacts, and the development of methods for evaluating potential fan blade materials with regard to foreign object impact resistance. This work was conducted during the period March 1976 through December 1977 and was jointly monitored by Dr. Theodore Nicholas and Captain J. S. Wilbeck of the Air Force Materials Laboratory. This program was partially funded with Air Force Materials Laboratory Director's Funds.

This report was submitted by the authors in January 1978 for publication as an Air Force Materials Laboratory Technical Report.

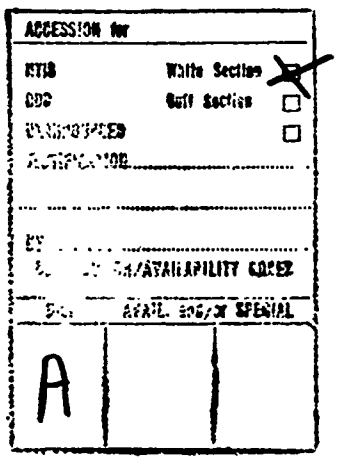

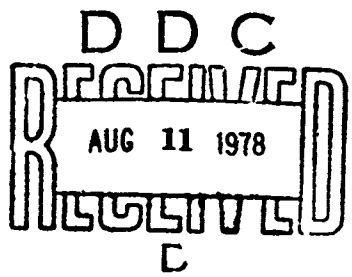

TABLE OF CONTENTS

LIST OF TABLES

LIST OF ILLUSTRATIONS

SECTION I

INTRODUCTION AND SUMMARY

1.1 BACKGROUND

The application of advanced organic and metal matrix composite materials in fan blades provides appreciable cost savings and performance potential in present and future jet engines. However, these materials must provide adequate resistance to damage from foreign objects, such as birds, stones, and ice balls, which may be ingested into the engines. The potential foreign object damage (FOD) problem increases with the higher blade velocities of improved performance engines. Little is known of the structural response of fan blades and the resulting mechanism of material damage resulting from hard and soft body impact loadings. In order for composites to be used in fan blades, the FOD problem must be solved.

To develop the necessary design methodology for FOD resistant structures requires the development of analyses, blade impact modeling methods, and screening techniques for evaluating candidate fan blade materials. Numerous blade impact analyses have been developed; for example, see References 1 through 12. However, the systematic evaluation and screening of candidate fan blade materials under various typical blade impact conditions is needed. To accomplish this by constructing and testing full-scale blades is impractical because of the prohibitive cost. This is particularly true because of the large number of impact variables, such as relative velocity, impact angle, impact location, missile characteristics, and blade characteristics, and the large number of material variables in composites, such as fiber and matrix types, spacing, layup, and orientation. It appears that the only rational scientific approach to the FOD problem is the use of laboratory specimen or coupon tests and complimentary analysis methods for simulating and predicting the performance of composite materials in full-scale blades subject to impact loads.

1.2 OBJECTIVE AND APPROACH

The objective of this study is to provide analytical guidance in the development of laboratory coupon tests for evaluating potential fan blade materials, especially composites, for FOD resistance and to refine and evaluate the methodology for predicting coupon and gross blade impact results.

Using previously developed blade impact analysis methods (see References 1 through 8) a three-phase study was conducted to assist AFML in fulfilling the above objective. The first phase consisted of analyzing at least twenty of the simply-supported and cantilevered specimens that had been impacted by soft bodies to see if the results could be satisfactorily predicted. These specimens consisted of numerous materials - titanium, aluminum, boron aluminum, boron titanium and/or organic matrix composites; their test results are reported in References 15 and 16. The second phase was to evaluate at least five FOD blade cases using available blade impact analyses to determine the significance of the stress conditions with regard to the damage. The third phase was to develop a viable impact test specimen or specimens for evaluating the FOD resistance of materials for fan blades.

In order to accomplish the above tasks it was found that the two available analytical blade impact computer programs - The Three-Degree of Freedom Blade Impact Program, References 1 through 7, and the Multi-Mode Blade Impact Program, Reference 8, had to be modified in order to handle normal impact and the simply-supported specimen. This was because they were originally formulated for cantilevered blades with shallow impact angles. Section II, therefore, not only briefly describes the two impact programs, but also the improvements made to them so that they could be applied to the typical specimen tests. Sections III, IV, and V summarize the work done under the three phases of this program.

1.3 SUMMARY AND CONCLUSIONS

It was found necessary to modify and improve the Three-Degree and Multi-Mode Impact Programs so that they could analyze normal impacts. Although the Three-Degree Impact Program was written for cantilever beams or fan blades, it was possible to make it accurately analyze simply-supported and

fixed-fixed beams by using special modeling techniques.

Considerable difficulty was encountered in reducing the strain gage results for three cantilever and two simply-supported impacted specimens. Both elastic impact programs predicted quite well the maximum and time history measured stress values when the yielding effects were included. The overhang of the simply-supported specimen was found to affect the results significantly and appears to cause a nonlinear pulse at the support. The elastic impact analyses were found to predict in all but two instances the likelihood of damage or fracture in the root or impact site of the 24 specimens analyzed. The calculated strain rates of 10 to 250/sec appear to be low enough so as not to influence the material strengths appreciably. The analyses show that the gross and local spanwise impact critical stressing occur at separate places on the cantilever specimen, whereas they occur at the same location on the simply-supported specimen. Because of this and the nonlinear support effects of the simply-supported specimen, the cantilever specimen is the better specimen to study the gross resistance of materials to impact.

The six rotating blade impact cases evaluated in this study illustrate the difficulty in performing rotating impact tests and accurately measuring the resulting response and stressing. The test results showed that once some type of damage occurs the blade response and subsequent damage modes change. Thus, to properly evaluate the impact of blades causing damage requires much more sophisticated and extensive measurement and analytical techniques than elastic or threshold damage impacts. For moderate and large missile impacts the elastic analyses were found to predict the stressing and fracture origin quite accurately. For small missile impacts, however, the accuracy of the elastic analyses was not very good.

The experimental and theoretical blade impact results show that three critical-stress regions occur due to impact - 1.) locally at the leading edge impact site, 2.) grossly at the blade impact station, and 3.) grossly inboard at the maximum fundamental mode stress locations. The peak stressing at these three regions occurs progressively later in time and damage in any one can

significantly affect the stressing in the other regions. For small missile impacts the chordwise response is very important and must be included in any impact analysis, whereas for moderate or large missile impacts the chordwise effect is minor and can be neglected. For moderate missile impacts the total combined stress state was not appreciably greater than the normal spanwise stress.

Typical impact analysis of a Q-Fan blade impacted by a 1-lb. missile at 30° and 830 fps resulted in mid-blade and impact station elastic, spanwise bending stresses of about 150,000 psi and a corresponding interlaminar shear stress at the impact station of about 10,000 psi. The resulting maximum strain rate in the Borsic/Aluminum shell and titanium spar were about 25/sec and 15/sec, respectively, which are probably not sufficient to influence the material properties significantly. These blade studies showed that elastic impact analyses can be used to define adequately the elastic state in fan blades so that corresponding material specimens can be designed for evaluating the impact resistance of materials.

Both the blade test and analysis results showed that two types of specimens are needed to evaluate the impact resistance of fan blade materials - one for the gross spanwise blade stressing at the impact station and the maximum stress inboard station, and the other for the local leading edge stressing. The former is best accomplished using a cantilever specimen so as to separate the two stressed regions. Parametric analysis of realistic 8" x 2" cantilever specimens (9" x 2" coupons) shows that by choosing the appropriate thickness, impact site, missile size, and velocity, the specimen bending and interlaminar shear stressing can be made approximately equivalent to the gross stressing present in a fan blade. Although the resulting strain rate tends to be about twice that present in blades, it is doubtful that this will have adverse effects. Typical specimens and missiles for simulating the stressing in a Q-Fan blade are 8" x 2" x .20" for a 1" spherical missile and 8" x 2" x .14" for a 7/8" spherical missile.

The evaluation of leading edge specimens showed that for small-sized and/or high velocity soft body impacts, simple specimens, such as the AFML fixed-fixed beam specimens, are satisfactory. However, for larger and/or slower missiles the effect of the gross blade response is important, so that the leading edge specimen must be designed to include the effects of the gross blade response. The studies further showed the importance of including chordwise response in the impact analysis for evaluating small missile impacts. For large missiles the chordwise response has only a minor effect. Although the centrifugal loading in fan blades can influence the dynamic characteristics and steady stressing, in general, the former can be accounted for and the latter can be neglected without significant error in the design of material impact specimens.

In conclusion, this study shows that blade impact analyses can be modified to satisfactorily predict the elastic stressing and response and, therefore, the threshold of damage and fracture of specimens and fan blades. For smaller missiles the impact analysis methods must include the chordwise response at the impact site. Except for the strain rates, which tend to be a little high, it appears possible to design coupon specimens to evaluate the impact resistance of materials under the same stress conditions as in fan blades. The gross blade stressing is best simulated by cantilever specimens so as to separate the initial impact and later inboard stressing. The local leading edge resistance of materials is best evaluated using special leading edge specimens that include the gross blade effect, which is very important for large missiles. The AFML leading edge specimen appears to be satisfactory for small missiles and high velocity impacts. Finally, this study shows that, through the use of available elastic blade impact analyses and programs, it is readily easy to develop viable gross and leading edge specimens for evaluating the FOD resistance of materials for fan blades.

SECTION II

BLADE IMPACT COMPUTER PROGRAMS

During the past few years Hamilton Standard developed two computer programs for predicting the impact load and gross blade response from impacts of soft and frangible objects such as birds and ice balls. Although the two analyses and programs differ considerably in their degree of sophistication, both programs have been found to correlate quite well with limited test results. Both of these programs, the Three-Degree and the Multi-Mode Blade Impact Programs, are based on beam models of the blade and are presently being expanded and improved under NASA-Lewis Contract NAS3-20091. It was originally hoped that these improvements would be available for use in this study. However, schedules of the NASA contract were such that the improvements could not be fully utilized. Because both of these programs were used extensively in this study a brief description of their formulation and features is presented in this section. Also, in order to accomplish several of the tasks both programs had to be modified slightly. These modifications are discussed along with the descriptions of the features of the programs.

2.1 THREE-DEGREE BLADE IMPACT PROGRAM

As pointed out in the introduction, this section is divided into two parts. The first part describes the formulation and features of the Three-Degree Blade Impact Program, whereas the second part presents the improvements made in the program and special application procedures in order to accomplish some of the tasks of this study.

2.1.1 Basic Program

The Three-Degree Blade Impact Program is the outgrowth of a single degree of freedom interactive impact program; see Reference 4. In this simple, single degree of freedom analysis the specimen or blade is represented by a one degree of freedom dynamic system. Because of its simplicity, this simple impact analysis permits a general understanding of the effects of the various blade or specimen characteristics and impact factors on their response and stressing.

A general Parametric Blade Impact Diagram developed from this single degree impact analysis is given in Figure 1. This chart gives insight into the impact phenomenon and can be useful in quick evaluation of simple cantilever specimens. The single degree analysis can also be used to obtain the approximate response of a two degree of freedom system (torsion and bending) by proper adjustment of the parameters of the dynamic system; see References 4 and 5.

The Parametric Blade Impact Diagram, Figure 1, shows how the interactive effects given by $\eta_\theta/\omega_\theta$ or η_x/ω_x decrease the maximum gross blade loads and the resultant stressing and how low, natural torsional and bending frequencies, ω_θ and ω_x, also decrease the loads. The larger the missile mass, m, is relative to the effective specimen or blade inertia, M or I, the greater is η_θ/ω_o or η_x/ω_θ and, therefore, the lower is the maximum gross response compared to that given by regular impulse theory (the upper boundary of the curve). Because of the specimen or blade dynamics the maximum effective gross response load can be up to twice that for a rigid blade if $\omega t_R > \pi$. In general, the dynamic characteristics of fan blades and impact durations are such that usually $\omega t_R < \pi$. Most impact specimens have extremely low natural frequencies, so that they fall in the lower left corner of the Parametric Impact Diagram.

The Three-Degree Blade Impact Analysis assumes the gross blade response can be satisfactorily defined by the first three fundamental blade modes - the first flatwise bending mode, the first edgewise bending mode, and the first torsional mode. The two bending modes are assumed normal to each other, and a correction is later applied to account for nonorthotropic motion. The dynamic system is represented by a lumped mass system with the equivalent mass and rotational inertia of the blade being at the impact station such that the corresponding two bending and torsional blade frequencies and stiffnesses are consistent with those derived from a separate blade coupled modal beam analysis or its equivalent. The analysis assumes the impacting missile is a

single fluid jet or a series of parallel fluid jets, whose impacting force depends on the instantaneous normal relative velocity of the missile and blade. Figure 2 presents the basic dynamic model of the Three-Degree Blade Impact Analysis. The analysis includes gross structural damping, torsion-bending coupling, and variation of impact force and location with blade deflection and time. The interactive effects permit the calculation of impact duration based on three criteria: the deflection of the entire missile, the impact force going to zero due to the normal velocities of the missile and blade becoming equal, and the missile running chordwise off the blade before it is completely deflected.

In order to define the local stressing at the impact site a perturbation post processor program was developed based on minimum energy. This post processor program not only gives the local deflection and stressing at the impact site but for the entire blade or specimen. The program plots out the variation of the deflection and loads with time at the impact site, and also the deflection, loads, and stress distributions for specified times during and after impact. Table 1 gives a summary of the features of the Three-Degree Blade Impact Analysis and References 1 through 7 present the details of the basic analysis. Figures 3 and 4, and Table 3 show the good correlation of the calculated results with test data using this program.

2.1.2 Improvements in Program and Special Applications

As Figure 2 shows, the original program was developed for the impact of fan or propeller blades, which can be represented by a cantilever beam with shallow impact angles. Because most specimens are impacted normally in laboratory testing, the interactive effects in the original program had to be modified. Also, a procedure had to be devised so that the program could be used to analyze the impact of simply-supported specimens, which are frequently used in material coupon tests.

In the original interactive analysis the normal impact force is assumed to be given by the equation

$$F_N = (m\, V_o/a)\,(\text{Change } V_{\text{Relative}}) \qquad (1)$$

$$F_N = F\left[\text{Sin}(\alpha+\theta)\,\frac{\dot{\theta}C' + \dot{X}\text{Cos}(\beta-\theta)}{V_o}\right]$$

where the impact location relative to the center of twist is given by

$$C' = \left[b' \sin\alpha - X\cos(\alpha+\beta) - y \sin(\alpha+\beta) \right] / \sin(\alpha+\theta)$$

and the rigid body impact force, F , for a missile of mass "m" , length "a" , velocity V_o , and coefficient of restitution, ϵ is

$$F = mV_o^2 (1+\epsilon)/a$$

This equation assumes the relative flow velocity of the missile jet over the blade is not influenced significantly by the interactive effects. Only the change in relative velocity was assumed to be influenced by the blade motion. For shallow impact angles $(\alpha+\Theta)$, where Θ is the twist motion of the blade and α is the initial impact angle, these assumptions are satisfactory; however, for large impact angles, and particularly normal missile impact, significant error is introduced by not including the interactive effect on the relative flow velocity of the missile over the blade. For example, for normal impact of a specimen with motion $\dot{z}$, the impact force given by the original formulation is

$$F_N \approx mV_o(V_o - \dot{z})/a \qquad (2)$$

compared to the correct formulation of

$$F_N \approx m(V_o - \dot{z})^2/a \qquad (3)$$

In order to account for the interactive effects on the relative flow, an iteration loop was incorporated in the program which modified the assumed relative flow velocity V_o by a correction factor. This factor is based on the relative velocity impact vector diagram, which includes the velocity effects of

the three fundamental modes; see Reference 7. This modification was found to have an insignificant effect on typical impacts of fan blades such as given in Figure 3 and Table 3.

In order to analyze simply supported specimens using the Three-Degree Blade Impact Analysis it is necessary to "trick" the program by making the following changes in the input data:

a. A very large translational mass is specified for the station at the free end of the cantilever.

b. A short section with very low bending stiffness, which acts as a hinge, is specified at the built-in end of the cantilever.

Figure 5 depicts the above concept and Figure 6 shows that the resulting mode shape compares well with that for a simply supported specimen. A similar approach can be used to analyze fixed-fixed specimens.

Later on during this study it appeared that the overhang of the simply supported specimen might be influencing the impact test results. Because of this, a new model was developed which would simulate such a case. Figures 7 and 8 depict such a model and resulting mode shape, which uses the same approach as before but ordered so as to allow for specimen overhang beyond the supports. The only potential difficulty with this model is that it permits both positive and negative motion of the overhang, whereas for the actual case only motion in one direction is permissible because of the foundation. This latter effect could not be approximated because it is a nonlinear one.

2.2 MULTI-MODE BLADE IMPACT PROGRAM

This section is divided into two parts. The first part describes briefly the formulation and features of the Multi-Mode Blade Impact Program, whereas the second part presents the modification of the program with regard to applying it for some of the tasks of this study.

2.2.1 Basic Program

The Multi-Mode Blade Impact Program is a much more sophisticated program than the Three-Degree Blade Impact Program. By including as many normal

modes aa desired it can handle impacts anywhere on the blade or specimen and give the local impact results directly. The analysis assumes the blade or specimen responds in its normal modes upon impact, the magnitudes of the responses being such as to minimize the total blade strain energy; see Figure 9. Although the missile is again represented by a fluid jet, the analysis includes a simple hydrodynamic model of the missile spreading and squashing effects as well as the blade-missile interaction. The interaction and effect of blade camber are accounted for by using a time history solution. Table 2 summarizes the features of the Multi-Mode Blade Impact Program and Reference 8 gives the derivation of the analysis.

The Multi-Mode Blade Impact Program has been evaluated by applying it to a number of fan blades impacted by soft or frangible missiles and found to give quite good results. Figure 4 and Table 3 give examples of the accuracy of the program in predicting gross blade response to impact loads. The program has also been found to predict the local spanwise deformation and stressing fairly well.

2.2.2 Improvements in Program

The Multi-Mode Blade Impact Analysis and Program was developed based on shallow impact angles and, therefore, it had to be modified so that it could be used for normal impacts. It was found that the modified program can be used for analysis of normal impacts with good accuracy if the specimen velocity does not exceed about 30% of the missile velocity during impact; see Figure 10. In order to obtain this correlation, equivalent or dummy values of many of the impact parameters must be chosen so as to give the same magnitude and location of the impact force as a 90^{o} fluid jet does as the specimen responds. This is done by choosing a relatively small impact angle, like .01 Radians, and then determining the corresponding values of missile velocity, density, length, crushing factor, and impact location that will simulate the location and magnitude of the normal impact. In this way the shallow impact angle requirement is met but "tricked" into giving the desired normal results. Only minor coding changes were necessary in the program to accept normal impact cases.

It was possible to make a shallow impact equivalent to a normal one over a range of specimen to missile velocity ratios by using pseudo missile parameters and proper adjustment of the crushing factor. Figure 11 depicts the turning and crushing model used, and Figure 12 depicts the resulting forces on the missile segments. For shallow impacts the force on the specimen, see Reference 8, is given by

$$F_1 = \frac{V_1 \, m \, \mathrm{Tan}\alpha'}{t(\mathrm{Cos}\alpha' + \mathrm{Sin}\alpha' \, \mathrm{Tan}\alpha')} = A_1 \rho_1 V_1^2 \left(1 - \frac{V_S}{V_1} \mathrm{Sin}\alpha_1\right) \mathrm{Sin}\alpha' \tag{4}$$

where V_S is the velocity of the specimen; V_1, A_1, ρ_1, and α_1 are the missile velocity, cross sectional area, density, and impact angle; and α' is given by

$$\alpha' = \alpha_1 - \left(\frac{V_S/V_1 \ \mathrm{Cos}\alpha_1}{1 - V_S/V_1 \mathrm{Sin}\alpha_1}\right) \tag{5}$$

For normal impact the force is given by

$$F_2 = A_2 \rho_2 (V_2 - V_S)^2 \tag{6}$$

Thus, the objective is to define pseudo missile parameters A_1, V_1, ρ_1, and α_1 such that the shallow impact angle requirement is met and the force F_1 is the same as the desired normal impact force F_2. This is done by making the forces equal at $(V_S/V_2)=0$ and 0.2. Thus, at $V_S=0$

$$A_2 \rho_2 V_2^2 = A_1 \rho_1 V_1^2 \, \mathrm{Sin}\alpha_1 \tag{7}$$

so that for other specimen velocities (assuming small angles)

$$F_1/F_2 = \frac{\left(1 - V_S/V_1 \ \mathrm{Sin}\alpha_1\right) \mathrm{Sin}\alpha'}{(1 - V_S/V_2)^2 \, \mathrm{Sin}\alpha_1} \approx \frac{\alpha_1 \left(\frac{V_S}{V_2}\right)\left(\frac{V_2}{V_1}\right)}{(1 - V_S/V_2)^2 \, \alpha_1} \tag{8}$$

Then, for $(F_1/F_2)=1$ at $(V_S/V_2)=.2$, we find that for small α_1, $(V_2/V_1)=1.8\alpha_1$. Using this value and assuming $A_1 = A_2 = A$, we find that $\rho_1=(1.8)^2\alpha_1\rho_2=3.24\alpha_1\rho_2$. Then h_t and the proper crushing factor K_f are determined by the formulas

$$n = \alpha' + \text{arc Tan}\left(\frac{h_t - V_1 t \,\text{Tan}\alpha'}{V_1 t}\right) \tag{9}$$

$$(h_t - V_1 t\,\text{Tan}\alpha')^2 + V_1^2 t^2 = \frac{\left(h_o - \frac{V_1 t\,\text{Tan}\alpha'}{2}\right)\text{Cos}^2\alpha'}{\text{Sin}^2\eta} \tag{10}$$

so that the crushing factor is

$$K_f = \frac{8\rho_1 V_1 h_o^2 - \left(\frac{A}{4h_o}\right)^3\left[\frac{h_o}{h_t} - 1\right]}{3t\; h_t^2 A_2 \rho_2 V_2^2} \tag{11}$$

The proper pseudo impact position on the specimen is obtained from torque equation 3.8 of Reference 8 by letting the torque be zero. This results in an impact position of LT=$(V_1t/2)$, HT=0, and DISLE=0; see Figure 9. Because the missile length, a_2, is broken into five sections, the incremental time is $t \approx a_2/5V_2$. In order to simplify the above equations a value of $\alpha_1=.01$ is used so that $\alpha_1 \approx \text{Sin}\;\alpha_1 \approx \text{Tan}\;\alpha_1 \approx .01$ and Cos $\alpha_1 \approx 1$. Then, $V_1=(V_2/.018)$, $V_1t=(11.111a_2)$, $A_1=A_2=A$, $\rho_1=.0324\rho_2$, $a_1=(a_2/1.8^2)$ and

$$K_f = \left\{\frac{3}{8}\left(\frac{h_o}{h_t}\right)^2 \frac{A^2}{h_o^3 a_2}\left[\frac{h_o}{h_t} - 1\right]\right\} \tag{12}$$

where

$$(h_t/h_o) = \left(1 - \frac{V_2 t}{3.6\; h_o}\right) = \left(1 - \frac{a_2}{18h_o}\right) \tag{13}$$

The Multi-Mode Blade Impact Program was modified to accept three correction factors in order to expedite normal impacts. These factors were $C_\rho = (\rho_2/\rho_1) = (1/3.24\alpha_1)$, $C_V=(V_2/V_1)=1.8\alpha_1$, and $C=(\pi/2)-\alpha_1$. For $\alpha_1=.01$, $C_\rho=30.8642$, $C_V=.018$ and $C=1.5608$ radians. Because the mass of the pseudo missile must be the same as the actual missile, $a_1\rho_1A_1=a_2\rho_2A_2$ or $a_1=\left(\frac{\rho_2}{\rho_1}\right)\left(\frac{A_2}{A_1}\right)=\left(\frac{\rho_2}{\rho_1}\right)=\frac{a_2}{1.8^2\alpha_1}$. Thus, for an $\alpha_1=.01$, the pseudo missile length $a_1=30.864a_2$.

Although the original Multi-Mode Impact Program was supposed to include damping, an error existed in the original formulation so that the effective damping was negligible. The discrepancy was corrected so that proper damping of the response due to impact was realized. It was found that realistic damping must be included in the analyses to obtain good correlation with test results.

SECTION III

ANALYSIS OF SPECIMEN IMPACT TESTS AND RESULTS

Several years ago the Impact Mechanics Laboratory at AFML conducted numerous specimen coupon impact tests to study the ability of different materials to withstand soft body impacts. These tests encompassed specimens of various types of composite materials and layups, titanium, and aluminum; see References 15 and 16. Two types of specimens were used in these tests. One was a four-inch cantilevered specimen and the other was a 4.5" simply supported specimen; see Figure 13.

In order to analyze these specimens using the Three-Degree and Multi-Mode Impact Programs, it was necessary to define their dynamic characteristics - e.g. natural frequencies, mode shapes, and equivalent masses and stiffnesses. This was done using both classical and Finite Element (NASTRAN) models; see Figure 14. A study was made to determine the number of flatwise modes needed to properly define the response of the specimens to impacts for the Multi-Mode Impact Analysis. It was found that at least four flatwise modes are needed for the cantilever specimen and six for the simply-supported specimen. Typical impact deflection, moment, and stress distributions for cantilever and simply-supported specimens are depicted in Figures 15 to 19.

Figures 15 and 16 show how the deflection and moment distributions vary with time during and after impact for the impact of a typical cantilever specimen. Note that initially the deflection and moment (proportional to the stressing) are very local at the impact site but progressively the deflection and loading travel toward the clamped end and finally are approximated by those for the fundamental normal bending mode. Figures 17 to 19 show similar results for a typical simply-supported specimen without overhang. Again, initially the deflections, loads, and stressing are very local but ultimately approach those for the fundamental normal bending mode long after the impact ends. Similar results were obtained when the overhang was included but the stressing goes to zero at the ends of the overhang of the specimen rather than at the supports; see Figure 20. This

is much more realistic and gives much better correlation with the test results, particularly near the supports.

Only five of the specimens tested were strain gaged with the resulting impact stresses measured. Also, many of the specimens tested were subjected to multiple impacts, so that they could not be used to evaluate the ability of impact analyses to predict the location and damage for various impact conditions. In all, 147 specimen test cases from References 15 and 16 were found to be acceptable for evaluation to see if the test results, both damage and stressing if available, could be predicted. The cases from Reference 15 are summarized in Table 4, whereas those from Reference 16 are summarized in Table 5. A number of the tests of Reference 16 included high speed movies of the specimen deformation, which could also be used for checking the ability of analyses to predict the results of specimen impacts.

3.1 ANALYSIS OF STRAIN-GAGED IMPACT SPECIMENS

The five specimens in Table 6 that were strain gaged were analyzed using both the Multi-Mode and Three-Degree Impact Programs; see References 1, 3 and 8. Because the Multi-Mode Analysis uses an energy approach it could readily handle directly both the three cantilever and two simply-supported specimens. However, because the Three-Degree Impact Analysis was written for cantilever beams, it had to be tricked into handling the simply-supported specimens; see Section 2.1.2. Both programs were modified so as to give normal impact; see Sections 2.1.2 and 2.2.2.

Table 6 and Figures 21 to 28 present comparisons of the peak measured and calculated stresses at the root and impact site of the five specimens using the two impact programs and an assumed damping of .08 and .12 critical. The measured values were very difficult to define accurately because of the poor resolution of the photographic strain history from the small oscilloscope screen. It is estimated that the error in reading the experimental results could be as much as ±20% and during the early stages of impact by possibly even more. Some of the test results had considerable higher order content, whereas others

were nearly pure fundamental mode after the initial impact period. This, coupled with the fact that several gages went out during the impact, raises the question whether some of the apparent strains might not be instrumentation induced. The estimated yield and ultimate bending strengths of 148 KSI and 226 KSI are standard engineering values.

Referring to Table 6, it is seen that the two impact programs predict values that are fairly consistent with the measured values. Because the test values are based on strain readings, they include yielding and, therefore, will be equal or greater than the predicted elastic stresses given by the programs. The two methods of calculation give results that agree within about 20% of each other and predict the yielding that was experienced by the specimens. At the support gage position of the simply-supported specimens two test values are given. The positive value is from an extremely sharp strain spike at the beginning of the reaction, whereas the negative value is the maximum of the main impact response. The Three-Degree Program only predicts the latter. This initial reverse kick is probably due to the restraint on the overhang, e.g. it can move in only one direction, whereas the theoretical modes do not include this effect.

Two calculated values are given in Table 6 for Specimen 7611 using the Three-Degree Program, one for a simply-supported specimen without the overhang and one with the overhang. It is apparent from these results that the overhang significantly affects the results and should be included in any analysis of such specimens. It is not understood why the Multi-Mode Program gives values about 50% too high at the support gage, for it agrees within 10% of the Three-Degree Program at the impact site.

The results of all of the above cases are plotted in Figures 21 to 28 as apparent stress vs time. The test results are only approximate because of the poor resolution of the strain recordings. Figure 21, for the root stressing of the cantilever beam hit at 713 fps, shows good time history correlation between test and the two theories when it is recognized that yielding should occur above about 148,000 psi.

For the impact site, see Figure 22, again there is good correlation of theory and test for the general transient stress trends and magnitudes if the permanent set is removed from the test results. The higher frequency aberations of the test results are approximated by the Multi-Mode Impact Program except the frequency is a little high. The Three-Degree Impact Program does not give these aberations.

Figures 23 and 24 give similar root and impact site apparent time history stress results for Specimen 7608, which was hit at 936 fps. Here again the correlation of the two programs and tests are good if yielding is taken into account. The measured permanent set at the root is probably not accurate because of the fracture at the root. Apparent from the Multi-Mode Program impact results is the need to include proper damping in the higher modes or unrealistic results will be obtained. This is particularly apparent in the results for the stressing at the impact site; see Figure 24. This figure shows reasonably good correlation between theory and test at the initial stress peak. However, because of yielding the test results for later times differ from the two calculated results, which agree quite well.

The corresponding impact site time history stress results for cantilever Specimen 7610 impacted at 1076 fps are shown in Figure 25. The test results were not available for the root because of gage failure, probably from the high strain rate due to fracture. Again fairly good correlation is present between the two calculated results and measured values. The measured higher order variations are approximated to some degree by the Multi-Mode Impact Program but not by the Three-Degree Impact Program. The initial measured peak is difficult to ascertain and appears to be between 140 and 240 KSI. This figure again shows the importance of damping in controlling the higher order modes.

Figures 26 to 28 give the time history test and calculated apparent stress results for the two simply-supported specimens. The test results are only approximate, particularly the time history results because of the very poor resolution of the recorded data. In Figure 26, the time history apparent

stressing for 933 fps impact, the correlation between the two calculated values and test is quite good when the permanent set is taken into account. Apparent is some discrepancy in defining the time for the test results. The corresponding results for the strain gage position near the support are given in Figure 27. Except for the initial measured positive spike and the dip at .3 milliseconds, the measured and calculated results agree quite well. The reason for the dip in stressing at .3 milliseconds is not apparent unless yield in the center of the beam might be involved. Figure 28 gives the time history of the apparent stressing for Specimen 7612 under a 1155 fps impact. Again similar time history correlation is reasonably good between the calculated and apparent stress test values when the yielding is taken into account. The Multi-Mode Impact Program results give a large dip in stress after the initial stress peak which might or might not be correct, because of the poor time resolution of the test results. The Three-Degree Impact Program only indicates a shallow dip.

3.2 ANALYSIS OF NONGAGED IMPACT SPECIMENS

A review of the virgin specimen test results given in Tables 4 and 5 shows that only about 36 of the 114 cases in Table 4 and 21 of the 33 cases in Table 5 were worthwhile to evaluate. These 57 specimens are designated by an asterisk and include specimens that had visual damage and/or are specimens impacted with the highest velocity for which no apparent damage occurred.

The importance of using virgin specimens is illustrated by the analysis of cantilever specimen 2419/20 of 5.6B/6061 $\left[\pm 45/0^{\circ}\right]$, which had been subjected to multiple impacts, was analyzed for an impact at 331 fps. Using the Multi-Mode Impact Program resulted in maximum elastic stresses of 54,000 psi and 162,000 psi at the impact site and root, respectively. These results are consistent with the yielding that was observed at the root but inconsistent with the observed yielding at the impact site. This multiple impact test result is in variance with the single impact test result on the same type specimen in which

no deformation occurred at impact up to 383 fps; see Table 4. It is apparent from this cursory study that only virgin specimens should be used to evaluate damage from impact and to correlate with analysis.

Table 7 summarizes the stress results for the 24 specimens that were analyzed for impact stressing and compares them to the observed damage. The damage occurred either as yielding or fracture at the root and/or impact site. Also included in the table are the engineering properties for the materials. These properties were obtained from References 15, 18, and 19 or from internal reference information. Because of the high strain rates during impact, usually about 50/sec to 250/sec, the appropriateness of using engineering values is questionable. References 14 and 17 indicate that beyond strain rates of about 10/sec the yield and strength of the material is usually increased.

Comparison of the observed damage with that predicted by the calculated elastic stressing and material properties shows good agreement for all specimens and damaged locations except for a few instances. For the Ti-6AL-4V cantilever specimen 7548, yielding was observed at the impact site as well as root. The analysis predicts sufficient stressing at the root for yielding but not high enough stressing at the impact site to result in yielding. The other discrepancy involves cantilever specimen SN129 made of 5.7 B_S/Ti-6AL-4V$\left[0\right]$ with .003" Ti-6AL-4V facing. According to Reference 15 this specimen showed some deformation after impact at 336 fps, but the calculations by both the Multi-Mode and Three-Degree Impact Programs indicate the root stressing is only about 2/3 of the likely yield. The good correlation of these elastic stress results and engineering material properties with the observed damage indicates that the increase in yield and ultimate strengths at moderate strain rates of 50/sec to 250/sec is probably not significant.

Deflections with time were measured for the aluminum cantilever Cases 7550 and 7552 of Table 7 using high speed moves. Although the resolution was only good to approximately ±10%, the photograph deflections agreed quite well

with those calculated using the Three-Degree Impact Program. Figure 3 compares the measured and calculated results for Case 7552, which was impacted by a velocity of 125 fps. The theoretical results shown in this figure are a little lower than those given in Reference 3, because of the correction introduced to account for high impact angles; see Section 2.1.2. The theoretical prediction now falls slightly below the test results instead of slightly above. Figure 15 compares the theoretical and photographic measured deflections for Case 7550, which was for an impact at 527 fps. The correlation is quite good. Of note is the initial local deformation at the impact site, which after a period of time develops into the normal fundamental bending mode shape. Figure 16 depicts the corresponding moment distributions (stressing) which shows the peak impact stress occurring at .1 ms, whereas the peak root stress occurs at about 2 ms and is about twice as high. Permanent set was observed at both regions because the peak stressings were above the yield; see Table 7.

3.3 DISCUSSION OF SPECIMEN IMPACT RESULTS

The results of Section 3.1 show that the elastic stressing of both cantilever and simply-supported specimens can be quite accurately predicted using available impact computer programs. This is true not only for the peak stressing at the support and impact site but also over the early initial impact period. Apparent from the good correlation of the results and the various check cases, see Figures 6 and 8, is the fact that the simply-supported specimen can be adequately modeled for the Three-Degree Impact Program by a simulated cantilever beam of Figure 7, and that normal impact can be satisfactorily simulated for the Multi-Mode Impact Program using the approach given in Section 2.2.2.

The results of Section 3.2 show that elastic impact analyses can predict the likelihood of damage by yielding or fracture with a reasonable degree of accuracy. However, it is apparent that there is need for better information on material properties, particularly at moderate strain rates of 10 to 250/sec. It also appears

desirable to apply plastic impact analyses to better define the strains and damage. It also indicates that basic fan blade materials can be screened by using elastic impact analyses and conventional engineering material properties.

These studies show that it is undesirable to impact specimens more than once even though there is no visual damage. Analysis of such specimens, as well as test results, indicate nonvisual internal damage, such as internal delamination, might occur from the initial impact which can adversely affect the capacity of the specimen to withstand the second impact. The difficulty in reducing the measured strain and deflection data combined with poor resolution, shows the need for improved impact measurement techniques. It is also important to measure the rebound velocity of the missile to properly evaluate the effective impact; see Figures 3, 15, and 16. It would be better to use a missile material which does not rebound, although the effect of the rebound velocity can be included in the data reduction and prediction analyses.

Apparent from the calculated impact stress distributions for the cantilever and simply-supported beams is that the former develops two high stress areas, whereas the latter only develops one. The peak stress at the impact site of the cantilever specimen occurs very soon after the impact ends but the peak stress at the root occurs much later, i.e. the two stressings are separated, both in time and location. For the simply-supported specimen the local and gross stressings occur at the same location, the center of the span; see Figures 18 and 19. Because of this a glitch occurs in the stressing with time as indicated in Figures 26 and 27. The basic local impact site stressing of the cantilever beam is of the same order as that for the simply-supported beam before the gross action takes over. In general, the local stressing is about 70% of the gross-root stressing for cantilever and center stressing for simply-supported specimens for the specimens which are about .070" thick.

If both local and gross impact damage is to be studied, the cantilever specimen is probably the better specimen because it separates the two phenomena.

The relative magnitudes of the local and gross stressing can be controlled as discussed in Section 5. The simply-supported specimen also has the disadvantage of a nonlinear support and resulting unexplained apparent stress spike near the support at the beginning of the impact period. The only disadvantage of the cantilever specimen is that the gross deflection of the specimen results in non-normal impacts. However, the gross deflection is usually so small during the impact period that this effect should be insignificant.

SECTION IV
ANALYSIS OF TYPICAL FAN BLADES

In order to determine the significance of the stress condition of fan blades during impact with regard to the resulting damage, the instrumented results from the impact testing of four Q-Fan blades were evaluated analytically using the Three-Degree and Multi-Mode Impact Programs. These rotating tests were conducted for NASA-Lewis, see Reference 20, and consisted of six impact cases of various size missiles at a velocity of 925 fps and an impact angle of 30°. The results of this blade impact study and the specimen impact study of Section III give the basic information needed to develop a viable impact test specimen for materials, which would similate the stress state that fan blades experience under impact; see Section V. This study also gives some insight into the damage phenomenon of impacted blades.

4.1 REVIEW OF TEST RESULTS

The test results which were used in this study were designed for the Quiet Clean Short-Haul Experimental Engine (QCSEE) and tested under NASA Contract NAS3-17837. The blades were designed to operate at a tip speed of 925 fps and a pressure ratio of 1.325, and had a span of 18.2". The blade construction consisted of a solid Ti-6Al-4V titanium spar with an adhesively bonded Borsic(R)/6061 Al shell which formed the airfoil. Over the shell was an integrally-bonded surface of pure .0057" Ti-6AL-4V titanium skin. The leading and trailing edge cavities contained 38 lb/ft^3 aluminum honeycomb. An Inconel 625 leading edge sheath provided resistance to damage from both hard and soft foreign objects; see Figure 29. The details of the construction and geometry of these blades may be found in Reference 20. The blades had a ball retention to permit variable pitch capability (a wire was actually used during the impact tests for cost reasons). Some of the blades incorporated a retention rocking scheme, which was used to limit the maximum gross moment and stressing in the blade for large

impacts. The dynamic characteristics of the blade are shown by the Campbell Diagram given in Figure 30.

Four fan blades were instrumented as shown in Figure 31 to measure the gross and local stressing resulting from the impact. The impacting missiles were either made of simulated micro-balloon/gelatine birds or real birds, both of approximately .69 specific gravity. The simulated birds were cylindrical in shape with a length to diameter ratio of 2:1. The blades were impact tested in Hamilton Standard's G-5 whirl impact test facility shown in Figure 32. The test chamber was evacuated to 2.5 PSI. A pendulum ejection system was set up so that the simulated missiles were cut in approximate half and hit the blade at .8 span. Photographic documentation of the impacts was accomplished using two high speed movie cameras. The transient strain measurements were recorded on magnetic tape, which allowed greater flexibility for data reduction. A more detailed discussion of the test facility, procedure, and measurements may be found in Reference 20.

All of the large impacts were at a velocity of 830 fps and at an impact angle of 32°. Although only four tests were run, six distinct impact cases occurred. This is because the missile ingestion timing of two of the tests, Tests 5 and 11, resulted in first a small slice and then a major slice of the missile impacting the blade. The measured strain (stress) results for the resulting six impact cases are summarized in Tables 8 and 9. These results cover impact missile weights of .12 to 1.74 lbs. The magnitudes of the actual impact missile weight was based on the remains of the missile in the pendulum and from the high speed photographs for the two small, "chip" impacts. Figure 33 shows the resulting damage from the four larger impacts, and typical damage due to a smaller missile of .36 lbs. Reference 20 presents detailed photographs and discussion of the damage resulting from these test cases. A close inspection of the high speed movies showed that in all cases the initiation of the damage in the trailing edge started at a chordwise crack near the spar and then propagated towards the

trailing edge and along the spar to the tip. Thus, the significant stressing causing the trailing edge damage was the spanwise shell stress at the impact site. The origin of the initiation of the leading edge damage could not be ascertained.

4.2 THEORETICAL RESULTS

All six impact cases were analyzed by using both the Three-Degree and Multi-Mode Impact Programs; see Section II. The calculated results are summarized along with the test results in Tables 8 and 9 for the Three-Degree and Multi-Mode Impact Analyses, respectively. In all cases, the maximum stressing at the impact site is not influenced by whether the retention is fixed or of the rocking type because the local peak stressing occurs before rocking takes place. However, the inboard blade stressing is reduced by permitting the blade to rock.

Comparison of the calculated and test values for the gross blade stressing at the impact site shows reasonably good correlation for the four major impact cases when one realizes that yielding has occurred, making the test values larger than their elastic values. Also, there was undoubtedly a loss of impact energy not taken into account by the elastic analyses because of the yielding and fracture of the blades; see Figure 33.

The inboard stressing predicted by the two analyses are about the same but are considerably greater than the measured values. This is undoubtedly because of the loss of energy due to yielding and fracture in the impact region, which occurs well before the stressing peaks at the inboard region. Also, the presence of rocking reduces the inboard stressing some. Analysis shows that Case 4 just barely rocks if no energy is lost, whereas for the greater impacts of Cases 5, 10, and 11 rocking should occur, thereby reducing the maximum gross impact stressing of the blade. The Three-Degree Impact Program predicted 11 and 13 degrees of rocking for Cases 5 and 10, respectively. These values compare well

with the measured values of 10.3 degrees for both cases, especially if the energy loss due to fracture is taken into account.

For the two chip impacts of Cases 5 and 11, the correlation of the theoretical predictions with the test results is not very good, particularly for Case 5, being much less than measured. Significantly both theoretical methods predict about the same stressing, so that it appears that the discrepancy could be due to the poor definition of the actual size of the chip shot, due to possibly the local yielding at the leading edge which results in a greater impact angle, and/or the lack of chordwise dynamics in the theoretical programs. Both analyses neglect the chordwise bending response, which might be important for small, leading edge impacts. Preliminary results from the improved Three-Degree Impact Analysis being developed under NASA Contract NAS3-20091 shows that chordwise dynamics is much more important for small, leading edge impacts than for large impacts; see Section 5.2.

Figures 34 and 35 compare the predicted spanwise blade centerline stressing for Case 4 of Tables 3 and 9 with the material strength at certain key times after impact. Apparent is the prediction of spanwise structural damage of the shell but not of the spar at the impact station, which agrees with the fracture results. Some disagreement is apparent between the Three-Degree Impact Program, Figure 34, and the Multi-Mode Impact Program, Figure 35, for the inboard blade stressing at the time the peak stressing occurs at the impact station and at the root (the times differ because the initiation of impact differed). Also apparent is that the high root stressing is not realized because of the loss of energy and load due to the fracture of the tip region earlier in time.

Figure 35 also presents the combined maximum stressing in the region of the impact site. These combined stressings include the centrifugal stressing, the leading or trailing edge spanwise stressing due to torsion, the flatwise bending stressing, and the edgewise bending stressing. It is apparent from Figure 36 that most of the stressing is given primarily by the spanwise flatwise stressing.

The torsional shear stressing at the centerline at a time of .55 milliseconds is about 20,000 PSI at the 30" station and only about 5000 PSI at the 31.84" station. The magnitude of the centrifugal core and shell stressing with blade station is given in Figure 36 and shows that at the impact site the centrifugal stressing is of secondary importance.

The maximum core and shear stresses vs blade station for Case 4 are presented in Figures 37 and 38. These values occur at different times after impact. The values in the vicinity of the impact site occur during or just after impact, whereas the inboard values occur much later and are primarily due to the fundamental bending mode. The maximum shell shear stress at the impact site is about 12,000 PSI (6,000 to 15,000 PSI).

Figures 39 and 40 give the shell centerline strain versus time for various blade stations in the impact region for Case 4. Figure 39 shows the maximum strain occurs at about .55 ms with the maximum strain rate occurring at about .30 ms. To obtain the maximum strain rate the expanded strain rate curve of Figure 40 was used. This figure shows that the maximum shell strain rate occurs at the 31.23" station and is about 25/sec. The corresponding strain versus time curve for the spar at the impact site is given by Figure 41 and shows that the maximum again occurs at the 31.23" station and is about 15/sec. Figure 42 presents the strain versus time curve for the shank region (12.8" station) for Case 4. Note that the maximum strain rate of about 14/sec occurs at about .8 ms instead of .3 ms as for the maximum strain rate at the impact site. The early variations in the strain (below .50 ms) would indicate similar strain rates at about .35 ms and .05 ms, but these appear to be inaccuracies in the calculated results. Thus, both the root and impact site of the spar see strain rates of about the same magnitude. Such strain rates are high enough to influence the yield and ultimate strength some, but probably not by a major amount; see References 14 and 17.

The analysis of the chordwise stressing using the results from the two beam impact analyses is difficult and only approximate, particularly for hollow blades

such as the Q-Fan blade. The analysis assumes that the shell leading and trailing edges behave as cantilever beams built in at the spar leading and trailing edges, respectively; see Figure 43a. Assumptions must be made with regard to the incremental impact pressures over the chordwise and spanwise directions. The improved versions of the two impact programs under NASA Contract NAS3-20091 will have this feature but were not ready for this study. For each impact loading, which varies with time, the effective structural spanwise length of the blade shell relative to a particular pressure increment is obtained by assuming the load in the overhang spreads at 45° as shown in Figure 43b. The chordwise section properties, bending moments and stressing are then calculated using simple beam theory. Further complicating the analysis is the fact that the shell and filler inertia loading must be included in the analysis. This is obtained from the calculated gross, rigid torsional and bending motions of the blade. It neglects the chordwise dynamic (flexible) inertia loads which might be significant. Such an analysis was performed for Case II using the impact loading given by the Multi-Mode Impact Program. The analysis gave a chordwise stress at the spar edge at the impact station of -126,000 PSI compared to a measured value of -570,000 PSI. Undoubtedly, much of this discrepancy is due to the yielding and fracture that occurred at this location.

Although the improved version of the Three-Degree Impact Program with chordwise response was not completely checked out it was applied to Case 4 to determine if the effects of chordwise flexibility had a significant effect on the blade response and stressing for moderately large missiles of .97 lbs. Figure 44 gives the computer printout of the deflections of the blade, where x, y, z, and Θ are the flatwise, edgewise, chordwise, and torsional deflections. Apparent from this figure is the relatively small magnitude of the chordwise deflection compared to the flatwise deflection. Table 8 includes in parentheses the resulting stressing at the strain gage positions using this improved analysis.

Comparison with the results without chordwise dynamics shows that the chordwise dynamics have a secondary but significant effect on the stressing and improve the correlation with the test results.

4.3 DISCUSSION OF BLADE IMPACT RESULTS

The evaluation of the six impact test cases of the four Q-Fan blades not only gave values for the significant stress conditions during impact for designing material coupon specimens, but also gave insight into the impact and damage phenomena, and afforded a check on the capability of available impact analyses in predicting the impact stressing and damage.

Apparent from the results from these rotating tests is the difficulty in conducting such tests. Not only is it difficult to measure the blade dynamic stressing on a rotating system, but it is difficult to assure exact impact location, witness the two "chip" impacts, and to observe and record the response of a rotating blade. These tests show that static tests would be highly desirable from not only a cost standpoint, but from the ability to instrument and evaluate the test results. It is also apparent that once damage occurs in the form of yield and/or fracture, a whole new set of phenomena occur with respect to blade response, energy transfer and loss, and fracture locations. The instrumentation and evaluation needed to completely understand the conditions involved during the damage and fracture of blades due to impact is far more complicated than that required for elastic impact. Similar complexity can be anticipated in developing a theoretical analysis for predicting the damage and fracture of impacted blades because of the many ways blades can fail; see for example Figure 33.

The relatively good correlation of the predicted elastic impact blade stressing with test measurements for the four larger missile cases shows that relatively nonsophisticated beam impact analyses can be used to predict the elastic dynamic response of blades from impacts. It is also apparent from this correlation and the prediction of the trailing edge fracture origin of these blades, that such

elastic analyses can be used effectively for predicting the impact threshold of blades and the likely initial damage. However, above this impact threshold the ability of such elastic analyses to predict the ensuing damage is very questionable.

Both the tests and analyses for the subject fan blades show that there are three critically stressed areas - the leading edge at the impact site, the gross blade at the impact station, and the gross blade at the stations of maximum stress for the fundamental modes. The time at which these three areas are critically stressed varies appreciably, occurring during impact for the first and considerably after the impact ends for the last. Thus, the location and magnitude of any damage is determined not only by the relative maximum stressing of the three regions but their time of occurrence. For example, if the leading edge is overstressed during the initial stages of impact and fractures, the loading will be decreased such that the rest of the blade will never reach the predicted high stressing later on during the impact processes. Thus, the magnitude of the impact as well as the blade characteristics determine the damage location. The use of rocking retentions are effective only for limiting the gross inboard blade stressing after the initial impact is over.

The two, beam, blade impact analyses did not predict the blade stresses caused by small missile impacts very well. Although this could be due to local leading edge yielding or poor definition of the missile size, it appears that the lack of chordwise response in the analyses could be the major cause of this discrepancy. The inclusion of chordwise response in a new version of the Three-Degree Impact Program showed that the chordwise response improved the correlation with test for larger missiles and is very important for small missile impacts; see Section 5.2.

The combined maximum stressing at the impact site was found to be only about 20% higher than that given by the sum of the normal mode stressing. The centrifugal stressing was found to be less than 10% of the bending stressing, and therefore, is of secondary importance. However, the torsion shear stressing was found to

be quite large and, therefore, should be included in any evaluation. These results indicate that static impact tests should be satisfactory for evaluating the impact region providing the blade dynamic characteristics are made the same as they are under centrifugal stiffening. For the inboard regions, the centrifugal stressing can be significant and probably should be included.

The study of Q-Fan Case 4 for a .97 lb. missile impact at 32° and 830 fps showed that the maximum typical elastic impact and mid-blade spanwise bending stressing are about the same at about 150,000 PSI; see the test and analysis results given in Tables 8 and 9. The maximum shell interlaminar shear stress was found to range from 6,000 to 15,000 PSI or about 10,000 PSI, and the maximum strain rates for the shell and spar materials were found to be about 25/sec and 15/sec, respectively. These strain rates are probably high enough to increase the material yield and ultimate strength some but not appreciably. These results are for a moderate size missile, and a moderate impact velocity and angle and, therefore, the magnitudes of these values could be more or less than those quoted depending on the impact conditions and fan blade characteristics. Apparent from these blade studies is the ability to define quite well the important elastic impact stress conditions using available analyses, particularly if the chordwise response is included in the theory. This capability should be helpful in the design of coupon test specimens for evaluation of materials for impact resistance.

SECTION V

EVALUATION AND DEVELOPMENT OF IMPACT SPECIMENS

Apparent from the test and analysis results of Section IV is the fact that the impact of a blade results in three stress conditions - two at the location of the impact and another inboard of the impact site. The former two are at the leading edge and near the centerline and occur during or just after the impact. Both involve a complex stress condition, particularly the leading edge location, because of the presence of both chordwise and spanwise stressing. The latter one occurs much later in time and is primarily a result of the lower fundamental modes and their stressing. To design a single specimen to evaluate properly all three of these stress states simultaneously would be very difficult. Therefore, it was decided that the evaluation of materials for impact resistance would best be accomplished using a two-phase specimen program - 1.) A specimen program to evaluate the impact capabilities of the materials for gross bending and shear stressing, and 2.) a specimen program to evaluate the impact capabilities of the materials for local complex stressing. The former pertains to the spanwise stressing of the blade initially at the impact site and later inboard, whereas the latter pertains to the local leading edge impact resistance capability. Sections 5.1 and 5.2 discuss the development of specimens for studying the resistance of materials to these two impact criteria. Section 5.3 investigates the significance of impacting specimens without centrifugal load by evaluating impacted blades with and without centrifugal load. This is important because of the desire for conducting specimen impact tests without centrifugal effects.

5.1 CANTILEVER TEST SPECIMEN FOR STUDYING GROSS IMPACT OF MATERIALS

The purpose of this study was to develop a cantilever test specimen that has equivalent impact stresses of a typical fan blade. To achieve this goal, the Three-Degree Impact Program was used, which was improved to handle normal

impacts; see Section 2.1.2. The evaluation was limited to the development of cantilever beam specimens because the simply-supported specimen has both the local and gross stressing occurring at the same location (the impact point); see Section 3.3. Because of costs and testing equipment, it was decided to limit the length of the specimen to 8" (9" coupon) and the impacting missile to spheres of gelatin or similar material no more than 1" in diameter. Also, in order to demonstrate the interactions of various properties of the specimen and missile, a parametric study was conducted. From the results of the parametric study suitable specimens to simulate actual blade stressing were defined to evaluate fan blade materials. The parametric study allowed a wide range of variables, such as impact velocity, impact site, thickness, beam taper, and the size of the impact missile to be compared as to their effect upon the bending stresses, shear stresses and strain rates in the cantilever specimen. The impact velocity of the missile was varied at first to observe its effect on the behavior of the beam. Then the velocity was fixed to 830 fps, which is the impact velocity at which the Q-Fan blade was impacted; see Section VI.

For a given 830 fps impact velocity, cases were run with variations in impact site. The point of impact along the beam was defined as a percentage of the total length of the specimen. This allowed for a generalization of the impact site in relation to the stresses that evolved. Based on a 1" clamp length, the maximum cantilever specimen obtainable from a reasonable 9" coupon is 8". Cases were run with an 8" x 2" cantilever specimen with the impact site (Z) ranging from .65 to .85 or between 5.2" to 6.8" of an 8" beam. Another important variable is thickness, which was adjusted from a very thin specimen of .04" to as high as .75" depending upon the desired impact stress state.

In the evaluation process of defining a specimen which would duplicate blade impact stressing, two other concepts were tried: tapering the beam and changing the missile size. The technique used in tapering the beam was to keep the tip the

same width (b) but increase the base (b_o) of the cantilever as shown in Figure 45. For example, a 1.5 taper is defined when the ratio of the width of the two ends (b_o/b) is equal to 1.5. The spherical missile was varied from .75" to 1.0" in diameter. The spherical missile was approximated for the Three-Degree Program by a cube of equivalent volume and mass - e.g. $V_{sphere} = \frac{4}{3}\pi r^3 = V_{cube} = \ell^3$ or $\ell = r\sqrt[3]{\frac{4\pi}{3}}$.

The parametric study revealed several important trends that are needed to properly design impact specimens for evaluating the impact resistance of fan blade materials. The first of these findings is that the velocity has a significant influence upon bending stress, shear stress and the strain rate. As shown in Figure 46, the root and local spanwise bending stresses were found to be directly proportional to the impact velocity. However, as shown in Figure 47, the shear stress and strain rates appear to increase at a faster rate with velocity than the bending stress. From these graphs, it can be concluded that the shear stress is proportional to the square of the velocity, V^2, while the strain rate is proportional to the 1.8 power of velocity, $V^{1.8}$. One important point to be noted from this study is that the ratio of the local impact spanwise stress to the root spanwise stress σ_i/σ_r, did not change significantly with the impact velocity.

The strain rate/local spanwise stress ratio increases almost proportionally to the local spanwise stress; see Figures 46 and 47, and increases slightly as the impact site moves towards the tip of the specimen; see Figure 48. Increasing the thickness of the specimen, tapering the specimen, and increasing the impact velocity all tend to increase the strain rate / local spanwise stress ratio. In general, the strain rate for specimens tends to be high compared to the desired value present in fan blades. Figure 48 shows that only very thin specimens with a low velocity impact will meet the strain rate/impact stress ratio equivalent to a .97 lb. bird impacting a 3D-Q-Fan blade. But such specimens are not practical and do not meet the other stress requirements. Therefore, the strain rate/impact

stress ratio for specimens will usually end up somewhat higher than that present in blades, perhaps double. However, it is doubtful if this discrepancy will have a major effect on the material properties; see References 14 and 17.

The results given in Table 10 and Figure 49 show that the thickness of the beam significantly influences the stresses. As expected, the bending stresses, shear stress and strain rate decrease with thickness. The results in Table 10 show that the bending stress decreases inversely proportional to $t^{1.5}$, whereas the shear stress and strain rate decrease approximately inversely proportional to $t^{1.2}$. From these trends, approximations can be made for bending stress, shear stress and strain rate of a particular specimen to obtain those properties that is closest to that of the fan blade under consideration.

In this study, the Q-Fan blade stress conditions given in Section IV were used to demonstrate the modeling of coupon specimens for evaluating materials for an engine fan blade. One condition was that the local spanwise maximum stress at the impact site should be greater than or equal to the root maximum stress. This, however, limits the choice of specimens, which can only be met under two conditions - The impact must be close to the tip; see Figure 50, or a smaller impact missile must be used; see Figure 46.

The effect of tapering was investigated with the hope of expanding the choice of the specimen and range of specimen and missile conditions. As was anticipated, the stresses were lowered by tapering the specimens. However, as shown in Figure 46 the root stress is higher than the local impact stress. Also apparent from Figure 46 is the fact that tapering worsens the impact stress/root stress ratio, compared to the nontapered case (or taper = 1.0). This result can only be due to the flexibility or dynamics of the specimen. Therefore, an impact very close to the tip and/or a smaller impact missile are the only apparent ways for obtaining a high local impact stress relative to the root stress.

To complete the parametric study, a comparison was made between the ratio of the shear stress and local spanwise stress and the effect of the variables of the parametric study. This is done in Figure 51. The shear stress over local

spanwise stress (f_s / σ_i) ratio is seen to decrease with increase in impact site (Z). The taper case tends to increase this ratio with increase in impact site. Obviously, an increase in velocity will also increase the shear stress/local spanwise stress ratio since the shear stress increases at a faster rate with impact velocity than the local spanwise bending stress does. This is also true for an increase in thickness. From Figure 51 a specimen can be carefully chosen which has approximately the proper shear stress relative to spanwise bending stress that is found in impacted fan blades.

From the combined use of the Figures 46 through 51 and Table 10, which summarize all the trends needed to clearly understand the effects of specimen dimensions and missile conditions, a specimen can be defined for studying the gross impact of materials for a given fan blade.

From these results a coupon specimen was designed for evaluating materials for the Q-Fan blade, which was impacted by a .97 lb. bird at an impact velocity of about 830 fps and an angle of 32°; see Section IV. From the various cases, the impact site was chosen to be about .85, which results in a local spanwise impact stress approximately equal to the root spanwise stress. It was also demonstrated that the specimen had to be relatively thick in order to lower the resulting stresses for impact velocities similar to those for the Q-Fan blade; see Section IV. As stated before, a tapered beam does not help the stress value relationship. It is shown in Figure 51 that only the thick specimen with high impact velocity (830 fps) had root and local spanwise bending stresses within 10 percent of those for the Q-Fan blade and a shear stress/local spanwise stress ratio close to those for the fan blade. The two specimens meeting these requirements are: 1.) An 8" x 2" specimen 0.2" thick, impacted normally at the .85 station with a 1" spherical missile at 830 fps; and 2.) an 8" x 2" specimen 0.14" thick, impacted normally at the .85 station with a 7/8" spherical missile at 830 fps. Figure 50 shows that the specimen with a 7/8" missile has the local stress equal to the root stress. The 1" missile is rather large on a beam whose width is only

two inches. For this reason, a smaller missile tends to lower the bending stress, shear stress, and strain rate; see Figures 46, 47 48, and 49. Obviously, the final designs of the specimen and missile depend upon the type of blade being impacted, the impact velocity and the size of the blade impact missile.

5.2 LEADING EDGE SPECIMEN FOR STUDYING LOCAL IMPACT OF MATERIALS

Apparent from the test and analysis work in Section IV and the work reported in the literature (see for example References 21 and 22) is that a special specimen is required to study the resistance of materials to the local impact conditions at the leading edge of fan blades. Realizing this, the Air Force Materials Laboratory (AFML) developed and performed impact tests on a leading edge test specimen consisting of plates 3" wide, 6" long, and .063" thick; see Figure 50d. The edge of the specimen is beveled down to a 0.010" edge thickness over a 1" width, and the specimen is clamped at each end. Impact damage on Ti-6AL-4V titanium using 1" RTV spherical missiles at 30° and velocities up to 1200 fps was found to compare favorably with what titanium blades experience in service; see Reference 23. Hamilton Standard had previously developed and tested a leading edge specimen consisting of a simulated 4" wide chordwise section of the leading edge of a Q-Fan blade clamped at the spar centerline; see Figure 50b. The resulting 4.8" cantilever specimen was then impacted with various missiles and velocities at 32°. The object of this study was to determine what type of specimen, such as these two, would best simulate the stress state under leading edge impact for evaluating materials.

Both the AFML and Hamilton Standard (HS) leading edge specimens were analyzed using the Three-Degree Impact Analysis to obtain an understanding of their dynamic response under impact. The required dynamic characteristics of both specimens were obtained using NASTRAN. The AFML specimen was analyzed for a 30° impact by a one-inch gelatin sphere traveling at both 830 fps and 1200 fps, whereas the HS specimen was analyzed for a 30° impact by both a one-inch gelatin

sphere and a 440 gram cylindrical missile traveling at 830 fps. For comparison purposes, the responses of an entire Q-Fan blade to these latter two impacts were also determined using the Three-Degree Impact Analysis.

The response results for the blade, HS leading edge specimen, and AFML specimen due to a 1" spherical missile impact, are given at the bottom of Figure 52. The reaction forces at the attachment points of the HS specimen is seen to be about 10% of the impact force at the time of peak impact, whereas it is virtually zero for the blade, indicating that the leading edge stresses in the specimen may be somewhat different than those in the blade. This indicates the need for including both the gross blade response and the chordwise response in both the analysis and test. The reaction forces at the support at the time of the maximum impact force for the AFML specimen are only about 1% of the impact forces, which are in between those for the blade and the HS specimen. The impact duration times are all about the same because of the small missile size; however, the deflections and maximum normal impact loads differ significantly between the blade and the two specimens. These differences can significantly affect the resulting stressing and, therefore, damage. Comparison of the two results under Columns d, for the AFML specimen, shows that the impact velocity does not affect the maximum loads and response during the impact period appreciably, only the length of the impact period.

In order to understand the difference between the blade and the HS specimen, an equivalent two-degree-of-freedom model of the flatwise response of the Q-Fan blade was developed. In this model, which is suitable only during the short period of impact, a small mass is used to represent the blade leading edge material in the vicinity of the impact site and a larger mass is used to represent the mass of the remainder of the blade. The spring connecting the two masses represents the chordwise flexibility at the impact site and the spring connecting the larger mass to ground represents the flexibility of the remainder of the blade. The effective width and, therefore, stiffness of the chordwise spring was based on Reference 24 for a point load applied to an overhung plate. This equivalent model was developed because the improved version of the Three-Degree Impact

Program was not available at that time. Later, the improved version with the chordwise effects became available and, therefore, was run for comparison purposes.

The results for the equivalent blade/leading edge model and the improved program with chordwise dynamics are given in Columns c of Figure 52. Comparison of the two results show relatively good correlation in load, deflection, and impact time considering the approximations made in the equivalent model. These results, when compared to those for the plain, leading edge specimen and the blade with no chordwise response given in Columns a and b, show that both the chordwise flexibility and blade flexibility are important. The dynamic deflections during impact are considerably more than those given by the rigidly-mounted, leading edge specimen, and by the blade. Also, the more realistic models give a much smaller load in the leading edge spring than the rigidly-mounted leading edge specimen, and a smaller blade spring load than the plain blade.

Figures 53 and 54 present a vivid display of the importance of chordwise response for small missile impacts. These figures were developed by the improved version of the Three-Degree Impact Program with and without chordwise effects, respectively. Apparent from Figure 53 is that the major chordwise response, z, with respect to the airfoil chordline and the influence of this motion on the gross flatwise, x, edgewise, y, and torsional responses of the blade. Figure 54 shows what the dynamic response would be if the chordwise response is not included. All of the interaction effects of the chordwise response on the gross motion is missing and the maximum gross flatwise and edgewise responses are about 20% and 50% greater, because none of the energy is absorbed by the chordwise response. The maximum magnitude of the torsional response did not change appreciably. Apparent from these results is the need to include both the gross and chordwise blade response in any analysis and test specimen design in order to properly evaluate small missile impacts. The AFML specimen appears to be too flexible, giving greater deflection and lower leading edge loads than those for a Q-Fan blade. However, these results indicate it probably gives

a fairly good representation of the impact response and, therefore, damage for thinner and narrower titanium fan blades or for smaller missiles.

For the large 440 gm missile impact, it was found that during impact the deflection of the rigidly-mounted HS leading edge specimen was of the same order as the deflection of the full scale blade model with a rigid chordwise airfoil. A more sophisticated model of the full blade, which would include both the gross spanwise and local chordwise deflection, would, therefore, have a different dynamic response and stressing at the impact site than the half-chord, rigidly-mounted, HS leading edge specimen. Therefore, for impact cases involving large missiles it is important to incorporate the gross mounting flexibilities in the leading edge specimen tests. This is quite apparent from Figure 44, which shows that the chordwise deflection time response of a Q-Fan blade has a secondary effect on the general dynamic response of the blade when impacted by large missiles. This is in contrast to the corresponding results given in Figure 53, which gives the blade time response of the same blade due to a small 1" spherical gelatin missile. Thus, as the size of the missile gets bigger, the gross effects become more important and the local effects become less important, unless their relative timing and magnitudes permit the latter to cause damage first.

5.3 EFFECT OF CENTRIFUGAL LOAD ON THE IMPACT OF BLADES

The results presented in Sections 5.1 and 5.2 indicate that both the gross and local dynamic stressing in blades due to impact can be approximated in simple cantilever specimens if properly designed. However, one important question with regard to using coupon specimen tests to study material impact resistance in blades is the important of the centrifugal load effect. Naturally the main advantage of such specimens is not only their low cost and simplicity, but also their ease of instrumentation and impacting without the complexity present in rotating blade impact tests.

The effect of centrifugal load influences two aspects of the blade impact process. One aspect affected by centrifugal load is the dynamic characteristics of the blade both as to the natural frequencies and mode shapes. The importance of the

centrifugal stiffening effects on the blade impact response depends on the size of the missile and its velocity; see Figure 1. Table II presents a comparison of theoretical results for stationary and rotating Q-Fan blades impacted by a moderate size missile. Although the differences in response and gross blade load are not large, they are sufficiently different so that the centrifugal loading effect on the dynamics should be included. Any sufficiently sophisticated impact analysis which includes at least the first fundamental modes (x, y, and Θ) should be adequate to evaluate the centrifugal effects on the blade dynamics, so that static specimen or blade tests can be devised equivalent to the rotating blade tests.

The other major centrifugal load effect is the steady stressing it causes. For the more common impacts over the outboard portion of the fan blade, the centrifugal stressing is usually small compared to that produced by the impact and, therefore, can be neglected; see Section 4.3. However, for small, leading edge impacts and larger impacts over the inboard portion of the blade, centrifugal stressing can be significant relative to the impact stressing and should be included. To include equivalent centrifugal stressing in stationary cantilever specimens would be difficult. Equivalent centrifugal stressing could be easily included in the AFML leading edge specimen; however, one must be sure the dynamic characteristics under such conditions are correct.

Table II also shows the effect of damping on the dynamic response of blades to impacts. Apparent is the secondary effect of damping on the gross response of the blade. Thus, in analyzing blades and specimens to determine their maximum impact stressing only approximate damping values need to be used. This is because the peak stressing and, therefore, the resulting damage occur early during the dynamic response.

The results of this parametric study show that properly designed leading edge and coupon specimens can be used for evaluating the FOD resistance of materials in fan blades. The necessary elastic blade impact programs and technology to analyze the blades and specimens are readily available and easy to use as shown

here. Two types of specimens are required to adequately similate the three critically stressed regions occurring in impacted blades. The type, geometry, and dynamic characteristics of the specimens depend on the speed and size of the missile and the blade impact characteristics.

REFERENCES

1. Cornell, R. W., "Elementary Three-Dimensional Flexible Blade Impact Analysis," Internal Hamilton Standard Report SA# 636, Division of United Technologies Corp., Windsor Locks, Conn., November 12, 1974.

2. Cornell, R. W., "Modifications to Elementary Three-Dimensional Flexible Blade Impact Analysis, Including Rocking," Internal Hamilton Standard Report SA# 636S, Division of United Technologies Corp., Windsor Locks, Conn., March 26, 1975.

3. Cornell, R. W., "Elementary Three-Dimensional Interactive Rotor Blade Impact Analysis," ASME Engineering For Power, Vol. 98, No. 4., October 1976.

4. Cornell, R. W., "Maximum Impact Blade Torques," Internal Hamilton Standard Report SA# 654, Division of United Technologies Corp., Windsor Locks, Conn., January 29, 1975.

5. Cornell, R. W., "Application of Single-Degree, Parametric Blade Impact Diagram," Internal Hamilton Standard Report SA# 688, Division of United Technologies Corp., Windsor Locks, Conn., February 5, 1976.

6. Cornell, R. W., "Parallel Jet Version of Elementary Three-Dimensional Flexible Blade Impact Analysis," Internal Hamilton Standard Report SA# 684, Division of United Technologies Corp., Windsor Locks, Conn., January 5, 1976.

7. Marti, J., "Parallel Jet Elementary 3D Flexible Blade Impact Analysis With Pre and Post Processors," Internal Hamilton Standard Report SA# 723, Division of United Technologies Corp., Windsor Locks, Conn., January 12, 1978.

8. Houtz, N., "Multiple Mode, Incremental Blade Impact Analysis and Computer Program," Internal Hamilton Standard Report SA# 664, Division of United Technologies Corp., Windsor Locks, Conn., August 25, 1975.

9. Rosenblatt, M., Eggum, G. E., & DeAngelo, L. A., "Numerical Analyses of Soft Body Impacts on Rigid and Deformable Targets," AFML-TR-76-202, California Research & Technology, Inc., December 1976.

10. Sun, C. T. and Sierakowski, R. L., "Studies on the Impact Structural Damage of Composite Blades," Foreign Object Impact Damage to Composites, ASTM STP 508. American Society for Testing and Materials, 1975.

11. Fulton, G., "Analyses of Fan Blade Impact," Fourth FOD of Composites Workshop, Cleveland, Ohio, March 1977.

12. Tsai, S. W., Sun, C. T., Hopkins, A. K., Hohn, H. T., & Lee, T. W., "Behavior of Cantilever Beam Under Impact of a Soft Projectile," AFML-TR-74-94, WPAFB, November 1974.

13. Chamis, C. C. & Minch, M. D., "Structural Response of Fiber Composite Fan Blades," ASME Preprint 75-GT-78, March 2-6, 1975.

14. Johnson, W., "Impact Strength of Materials," Edward Arnold, London, 1972.

15. Prevo, K. M., "Development of Impact Resistant Metal Matrix Composites," AFML-TR-75-216, WPAFB, March 2976.

16. Hopkins, A. & Chamis, C., Unpublished Soft Impact Test Data for Titanium and Aluminum Specimens, 1975.

17. Nadai, A., "Theory of Flow and Fracture of Solids," Volume 1, McGraw-Hill Book Co., 1950.

18. "Metallic Materials and Elements for Aerospace Vehicle Structures," MIL HDBK-5A, Feb. 8, 1966.

19. "Structural Design Guide for Advanced Composite Applications," Second Edition, Advanced Composites Division, AFML, January 1971.

20. Graff, J., Stoltze, L., and Varholak, E. M., "Fiber Composite Fan Blade Impact Improvement," NASA Report CR-135001, Feb. 1976.

21. Seibert, A. G., "Approximate Blade Leading Edge Impact Damage Analysis," Internal Hamilton Standard Report SA# 717, Division of United Technologies Corp., Windsor Locks, Conn., August 11, 1977.

22. Sayes, K. H., "Design and Analysis Methods for Soft Body Impact on Laminated Composite Materials and Metal Lift Engine Fan Blades," Fiber Science & Technology, (8), 1975, pg. 174-206.

23. Barber, J. P. and Bertke, R. V., "Experimental Simulation of Fan Blade Leading Edge Damage from Bird Impacts," AFML Technical Report to be Published in 1978.

24. Timoshenko, S. and Woinowsky-Kreiger, S., "Theory of Plates and Shells," Second Edition, 1959, McGraw-Hill Book Company, pg. 210-211.

TABLE 1. FEATURES OF THREE DEGREE OF FREEDOM IMPACT ANALYSIS
(COMPUTER TIME: 5 SECONDS)

Missile Model

- Improved single and multiple parallel jets

Blade Model

- No camber but approximate twist effect
- Centrifugal stiffening included
- Coefficient of restitution & damping included
- Lumped mass and rotational inertia at impact station
- Response in first and second bending and first torsional modes
- Bending and torsional stiffnesses based on blade properties
- Mass and rotational inertia defined by first bending and torsional frequencies and corresponding stiffnesses
- Second bending mode assumed normal to first bending mode and at much higher frequency
- Retention stiffness and orientation can be varied

Impact Model

- Interactive impact force and time based on first bending and first torsional modes
- Second bending mode impact force and time based on above
- Higher bending mode responses obtained from minimum energy perturbation analysis

TABLE 2. FEATURES OF MULTI-MODE IMPACT ANALYSIS
(COMPUTER TIME: 1-2 MINUTES)

Missile Model

- Improved segmental impact
- Bird crushing and spreading included

Blade Model

- Camber and twist effects included
- Damping included
- Centrifugal stiffening included
- Blade responds in its normal beam modes
- Response of each mode based on energy relationship
- Retention stiffness and orientation can be varied

Impact Model

- Bird and blade at impact station divided into elements
- Impact and blade response calculated for each bird element for each of a series of short time periods
- Impact force is approximately interactive for each short time period

TABLE 3. IMPACT OF Q-FAN SPAR-PLATE SPECIMEN

1.0 LB, 3.75" SPHERICAL MISSILE AT 605 FPS
IMPACT AT 30" STA. @ 30°

PARAMETER	STATION IN.	TEST	THREE DEGREE*	MULTI MODE+
DEFLECTION, X, IN.	30	0.86	0.86	0.64
TWIST, θ, DEG	(IMPACT POINT)	0.80	7.9	8.2
BENDING STRESS, PSI	14.9	28,600	21,000	31,000
TORSIONAL STRESS, PSI		4,100	3,700	3,800
BENDING STRESS, PSI	16.9	103,000	118,000	101,100
TORSIONAL STRESS, PSI		18,700	24,800	25,100

* $\epsilon = 0.17$

+FIVE FIRST COUPLED MODES

TABLE 4. CANTILEVERED AND SIMPLY-SUPPORTED BALLISTIC IMPACT SPECIMEN RESULTS

FROM UTRC REPORT R75-911866-5; SEPTEMBER 30, 1975;
RTV CYLINDRICAL MISSILE: 0.36GM; 0.295" D X 0.295" L

Type	Specimen	Material	E 10^6psi	UTS - 10^3 psi Tension	UTS - 10^3 psi Bend	E_f %	Impact Energy ft lbs	Thick t Mils	Impact Velocity (ft/sec) And Impact Damage* V_1	D_1	V_2	D_2	V_3	D_3	V_4	D_4	V_5	D_5	V_6	D_6	V_7	D_7
Cantilever Specimens	2419/20	5.6B/6061 $[\pm 45/0_3]_2$	29	170	170	0.88	1.1	70	126	NV	187	NV	383	NV	715	D	1437	F-I-R				
	2427/28	5.6B/6061 $[\pm 45/0_3]_2$	29	170	180	0.88	0.9	67	158	NV	202	NV	339	NV	390*	D	607	D	718	D		
	2479	5.6B/6061 $[\pm 22]_5$	30	148	226	1.35	1.5	69	188	NV	438	NV	702(A)	D-DI	713(A)	D-DI	938(A)	D-FR	1076(A)	D-FR	1233	FI-FR
	2422/24	5.6B/1100 $[\pm 45/0_3]_2$	–	152	143	–	1.3	67	129	NV	186	NV	282*	NV	381*	D	627	D	1132	F-I		
	2480	5.6B/1100 $[\pm 22]_5$	–	71	159	–	3.0	66	196(A)	NV	440(A)	D	950(A)	D-DI	1116(A)	CR-DI	1297	CR-FI	1324	FR-FI	1362	FR-FI
	2473/74	5.6B/1100(0) 0.003" T_I-6-4 Face	–	–	296	–	1.2	53	532*	D-DI	813	DI-FR	844	DI-FR								
	2475/76	5.6B/1100 (0) 0.009" T_I-6-4 Face	–	–	225	–	1.4	66	705*	D-DI	799	D-DI	845	D-DI	990	D-DI	1050	D-DI	1270	DI-FR		
	SN-129-1	5.7B$_S$/T_I-6-4 (0) 0.003" T_I-3-2½ Face	38	146	315	0.40	1.1	52	697	D	705	D	786	D-FI	816	D-FI	855	D-FI				
	SN-141-4/5	5.7B$_S$/T_I-6-4 (0) 0.012" T_I-3-2½ Face	34	130	266	–	2.4	63	902*	D	1011*	D-DI	1218	D-DI	1424	D-DI	1510	D-DI-FR				
	SN-129-2	5.7B$_S$/T_I-6-4 (0) 0.003" T_I-3-2½ Face	39	148	315	0.40	–	52	133	NV	173(A)	NV	337 336(A)	NV-I D-M								
	2578	8.0B/1100 $[\pm 22]_4$	–	66	147	–	1.9	75	446(A)	D	553(A)	D-DI	856	D-DI	1096	D-DI	1116	D-DI-CR	1359	FR-FI		
	2579	8.0B/1100 $[\pm 45/0_2]_2$	–	–	98	–	1.4	75	718	D-DI	791	D-DI	856	D-DI	880	D-DI	1136	FR-FI	1179	FR-FI		
	2580	8.0B/1100 3-0.005" T_I-6-4 Face	–	–	217	–	2.7	85	880	D-DI	1025	D-DI	1488	D-DI	1562	D-DI	1645	D-DI	1838	D-DI		
Simply Supported Specimens	2419/20	5.6B/6061 $[\pm 45/0_3]_2$	29	170	170	0.88	1.1	70	199	D	442	D	872	D	1043	D						
	2427/28	5.6B/6061 $[\pm 45/0_3]_2$	29	170	180	0.88	0.9	67	190*	D	439	D	897	D	1392	F-I						
	2479	5.6B/6061 $[\pm 22]_5$	30	148	226	1.35	1.5	69	846(A)	D	933(A)	D	1155(A)	D	1160	FI	1245	F-I				
	2422/24	5.6B/1100 $[\pm 45/0_3]_2$	–	152	143	–	1.3	67	199*	D	447	D	907	D	1283	FI						
	2480	5.6B/1100 $[\pm 22]_5$	–	71	159	–	3.0	66	352(A)	D	761(A)	D	941	FI	1193	FI						
	2473/74	5.6B/1100 (0) 0.003" T_I-6-4 Face	–	–	296	-	1.2	53	549	DI	872	FI	952	FI	1157	FI	1197	FI				
	2475/76	5.6B/1100 (0) 0.009" T_I-6-4 Face	–	–	225	–	1.4	66	967*	DI	1049	DI	1291	FI								
	SN-129-4/5	5.7B$_S$/T_I-6-4 (0) 0.003" T_I-3-2½ Face	39	148	–	0.40	–	52	801	D	803	D	853	D	970	D						
	SN-141-2/4	5.7B$_S$/T_I-6-4 (0) 0.012" T_I-3-2½ Face	34	130	266	–	2.4	63	1020*	D	1089	D	1124	D	1389	D						
	SN-129-2	5.7B$_S$/T_I-6-4 (0) 0.003" T_I-3-2½ Face	39	148	315	0.40	–	52	190(A)	NV	439(A)	D	903	D	1330	D						

(A) – Analyzed
\+ – Damage Code
NV – No Visible Damage
D – Deformation
F – Fracture
I – Impact Site
R – Root
C – Visible Cracking
□ Strain Gaged
M – Multiple Impact

TABLE 5. CANTILEVERED BALLISTIC IMPACT SPECIMEN RESULTS (HOPKINS & CHAMIS)

RTV CYLINDRICAL MISSILE: 0.295"D X 0.295"L $\frac{372\ MG}{351\ MG}$

Specimen	Case	Material	Thickness, t; Impact Velocity, V; Impact Damage, D +								
			Impact 1			Impact 2			Impact 3		
			t-mils	V-fps	D	t-mils	V-fps	D	t-mils	V-fps	D
C. Chamis 3.0" x 0.75" Cantilever, Impact 2.4" ~351 mg Missile	7517/18/19	G/E [0]	65	298*	NV	56	495*	S-FR	58	720*	B
	7522/21/20	B/AL [0] Diff.	61	309*	NV	61	489	DIm	61	711	D-CI
	7523/24/25	B/AL [0] Bonded	56	299	NV	55	496*	DIm	56	718*	D
	7526/27/28	B/AL [0] Adhes.	58	305*	DIm	62	496*	D-CI	62	718	D-Twist
	7531/30/29	B/AL [0] Bonded	60	305	NV	62	483	DIm	62	721	DIC-FR
	7532/33/34	T_I/B-AL Adhes.	65	310*	NV	67	495*	DIm	66	721*	DI
	7535/36/37	T_I/B-AL Bonded	62	306	NV	60	490	DIm	59	709	DI
A. Hopkins 4.0" x 0.40" Cantilever Impact 3.2" ~372 mg Missile	7547/48/58	T_I-6AL-4V	41	284⊛	NV	41	525*	YR&I	41	899	YR&I
	7556/57	T_I-6AL-4V	–	–	–	42	527⊛	YR&I	40	906	YR&I
	7553/54/55	6061-T6 Al	31	79*	NV	31	160*	YR	31	306	YR&I
	7552/51/–	6061-T6 Al	63	125⊛	NV	63	187⊛	YRm	–	–	–
	–7549/50	6061-T6 Al	–	–	–	63	282*	YR	63	527⊛	YR&I

+

NV – No Visual Damage
S – Shear Delamination
B – Breakup
D – Dent & Bulge
F – Fracture
R – Root
m – Minor Or Slight
Y – Yielding Or Bending
C – Cracking
I – Impact Region
⊛ Analyzed

TABLE 6. STRAIN-GAGED SPECIMEN IMPACT TEST RESULTS

0.069" THICK, 5.6B/1100 AL $(\pm 22°)_5$ SPECIMENS
36 GM, 0.295" DX 0.295" L, RTV MISSILE

SPECIMEN		IMPACT VELOCITY FPS	ROOT OR SUPPORT GAGE				IMPACT SITE GAGE			
			DAMAGE+	STRESS – KSI			DAMAGE+	STRESS – KSI		
				3D	MM	TEST		3D	MM	TEST
CANTILEVER	7609	713	YIELDING	208	176	344	YIELDING	166	164	290
	7608	936	FRACTURE	239	293	699	YIELDING	178	262	240
	7610	1076	FRACTURE	270	317	N.A.	YIELDING	232	305	242
SIMPLY SUPPORT	7611	933	–	-43* -100**	– -196**	– -120++	YIELDING	225* 270**	– 295**	– ~400
	7612	1155	–	-52*	-212**	-140++	YIELDING	280*	327**	~500

*NO OVERHANG
**WITH OVERHANG

+ YIELD <148 KSI, ULT. BEND ≈226 KSI
++ SHARP, POSITIVE INITIAL STRESS ~ 170 KSI

TABLE 7. ANALYZED CANTILEVERED AND SIMPLY-SUPPORTED BALLISTIC IMPACT SPECIMEN RESULTS

FROM UTRC REPORT R75-911866-5 SEPT. 30, 1975; HOPKINS & CHAMIS
RTV CYL. MISSILE 0.36GM , 0.295" DIA. X 0.295L

ROW	SPECIMEN NUMBER			MATERIAL	UBS KSI	YTS KSI	THICKNESS MILS	IMPACT VELOCITY FPS	ROOT OR SUPPORT			IMPACT SITE		
									DAMAGE	STRESS – KSI		DAMAGE	STRESS – KSI	
	NO.	TYPE	SHOT							3D	MM		3D	MM
1	2479	CANT.	7607	5.6B/6061 $[\pm 22]_5$	226	~148	69	702	Y	-187	–	Y	142	–
2			7609		226	~148	69	713	Y	235	–	Y	166	–
3			7608		226	~148	72	936	F	-239	–	Y	147	–
4			7610		226	~148	71	1076	F	270	–	Y	232	–
5		S.S.	7615		226	~148	69	846	N	–	–	Y	194	–
6			7611		226	~148	71	933	N	–	–	Y	225	–
7			7612		226	~148	72	1155	N	–	–	Y	280	–
8	2480	CANT.	7599	5.6B/1100 $[\pm 22]_5$	159	~ 71	67	196	N	54.5	–	N	28	–
9			7600		159	~ 71	67	440	Y	122	134	N	66.6	94
10			7616		159	~ 71	65	950	Y	264	–	Y	157	–
11			7618		159	~ 71	67	1116	F	310	–	Y	178	–
12		S.S.	7621		159	~ 71	66	352	N	–	–	Y	94	123
13			7620		159	~ 71	66	761	N	–	–	Y	193	–
14	SN-129	CANT.	–	5.7B/Ti-6AL 4V [0]	315	~148	52	173	N	46.5	–	N	33.5	–
15			–		315	~148	52	1/M 336	N/Y	88	111	N/N	75.2	62
16		S.S.	–		315	~148	52	190	N	–	–	Y	(71.1)	–
17			–		315	~148	52	439	N	–	–	Y	162	156
18	HOPKINS	CANT.	7547	Ti-6AL 4V	132	120	41	284	N	71.3	–	N	44.2	–
19			7556		132	120	41	527	Y	146	138	Y	(78.3)	138
20	2578	CANT.	7823	8.0B/1100 $[\pm 22]_4$	147	~ 66	75	446	Y	93	–	N	60.4	–
21			7822		147	~ 66	75	553	Y	116	–	Y	92	–
22	HOPKINS	CANT.	7552	6061 - T_6	42	35	63	125	N	38	–	N	16	–
23			7551		42	35	63	187	Y	51	37	N	20	21
24			7550		42	35	63	527	Y	132	–	Y	56	–

N – NO VISIBLE DAMAGE
Y – YIELD
F – FRACTURE
M – MULTIPLE IMPACTS
1 – SINGLE IMPACT
( ) – INCONSISTENT WITH DAMAGE

TABLE 8. NASA-LEWIS 3A DEMO F.O.D. BLADE TESTS
COMPARISON OF EXPERIMENTAL AND THREE DEGREE IMPACT ANALYSIS RESULTS

CYLINDRICAL MISSILES; IMPACT AT 830 FPS AT 32° AND 30.8' STA.

Parameter			Test Number					
			4	5		10	11	
				Major Impact	Chip Impact		Major Impact	Chip Impact
MISSLE	Material		Gelatin	Gelatin	Gelatin	Bird	Gelatin	Gelatin
	Weight-lbs		0.97	1.68	0.12	1.74	1.43	0.17
	Diameter-in		3.41	4.29	4.29	4.29	4.29	4.29
Retention Type			Rocking	Rocking	Rocking	Rocking	Fixed	Fixed
Shank 14.7" Sta.	Bending Stress–KSI	3D	104 (92)	166	16	181	179	22
		Test	76	83	34	91	102	33
	Shear Stress–KSI	3D	17	27	7	29	21	7
		Test	15	19	12	19	12	9
22" Sta.	Shear Stress–KSI	3D	40	48	12	53	38	12
		Test	54	67	40	67	42	33
26" Sta.	Bending Stress–KSI	3D	-126 (-132)	–227	–17	–249	–382	–24
		Test	–173	–223	–38	–173	–230	–31
30.8"Sta. Impact	Bending Stress–KSI	3D	132 (200)	231	24	255	239	33
		Test	182	201	69	231	154	48

(-) Includes Chordwise Flexibility

TABLE 9. NASA-LEWIS 3A DEMO F.O.D. BLADE TESTS
COMPARISON OF EXPERIMENTAL AND MULTI-MODE IMPACT ANALYSIS RESULTS

CYLINDRICAL MISSILES; IMPACT AT 830 FPS AT 32° AND 30.8" STA.

Parameter			Test Number					
			4	5		10	11	
				Major Impact	Chip Impact		Major Impact	Chip Impact
Missiles	Material		Gelatin	Gelatin	Gelatin	Bird	Gelatin	Gelatin
	Weight-lbs		0.97	1.68	0.12	1.74	1.43	0.17
	Diameter-in		3.41	4.29	4.29	4.29	4.29	4.29
Retention Type			Rocking	Rocking	Rocking	Rocking	Fixed	Fixed
Shank 14.7" Sta.	Bending Stress–KSI	MM	115	187	17	197	171	18
		Test	76	83	34	91	102	33
	Shear Stress–KSI	MM	30	41	8	45	42	11
		Test	15	19	12	19	12	9
22" Sta.	Shear Stress–KSI	MM	45	68	11	75	70	15
		Test	54	67	40	67	42	33
26" Sta.	Bending Stress–KSI	MM	--119	–194	–21	–220	–194	–29
		Test	–173	–223	–38	–173	–230	–31
30.8" Sta. Impact	Bending Stress–KSI	MM	113	150	23	164	141	31
		Test	182	201	69	231	154	48

TABLE 10. VARIATION OF IMPACT STRESS, ROOT STRESS, SHEAR STRESS, AND STRAIN RATE WITH SPECIMEN THICKNESS

(VELOCITY = 830 FPS, IMPACT SITE Z = 0.85)
TAPER = 1.0, MISSILE = 1"

THICKNESS	IMPACT STRESS KSI	ROOT STRESS KSI	SHEAR STRESS KSI	STRAIN RATE IN/IN/SEC
0.125	190	210	13.2	83
0.145	160	190	11.2	70
0.150	150	185	11.0	68
0.200	110	136	8.3	52
0.250	80	111	6.8	41

TABLE 11. EFFECT OF DAMPING AND CENTRIFUGAL LOAD ON BLADE IMPACT RESPONSE

IMPACT OF Q-FAN® TITANIUM SPAR-B/AL SHELL BLADE; 0.97 LB, 3.67" D X 3.67" L CYLINDRICAL MISSILE; IMPACT AT 32 DEG AT 30.8 IN. STATION; 9 DEGREE CAMBER EFFECT OR ϵ = .16; V_o = 830 FPS.

Parameter			Test	Theory		
				μ= 0.12	μ= 0.12	μ = 0.00
Rotation, RPM			3089	3,089	0	3,089
Response Angle, β			--	22.56°	19.45°	22.56°
Max. Normal Force-lbs			--	35,100	34,800	35,300
Impact Time-ms			--	0.92	0.93	0.92
Maximum Deflections	x - in.		--	2.27	2.77	2.72
	y - in.		--	0.520	0.457	0.603
	θ - Rd.		--	0.183	0.186	0.213
Maximum Stresses (Impact Station)	Shank 14.7"	Bend	76	104	119	124
		Shear	15	17	18	20
	22"	Shear	54	40	41	47
	26"	Bend	-173	-126	-214	-137
	30.8"	Bend	182	132	192	133

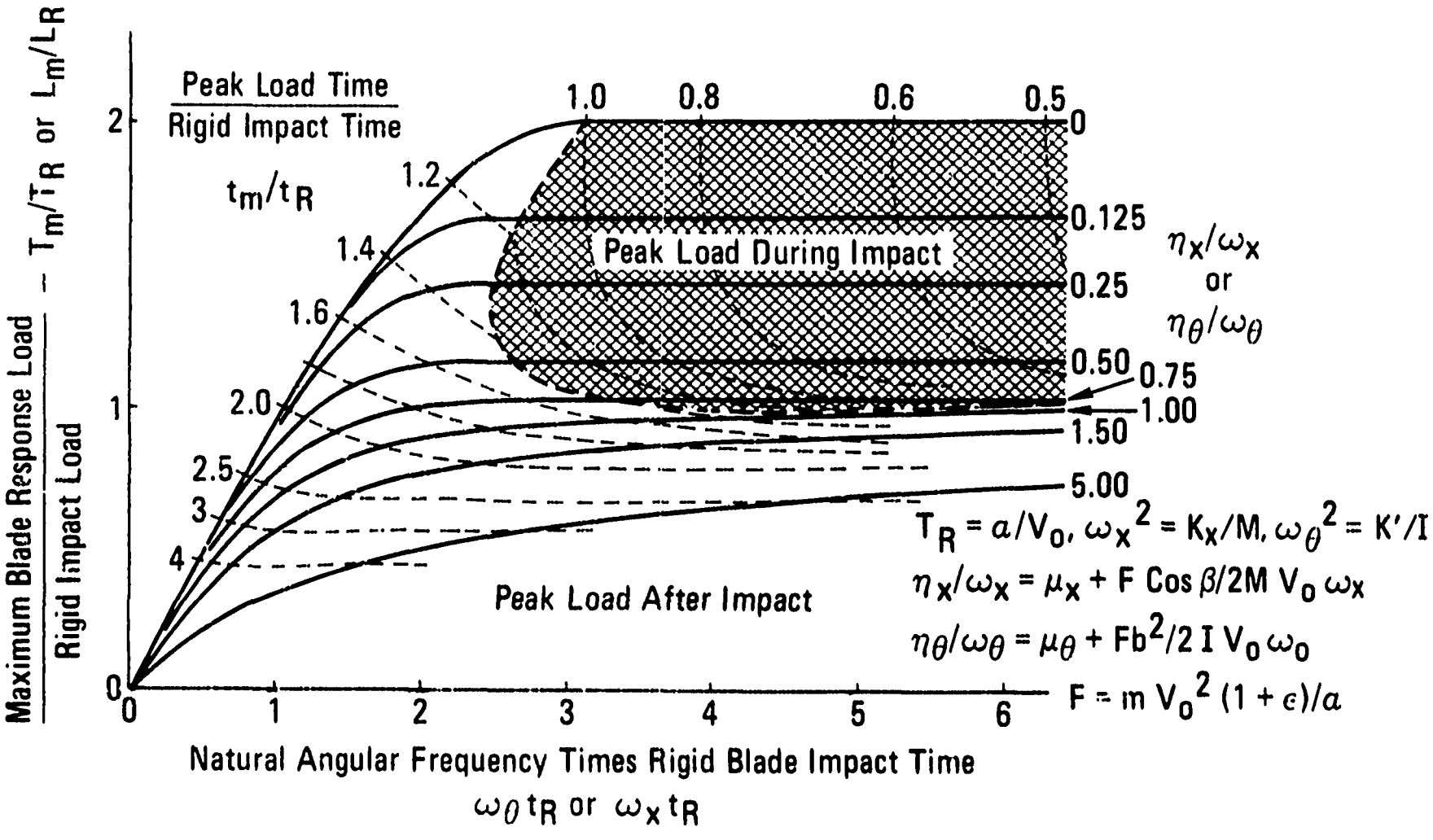

FIGURE 1. PARAMETRIC BLADE IMPACT DIAGRAM
MAXIMUM IMPACT RESPONSE LOAD FOR SINGLE DEGREE SYSTEM

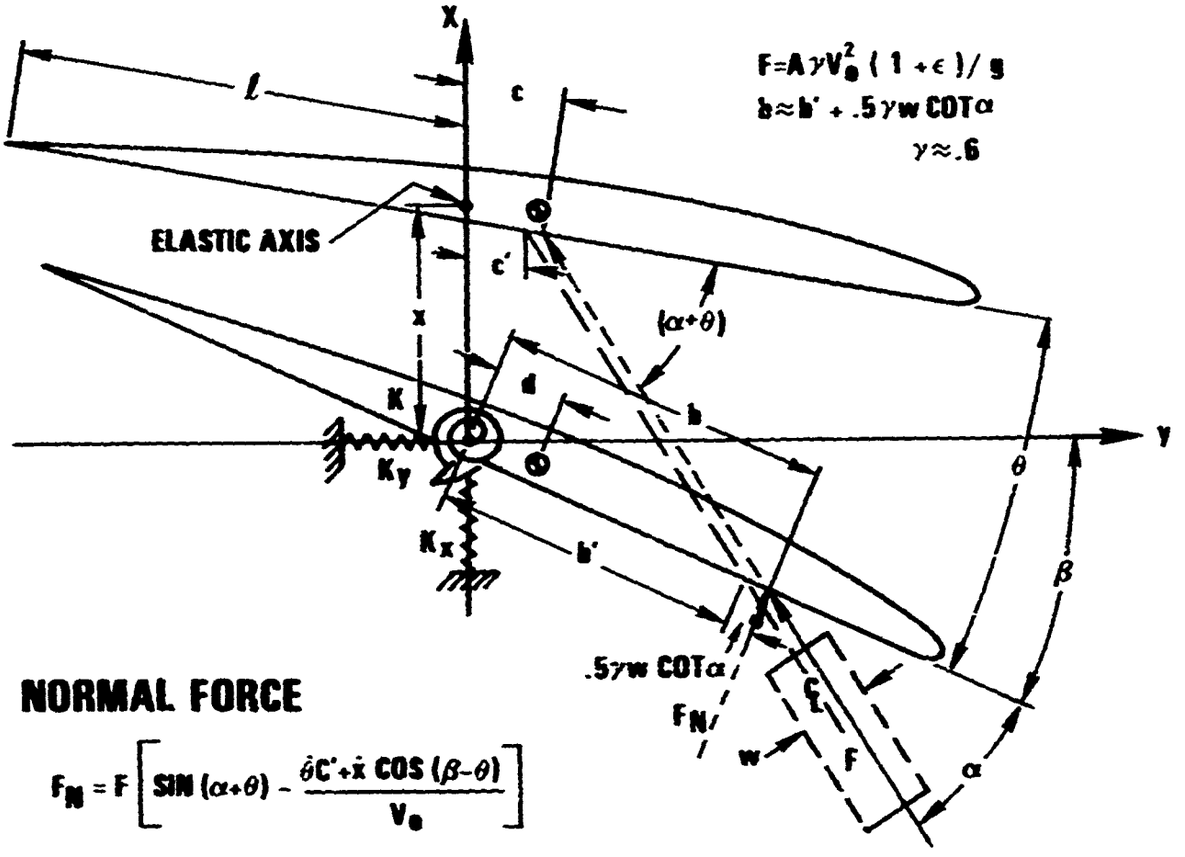

NORMAL FORCE

$$F_N = F\left[\sin(\alpha+\theta) - \frac{\dot{\theta}C' + \dot{x}\cos(\beta-\theta)}{V_e}\right]$$

DIRECTIONAL FORCES

$$F_X = F_N\cos(\beta-\theta) \qquad F_Y = F_N\sin(\beta-\theta) \qquad T = F_N C$$

TORQUE ARMS

$$C \approx \frac{b\sin\alpha - x\cos(\alpha+\beta) - y\sin(\alpha+\beta)}{\sin(\alpha+\theta)} \qquad C' = \frac{b'\sin\alpha - x\cos(\alpha+\beta) - y\sin(\alpha+\beta)}{\sin(\alpha+\theta)}$$

FIGURE 2. NOMENCLATURE AND LOADS FOR THREE DEGREE IMPACT ANALYSIS

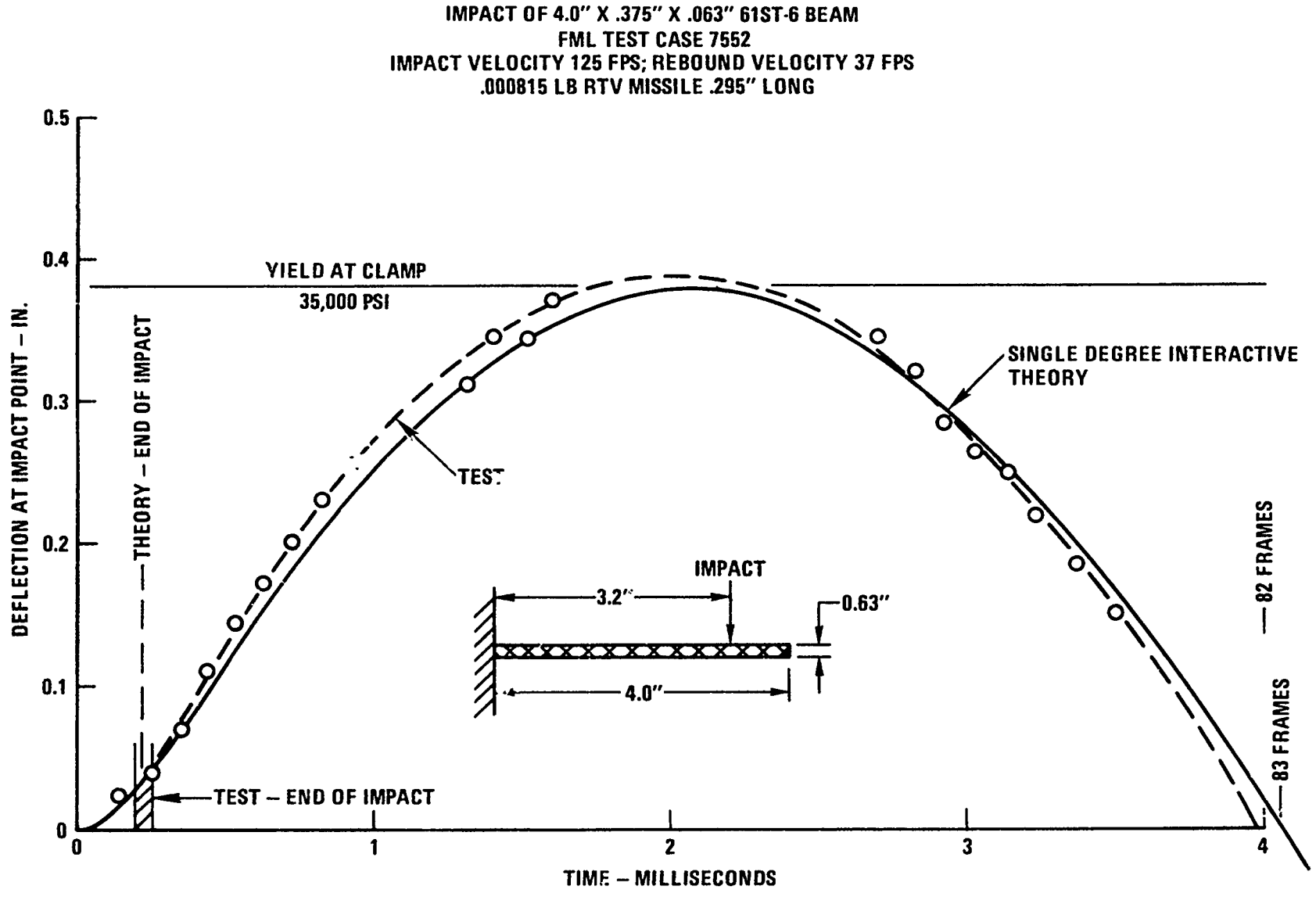

FIGURE 3. COMPARISON OF TEST MODE SHAPE WITH THEORETICAL FOD CANTILEVERED SPECIMEN

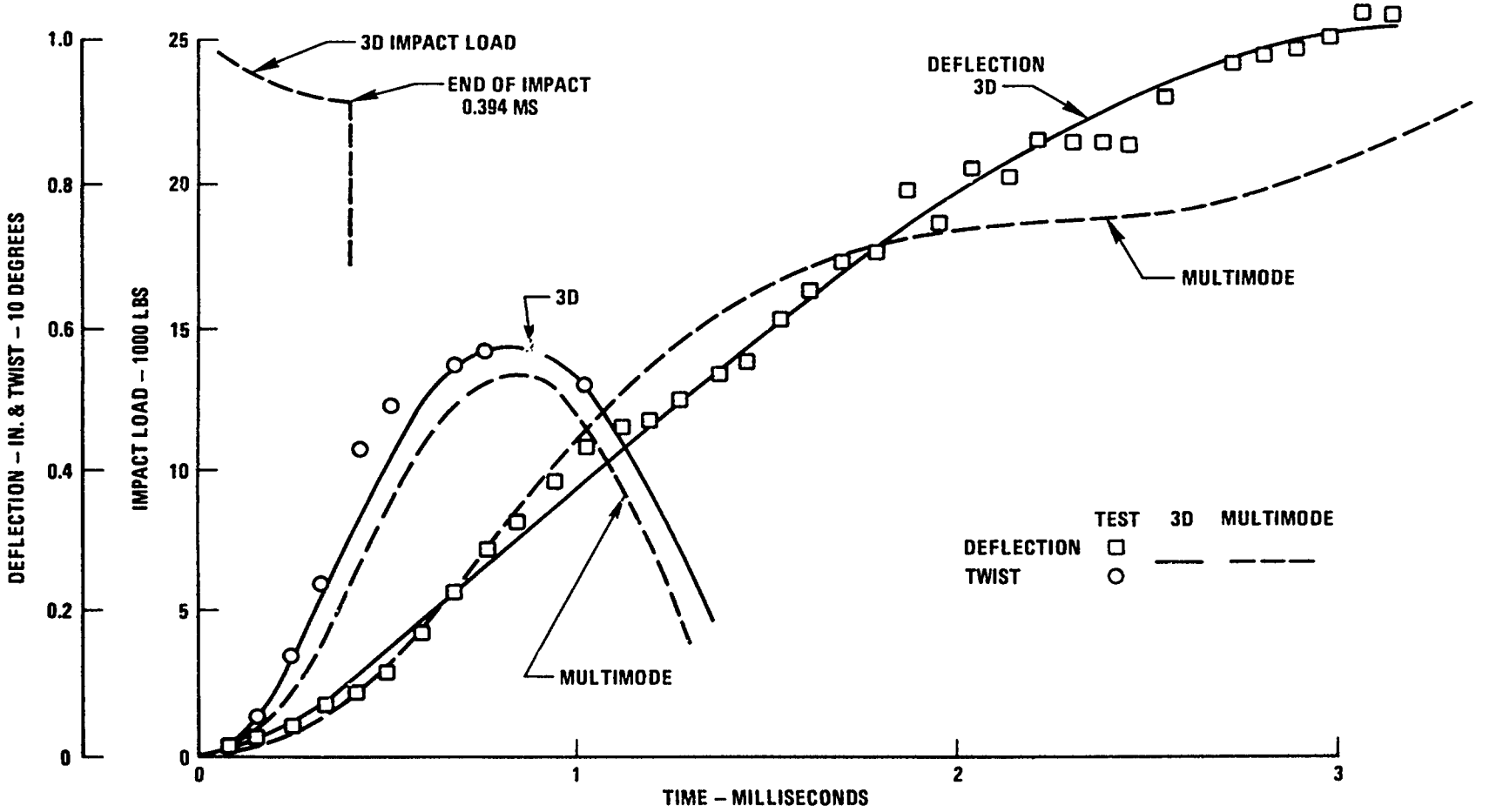

FIGURE 4. NAKED SPAR DEFLECTION AND TWIST FOR THREE-DEGREE AND MULTI-MODE ANALYSES

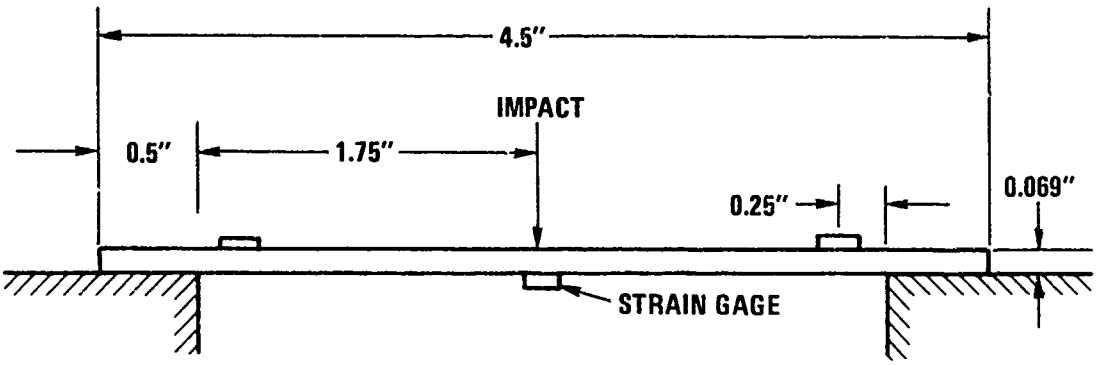

MECHANICAL PROPERTIES USED IN 3D BLADE IMPACT ANALYSIS TO OBTAIN ABOVE SIMPLY SUPPORTED CASE

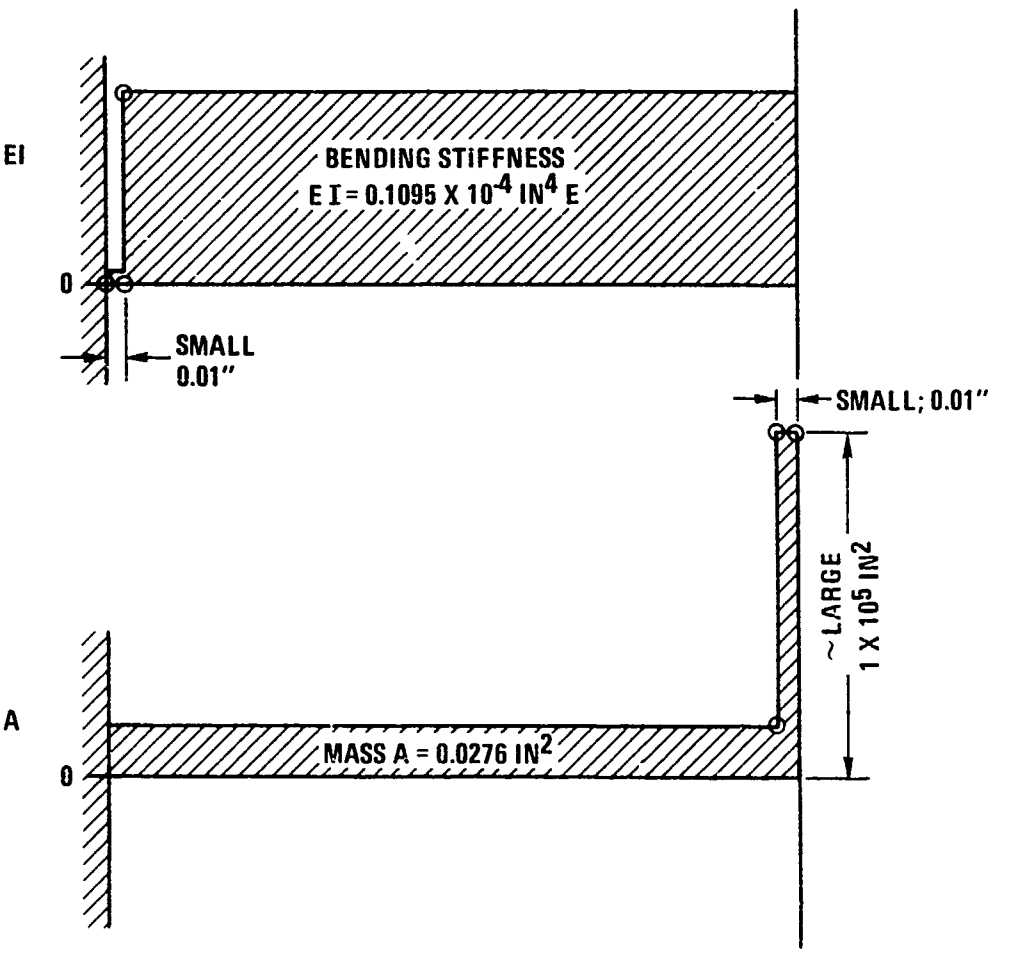

FIGURE 5. THREE-DEGREE IMPACT ANALYSIS OF SIMPLY-SUPPORTED SPECIMEN

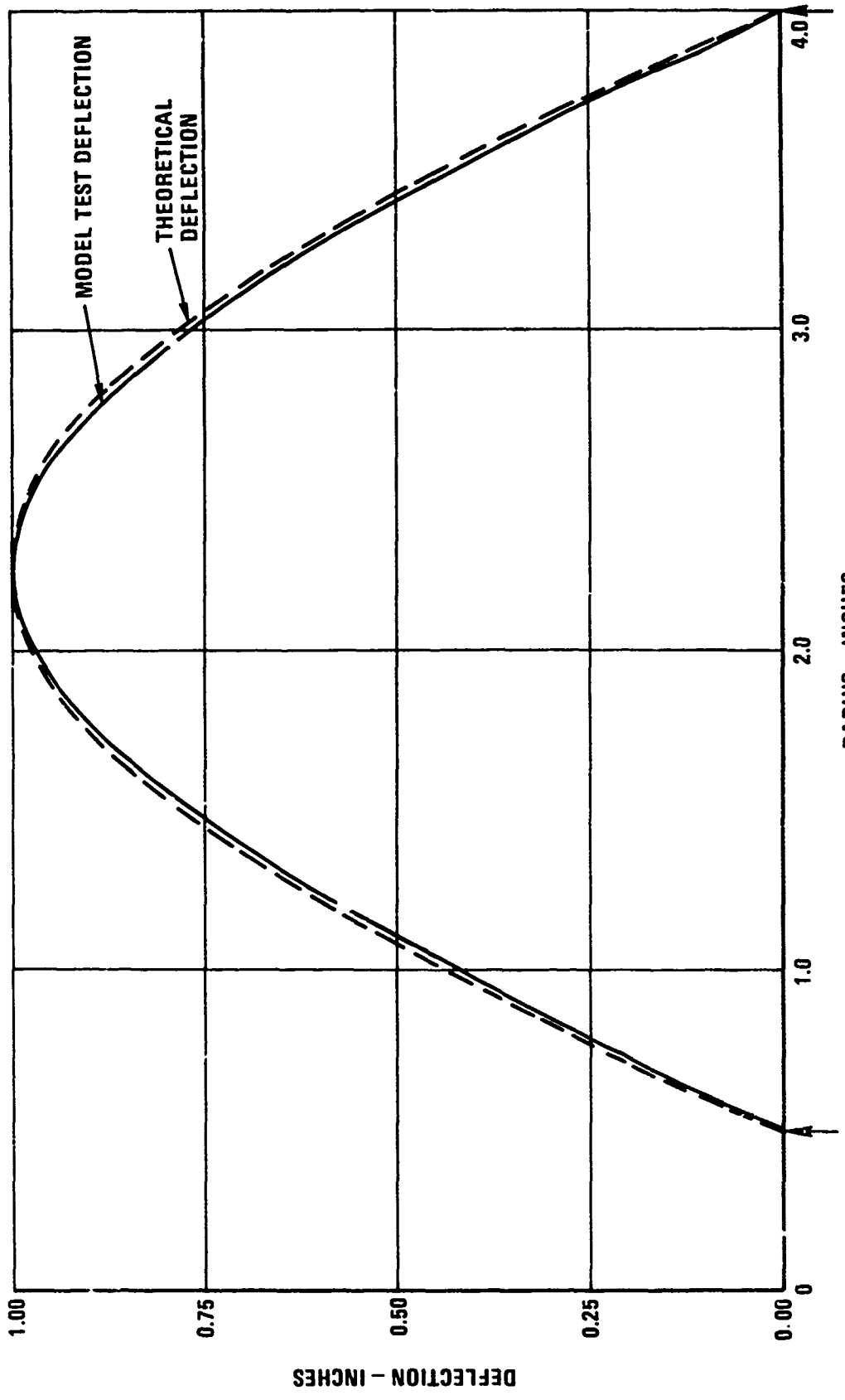

FIGURE 6. COMPARISON OF TEST MODE SHAPE WITH THEORETICAL FOR SIMPLY-SUPPORTED SPECIMEN

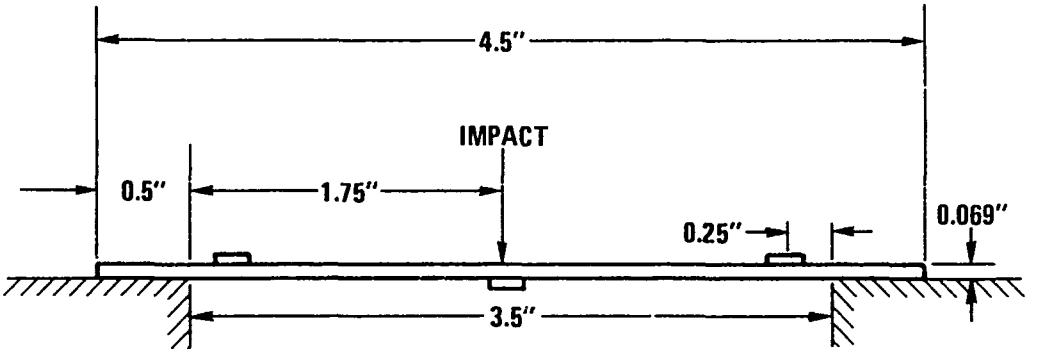

MECHANICAL PROPERTIES USED IN 3D BLADE IMPACT ANALYSIS TO OBTAIN ABOVE SIMPLY SUPPORTED CASE

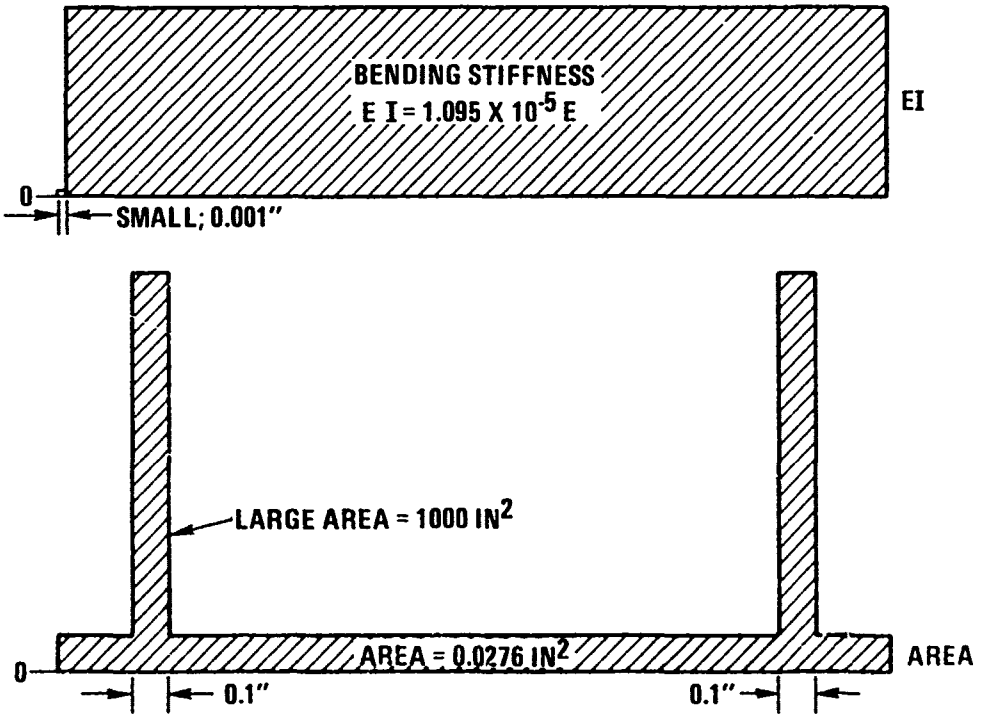

FIGURE 7. THREE-DEGREE IMPACT ANALYSIS FOR SIMPLY-SUPPORTED SPECIMEN WITH OVERHANG

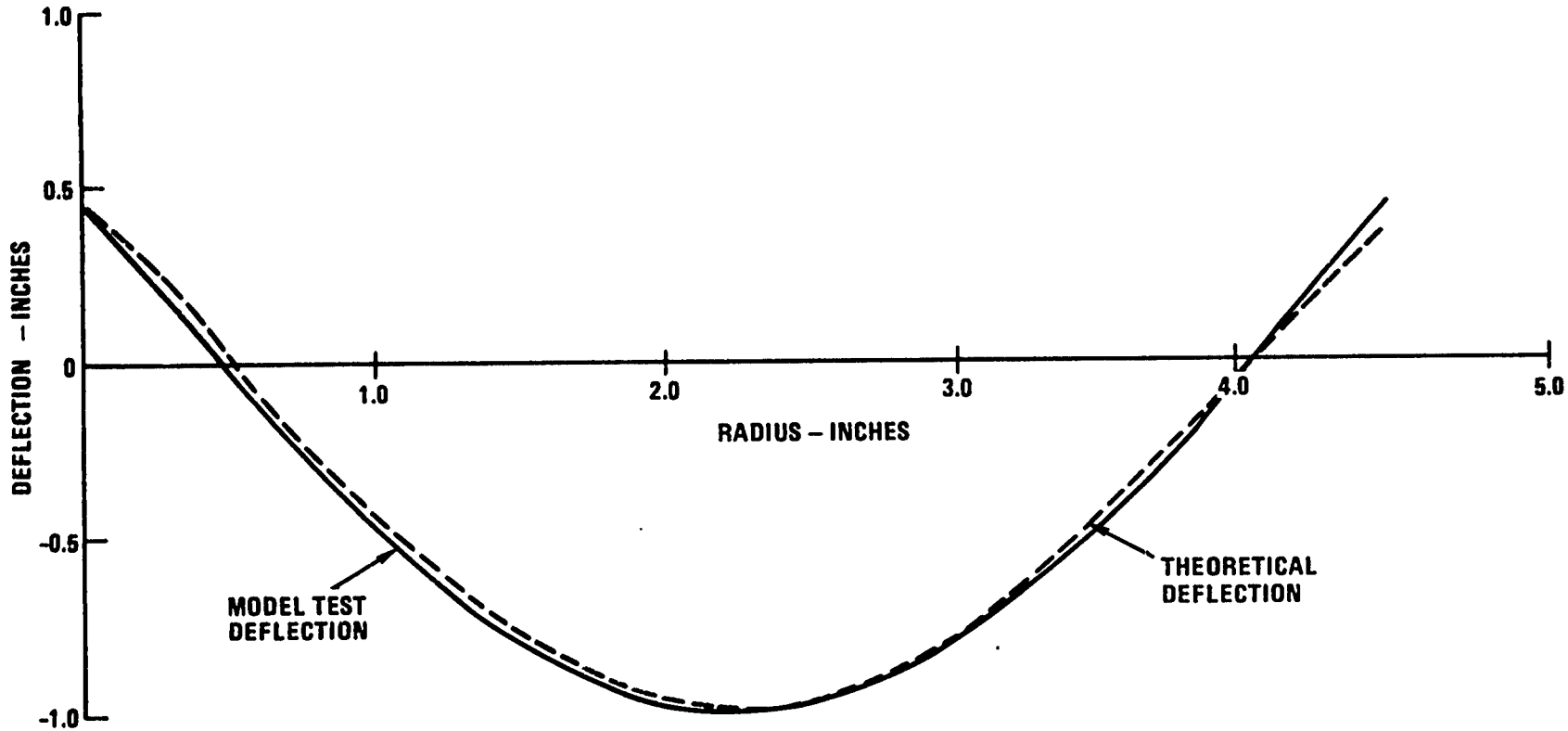

FIGURE 8. COMPARISON OF TEST MODE SHAPE WITH THEORETICAL FOR SIMPLY-SUPPORTED SPECIMEN WITH OVERHANG

DEFINITIONS

- MOTION OF i^{th} NORMAL MODE: $y_i = \Phi_i(x)\, q_i(t)$ WHERE $\Phi_i(x)$ = NORMALIZED MODE SHAPE
- MODAL MASS OF i^{th} MODE: $m_i = \{\phi_i\}^T [Mp] \{\phi_i\}$ $q_i(t)$ = TIP AMPLITUDE OF MODE
- ENERGY (GENERALIZED FORCE) IN i^{th} MODE FROM FORCING FUNCTION $\{P_p\}$: $\{P_i\} = \{\phi_i\}\{P_p\}$

EQUATION OF MOTION OF i^{TH} MODE

- $m_i \ddot{q}_i + c_i \dot{q}_i + k_i q_i = P_i(t)$ WHERE $C_i = B_i m_i$ AND $\omega_i^2 = K_i/m_i$

SOLUTION - SUM OF HOMOGENEOUS SOLUTION AND CONVOLUTION INTEGRAL

- $$q_i = F_i q_{i_0} + G_i \dot{q}_{i_0} + \frac{1}{m_i} \int_{t_0}^{t} G_i(t-\tau) P_i(\tau) d\tau$$

SOLUTION OF CONVOLUTION (DUHAMEL) INTEGRAL

- $q_i^c = A_i P_{i,t_0} + B_i P_{i,t}$ WHERE A_i & B_i FUNCTIONS OF M_i, B_i, ω_i

FIGURE 9. NORMAL MODE ANALYSIS (MULTI MODE ANALYSIS)

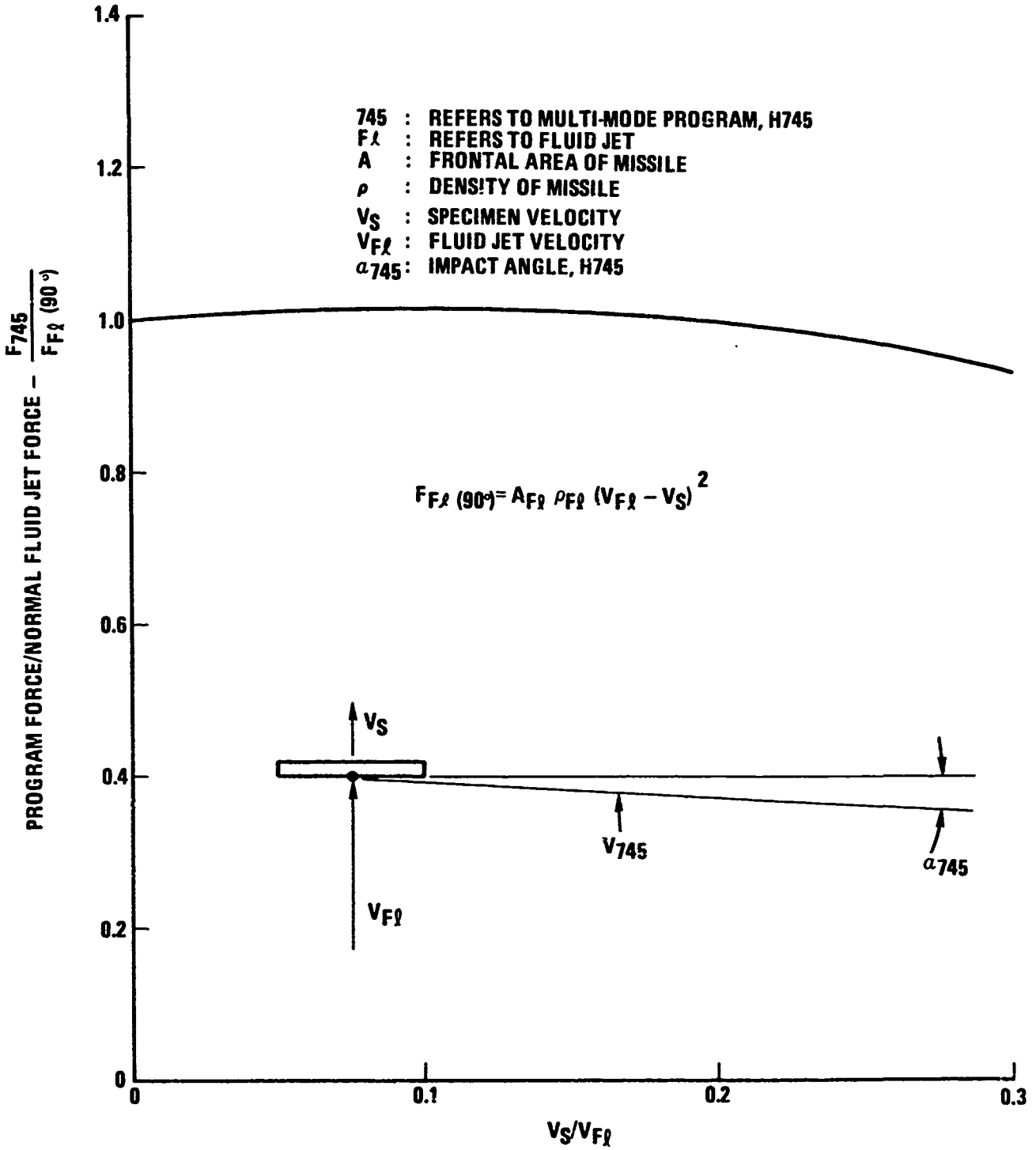

FIGURE 10. 90° IMPACT FORCE APPROXIMATION FOR MULTI-MODE PROGRAM

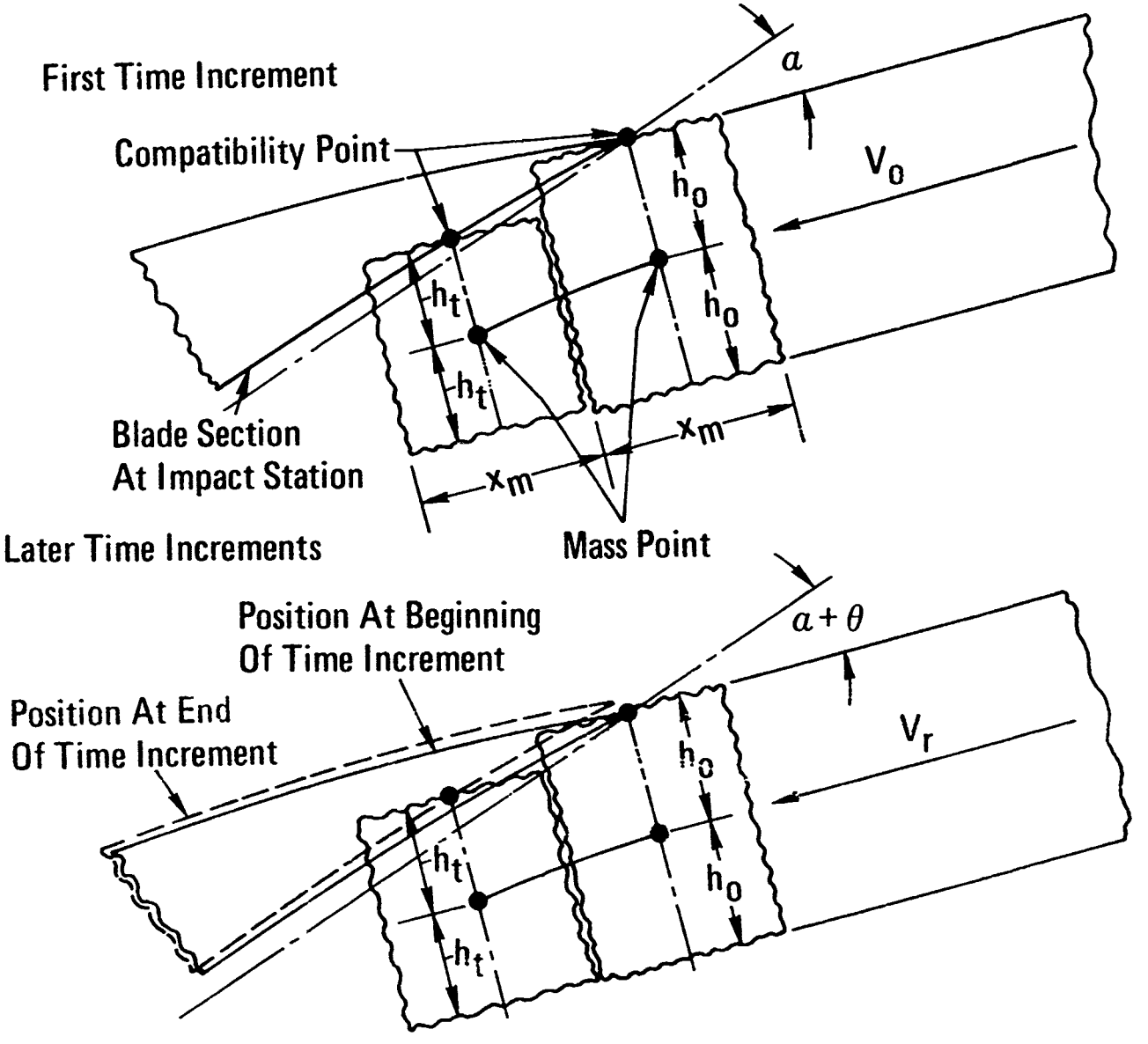

FIGURE 11. BLADE-MISSILE INTERACTION FOR MULTI-MODE IMPACT ANALYSIS

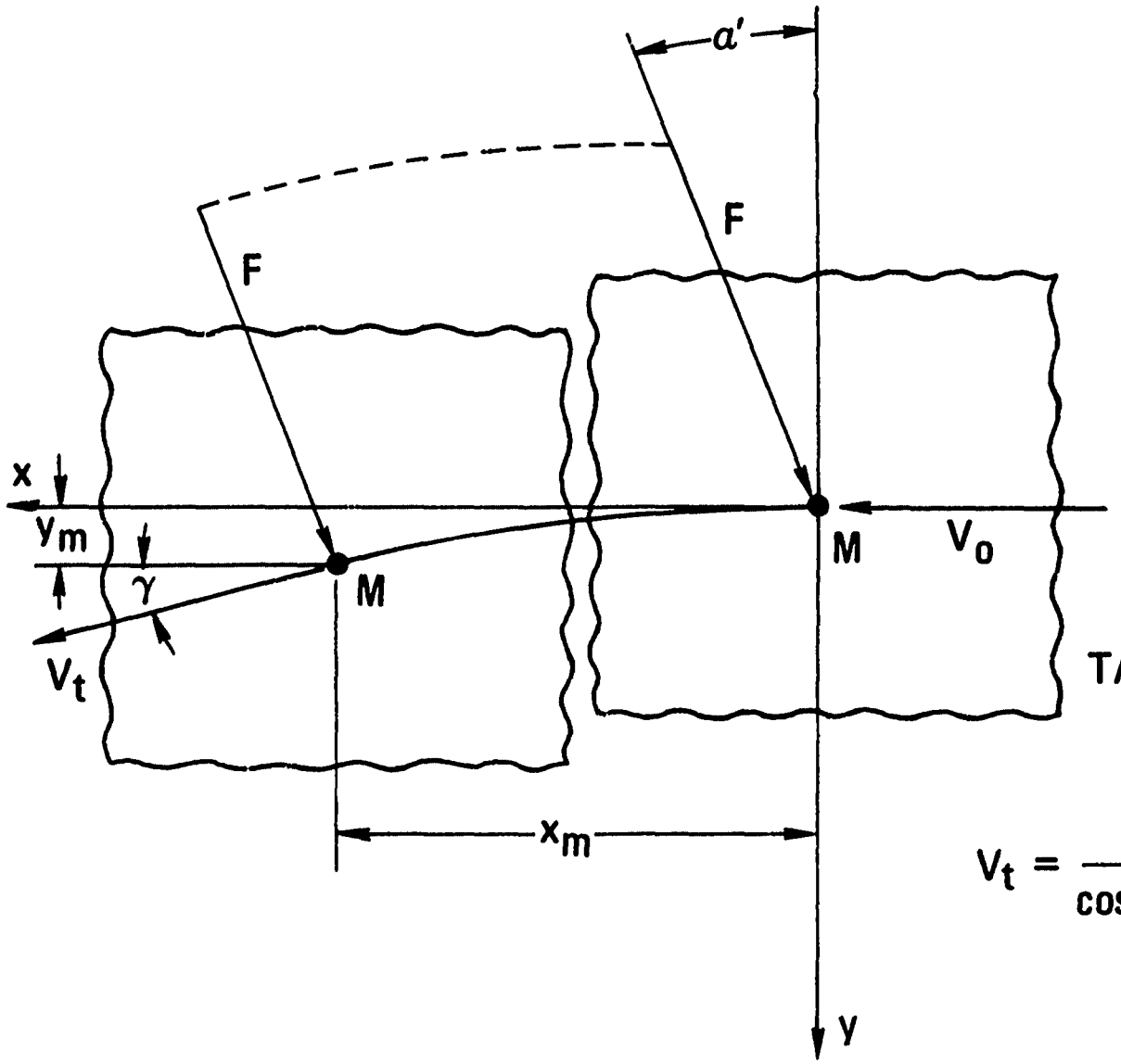

$$x_m = V_0 t - \frac{Ft^2 \sin a'}{2M}$$

$$y_m = \frac{Ft^2 \cos a'}{2M}$$

$$\text{TAN}\gamma = \frac{Ft \cos a'}{V_0 M - Ft \sin a'}$$

$$V_t = \frac{V_0 \cos a'}{\cos\gamma\,(\cos a' + \sin a'\,\text{TAN}\gamma)}$$

FIGURE 12. MISSILE ELEMENT EQUATIONS OF MOTION

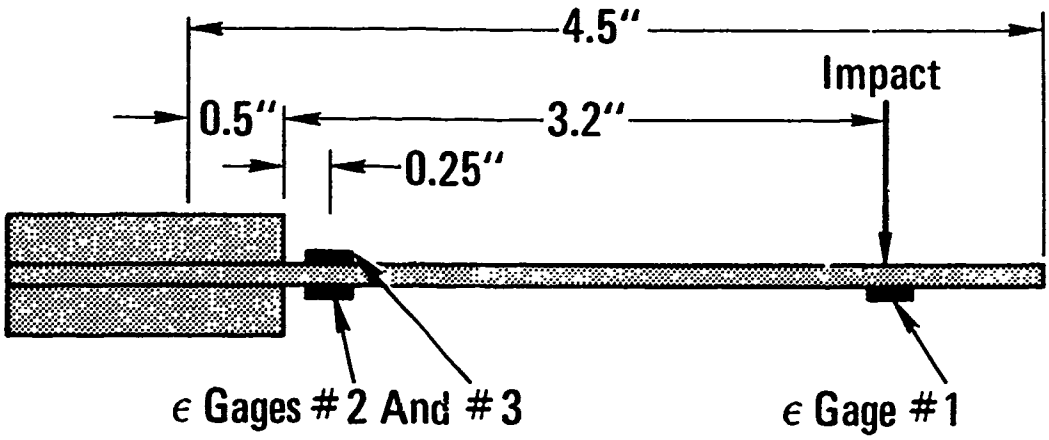

Catilevered Specimens

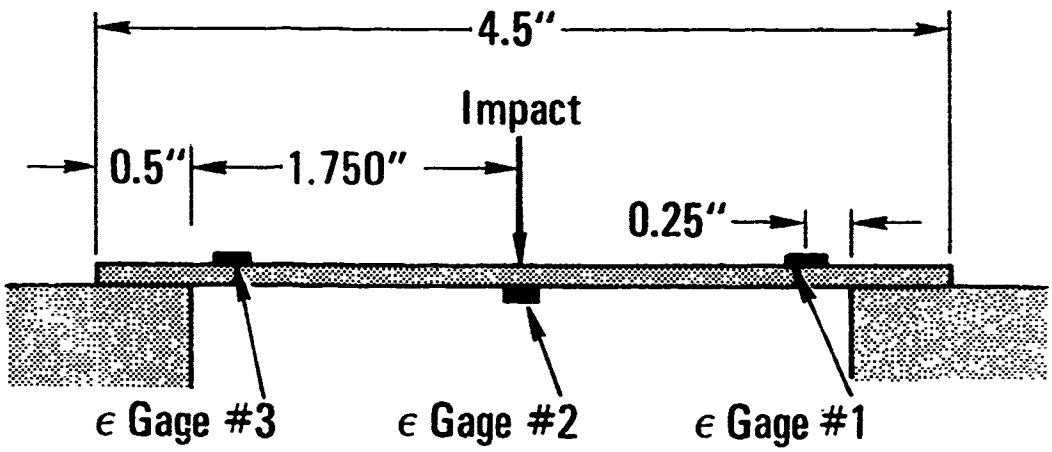

Simply Supported Specimens

FIGURE 13. BALLISTIC IMPACT SPECIMEN CONFIGURATIONS

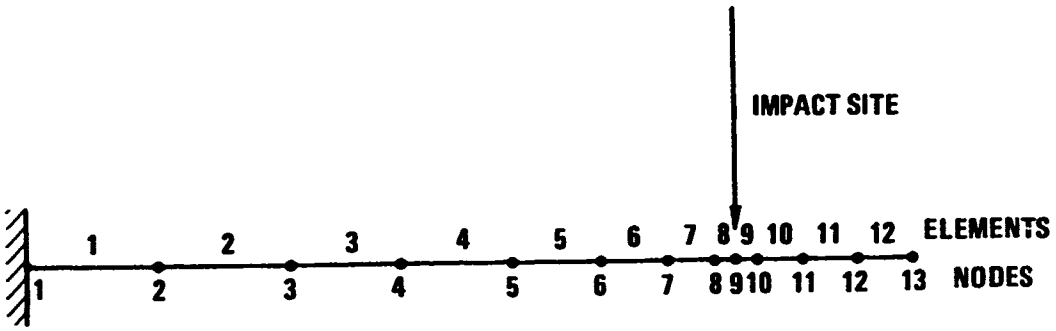

CANTILEVER SPECIMEN

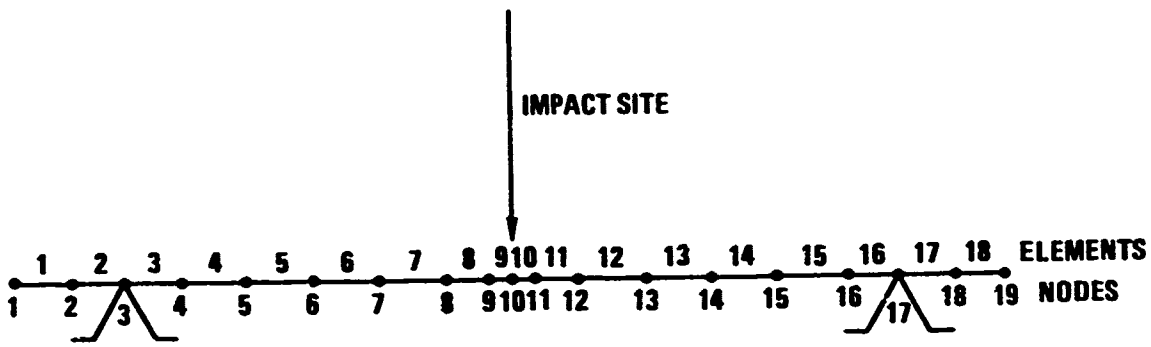

SIMPLY SUPPORTED SPECIMEN

FIGURE 14. FINITE ELEMENT SPECIMEN MODELS

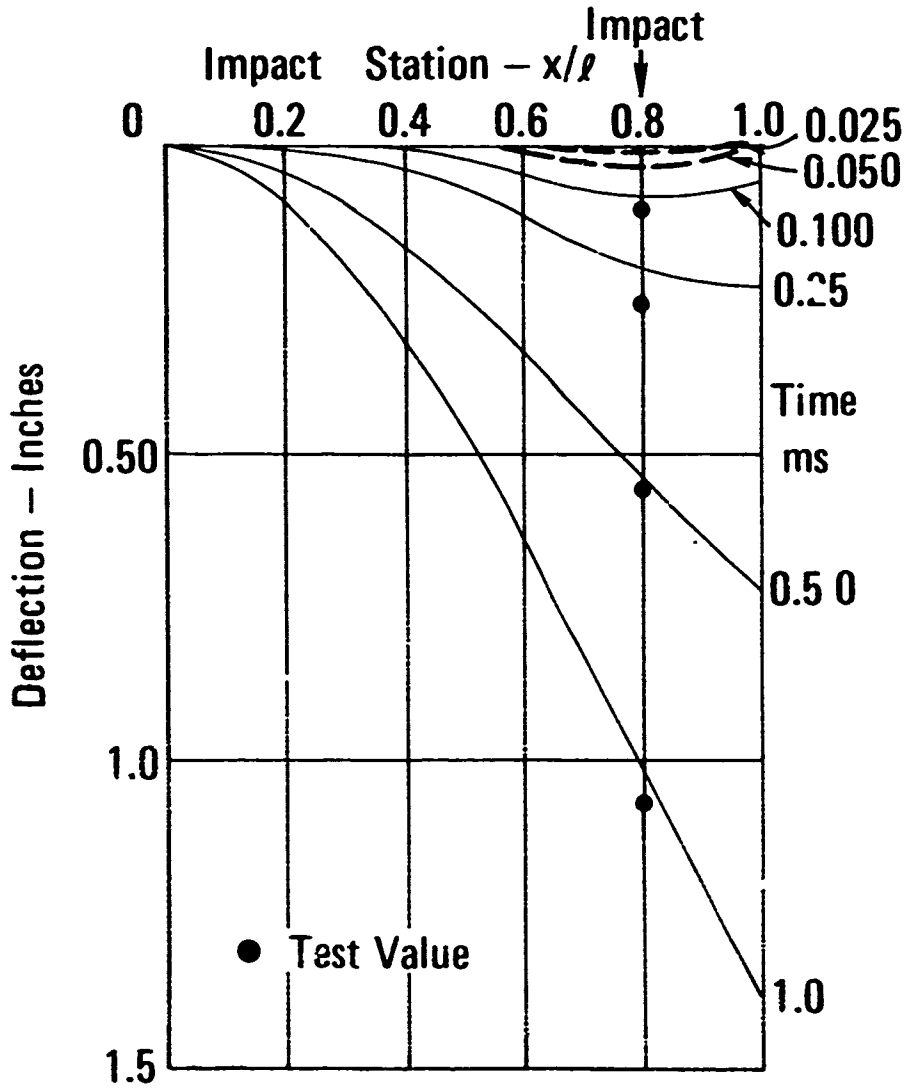

FIGURE 15. DEFLECTION DISTRIBUTIONS FOR IMPACT OF CANTILEVER SPECIMEN – CASE 7550

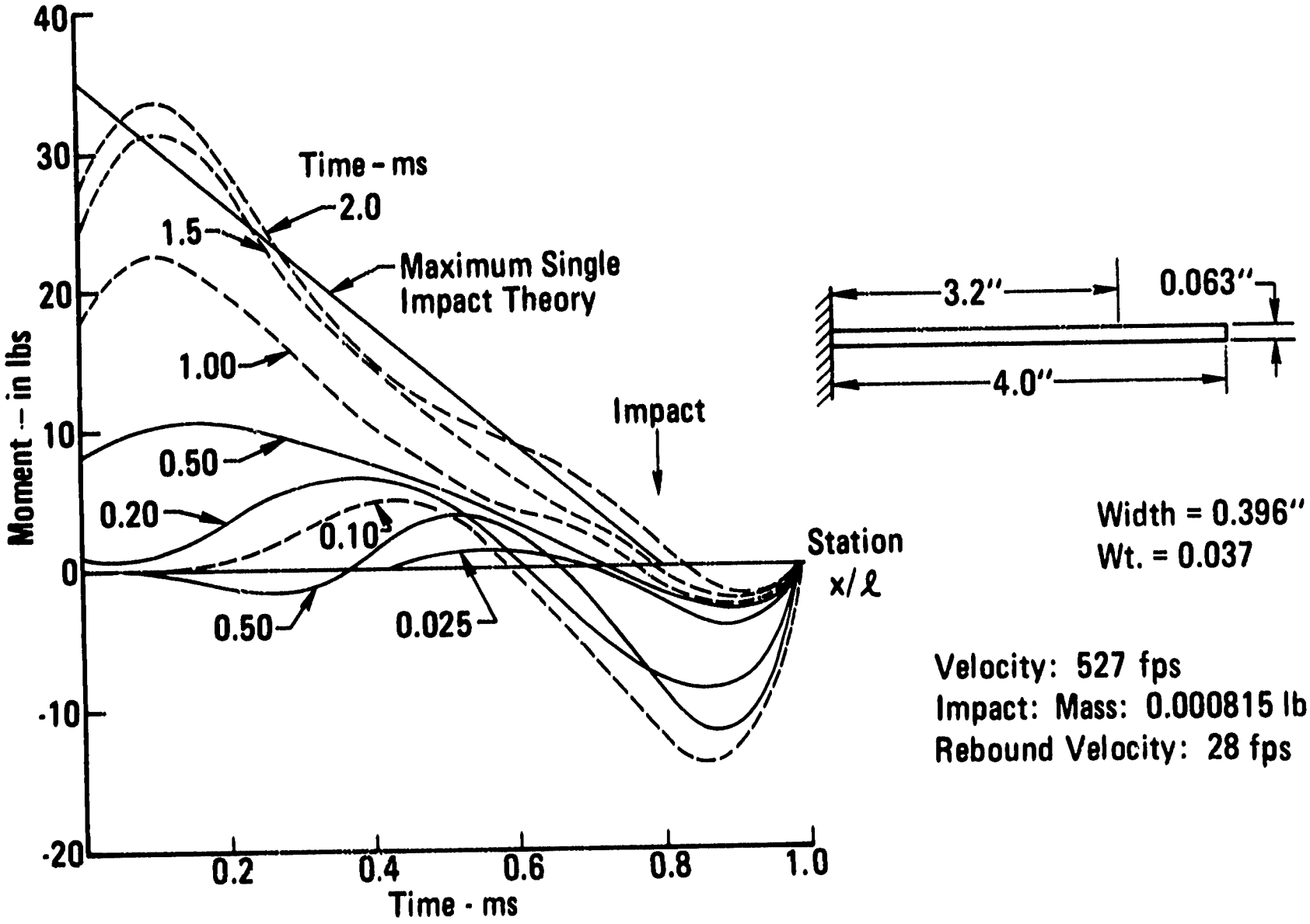

FIGURE 16. MOMENT DISTRIBUTIONS FOR IMPACT OF CANTILEVER SPECIMEN – CASE 7550

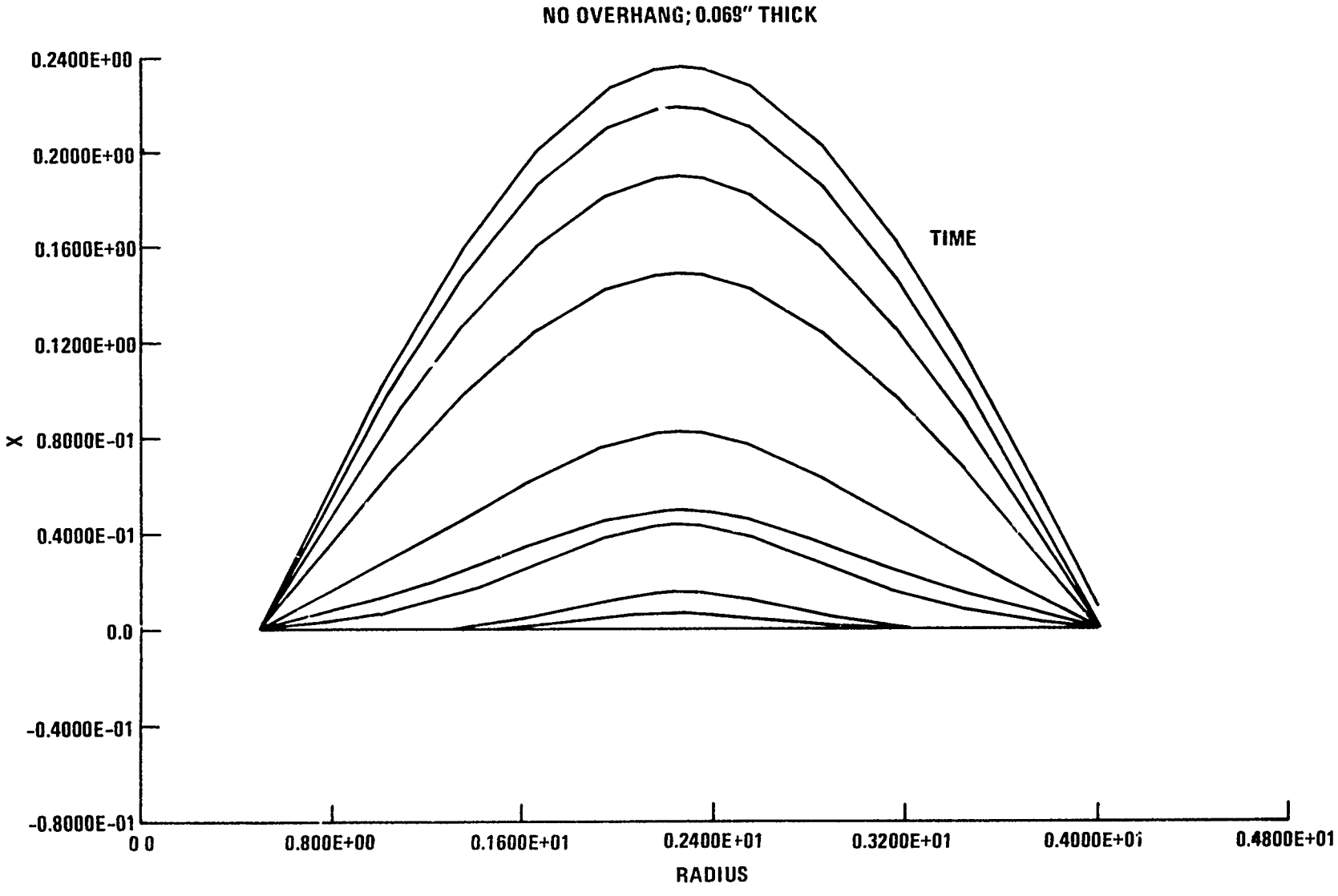

FIGURE 17. DEFLECTION DISTRIBUTION FOR IMPACT OF SIMPLY-SUPPORTED SPECIMEN

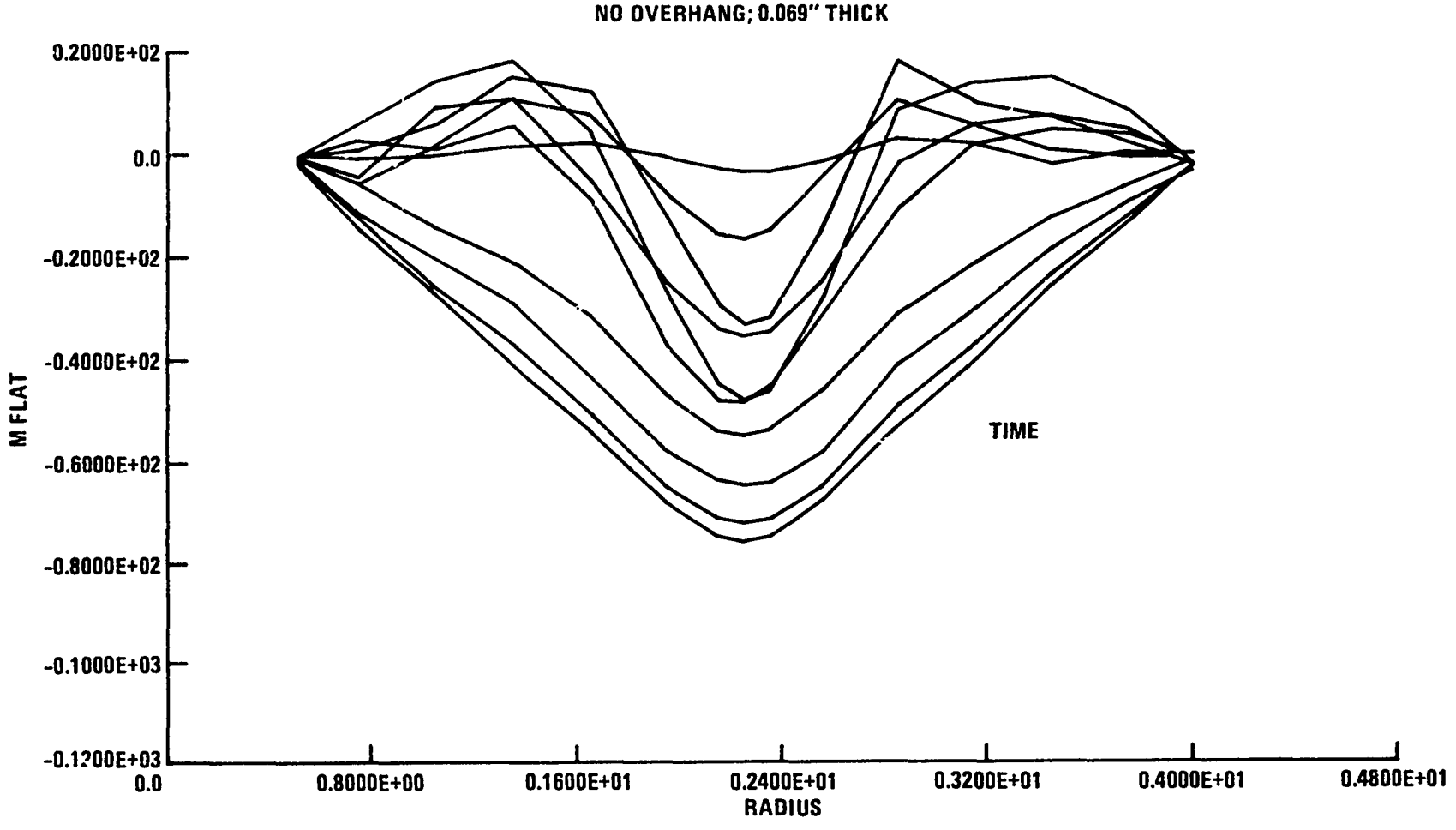

FIGURE 18. MOMENT DISTRIBUTION FOR IMPACT OF SIMPLY-SUPPORTED SPECIMEN

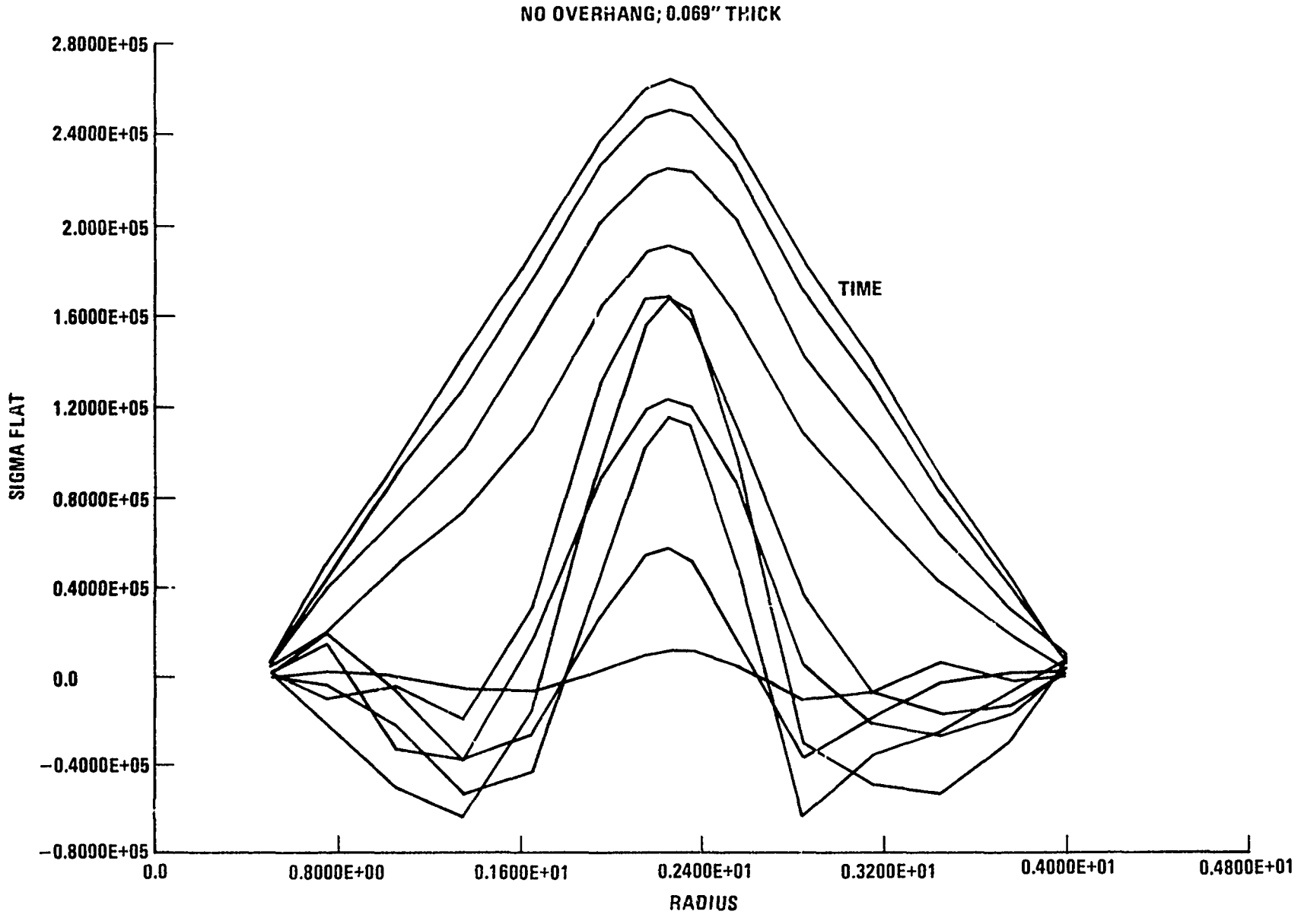

FIGURE 19. STRESS DISTRIBUTION FOR IMPACT OF SIMPLY-SUPPORTED SPECIMEN

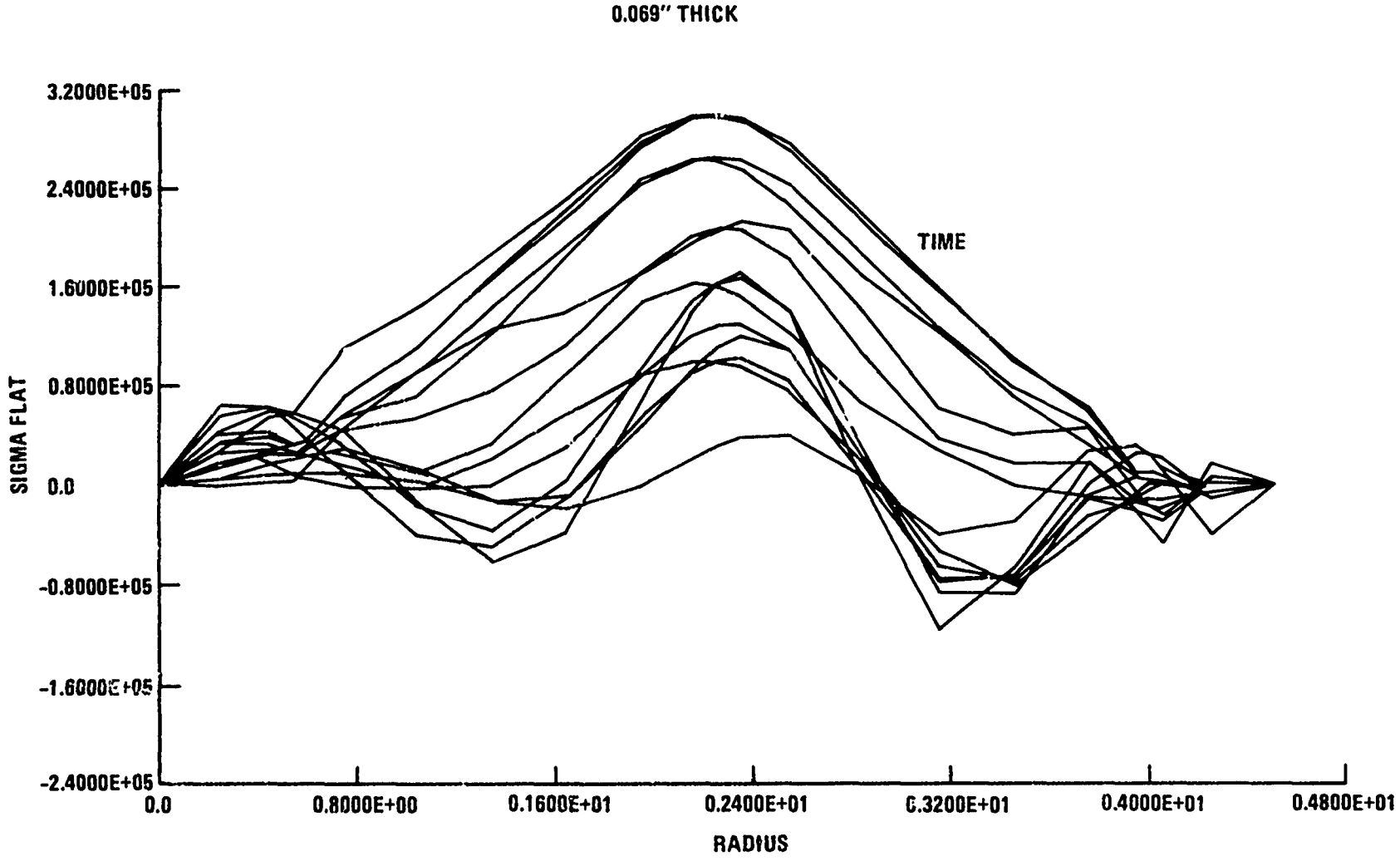

FIGURE 20. STRESS DISTRIBUTION FOR IMPACT OF SIMPLY-SUPPORTED SPECIMEN WITH OVERHANG

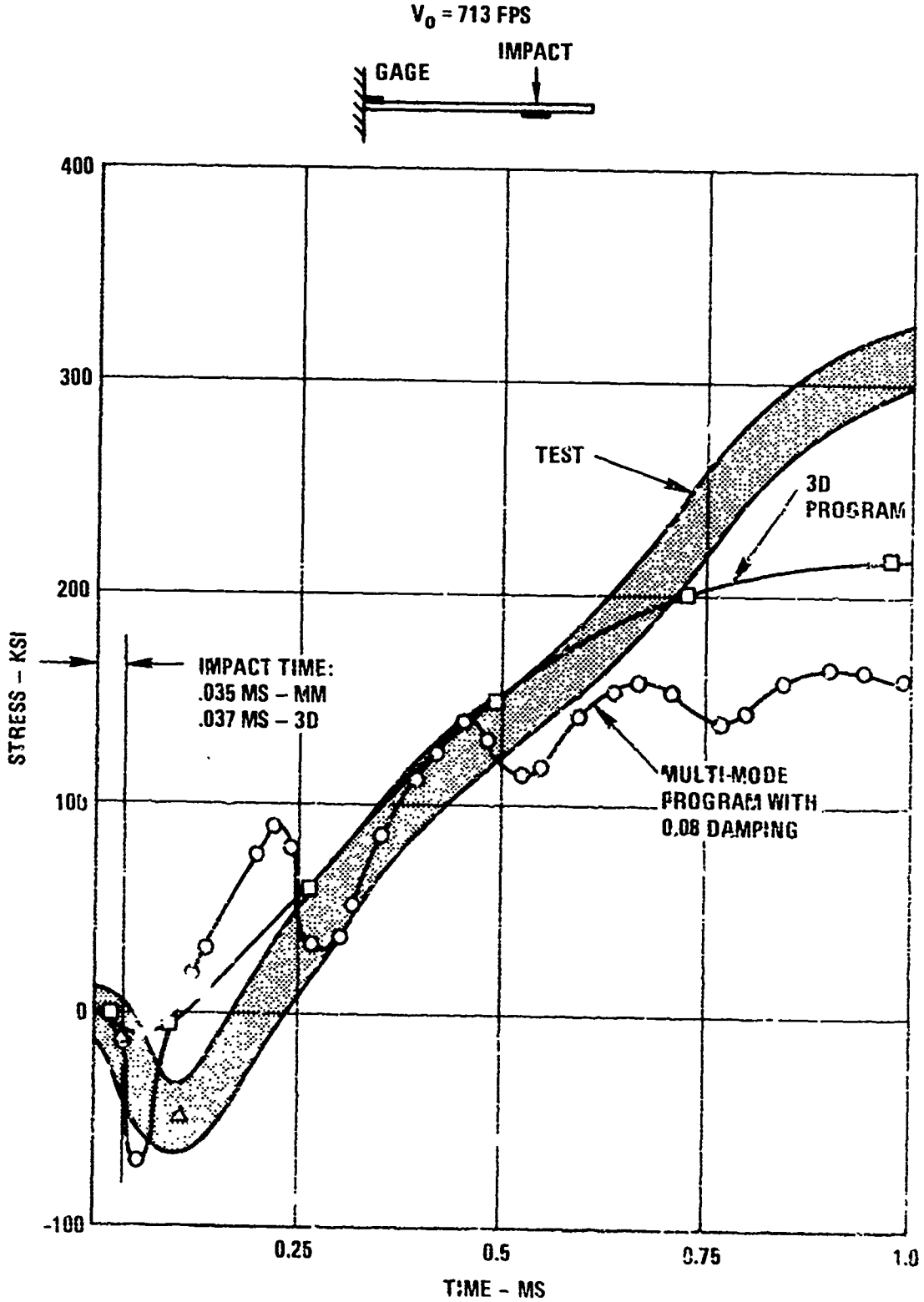

FIGURE 21. STRESSES AT ROOT SITE – CANTILEVER SPECIMEN CASE 7609

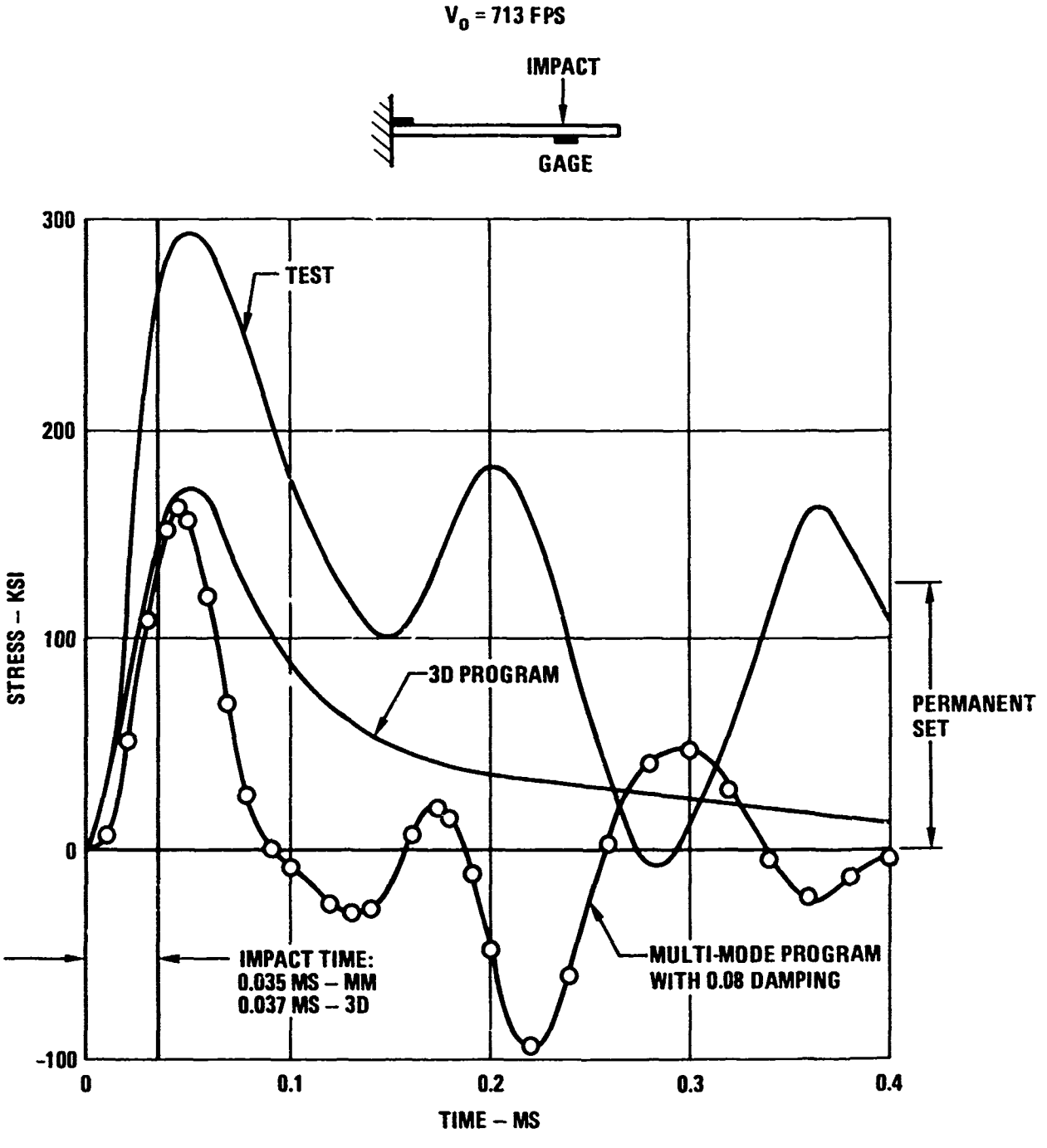

FIGURE 22. STRESSES AT IMPACT SITE – CANTILEVER SPECIMEN CASE 7609

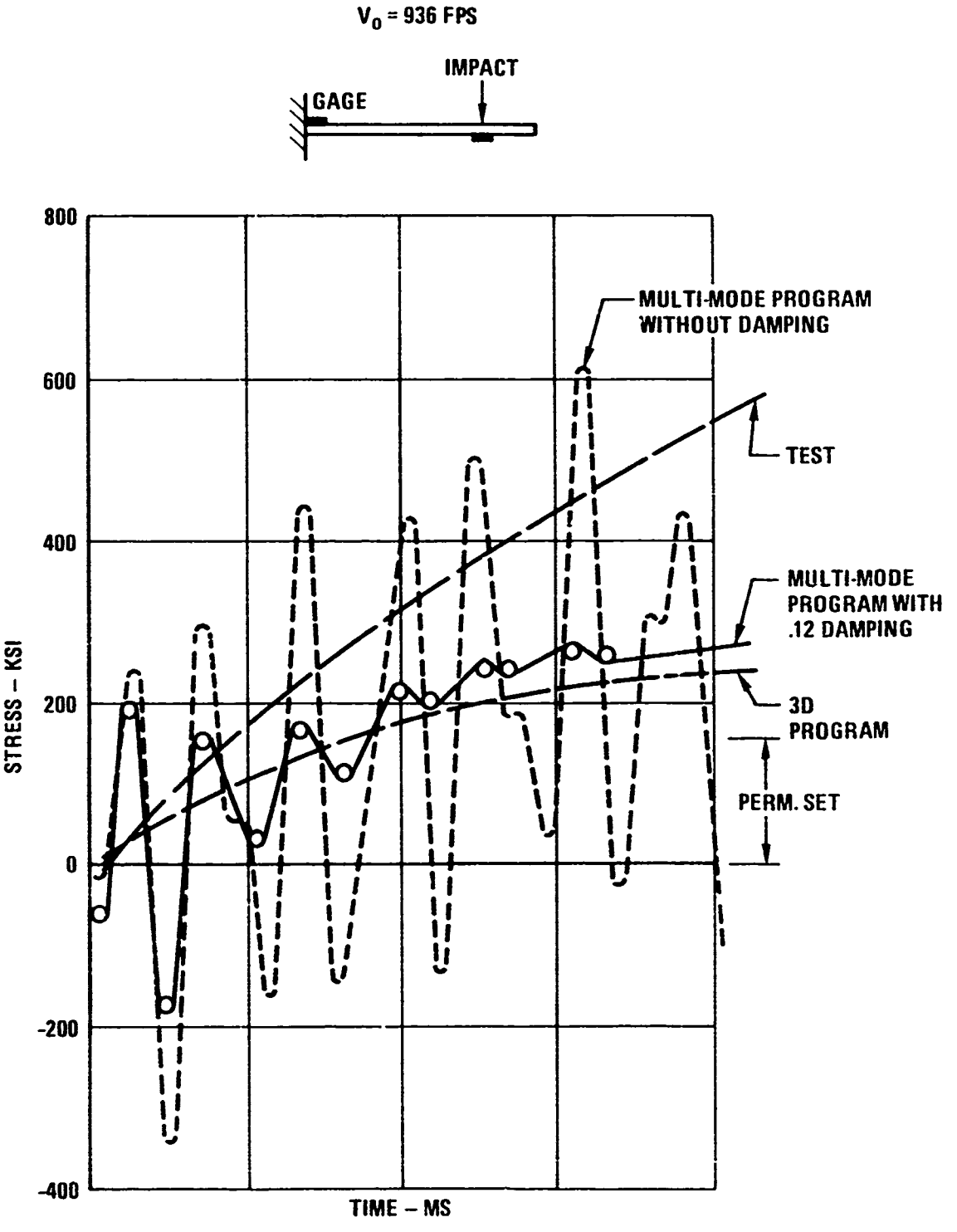

FIGURE 23. STRESSES AT ROOT SITE – CANTILEVER SPECIMEN CASE 7608

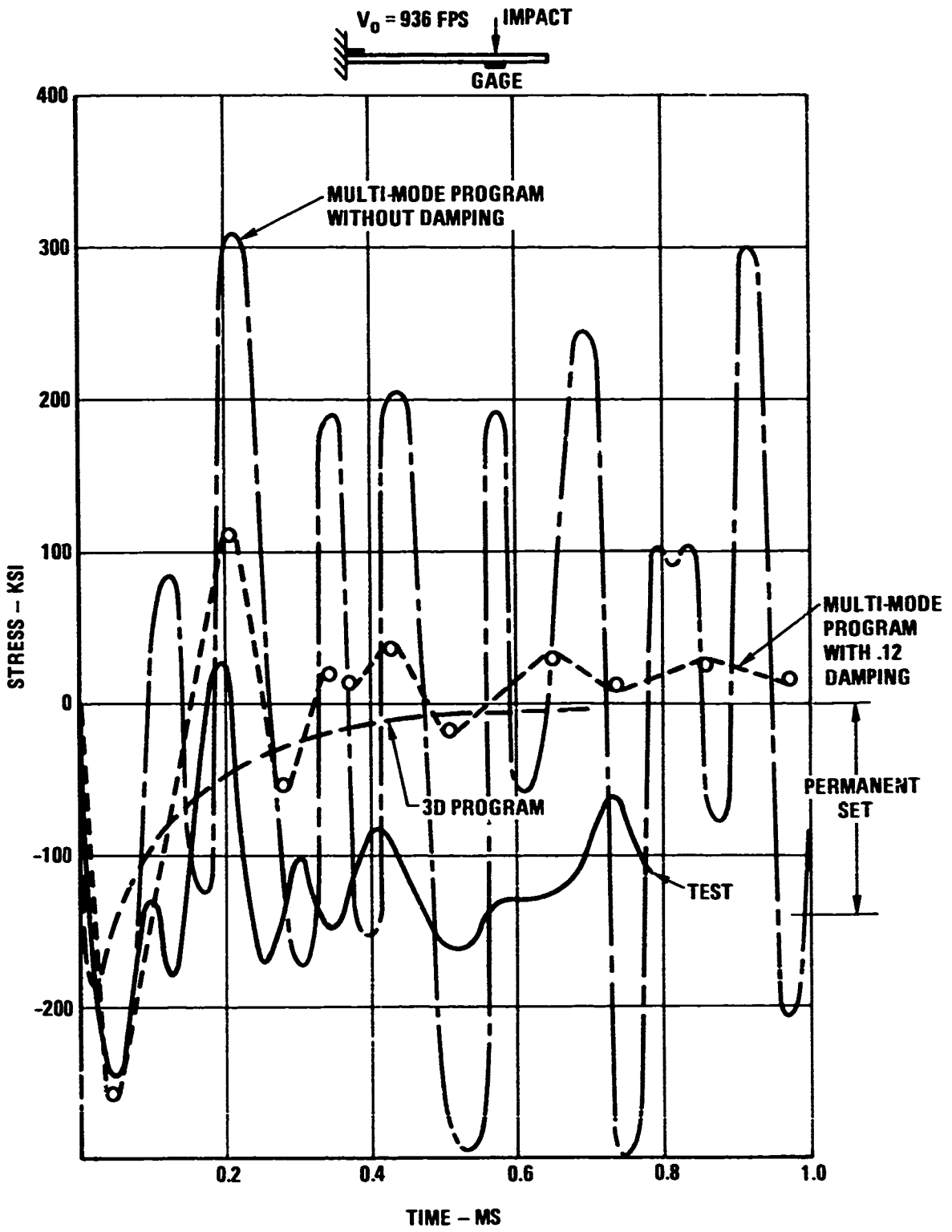

FIGURE 24. STRESSES AT IMPACT SITE – CANTILEVER SPECIMEN CASE 7608

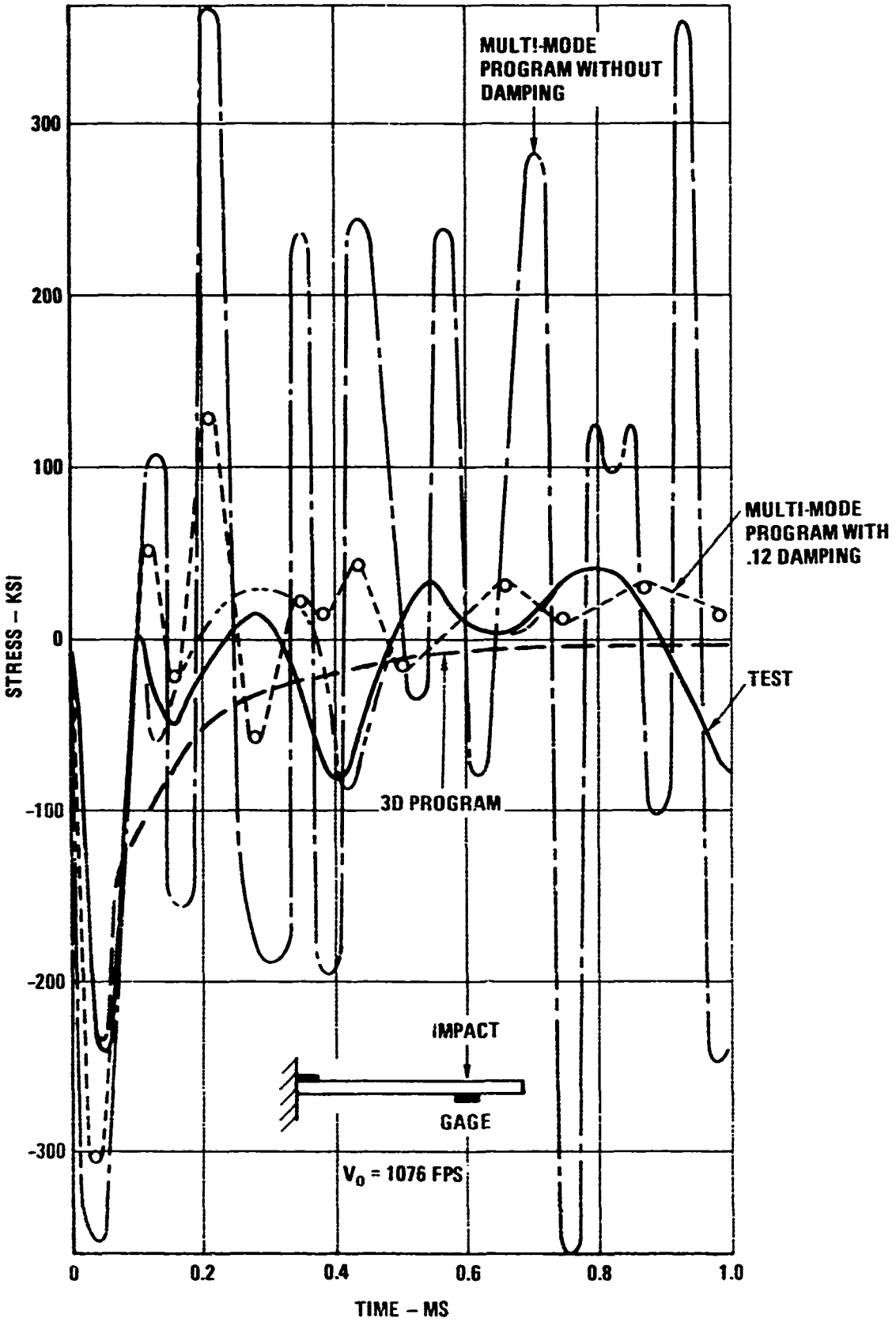

FIGURE 25. STRESSES AT IMPACT SITE – CANTILEVER SPECIMEN CASE 7610

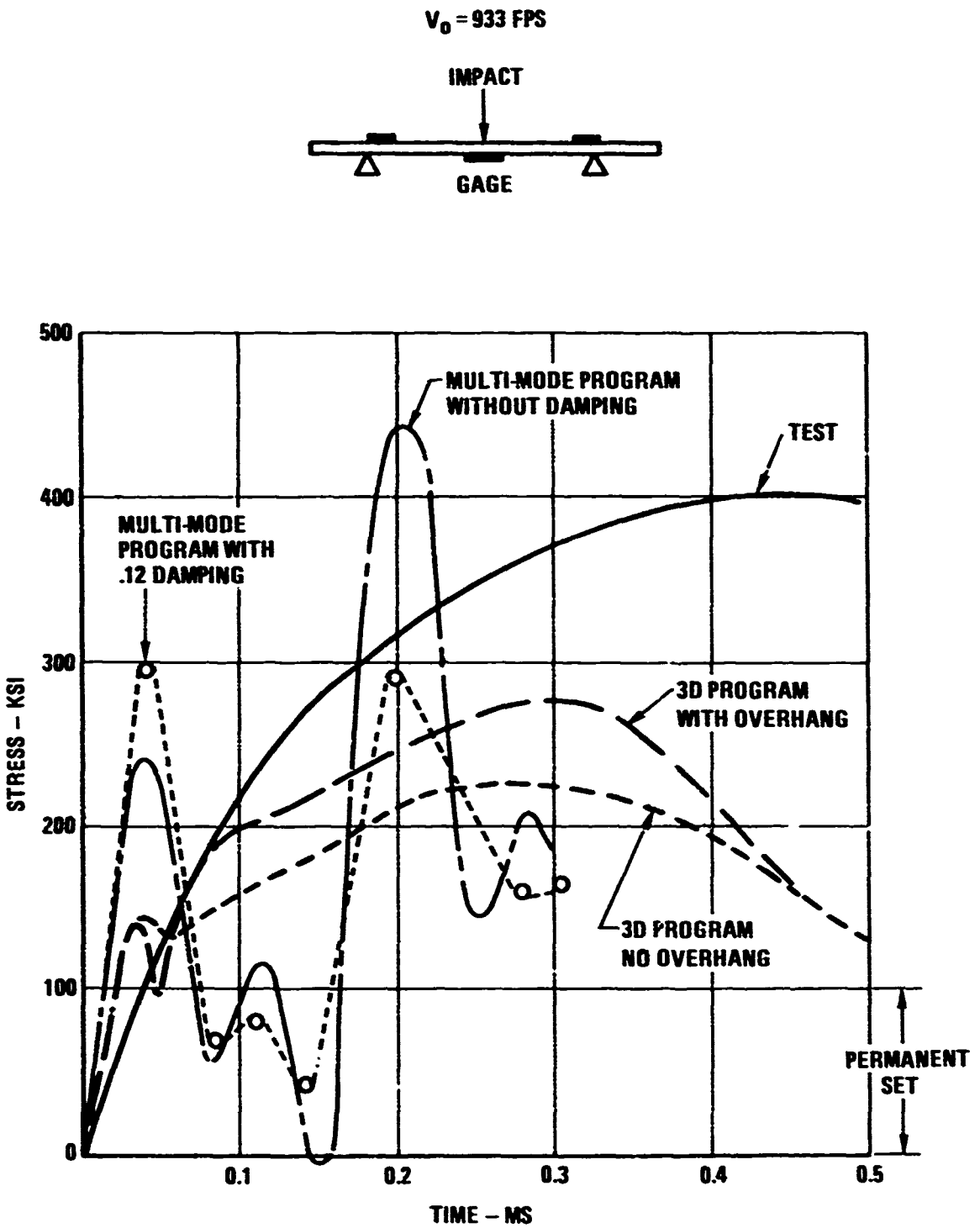

FIGURE 26. STRESSES AT IMPACT SITE – SIMPLY SUPPORTED SPECIMEN CASE 7611

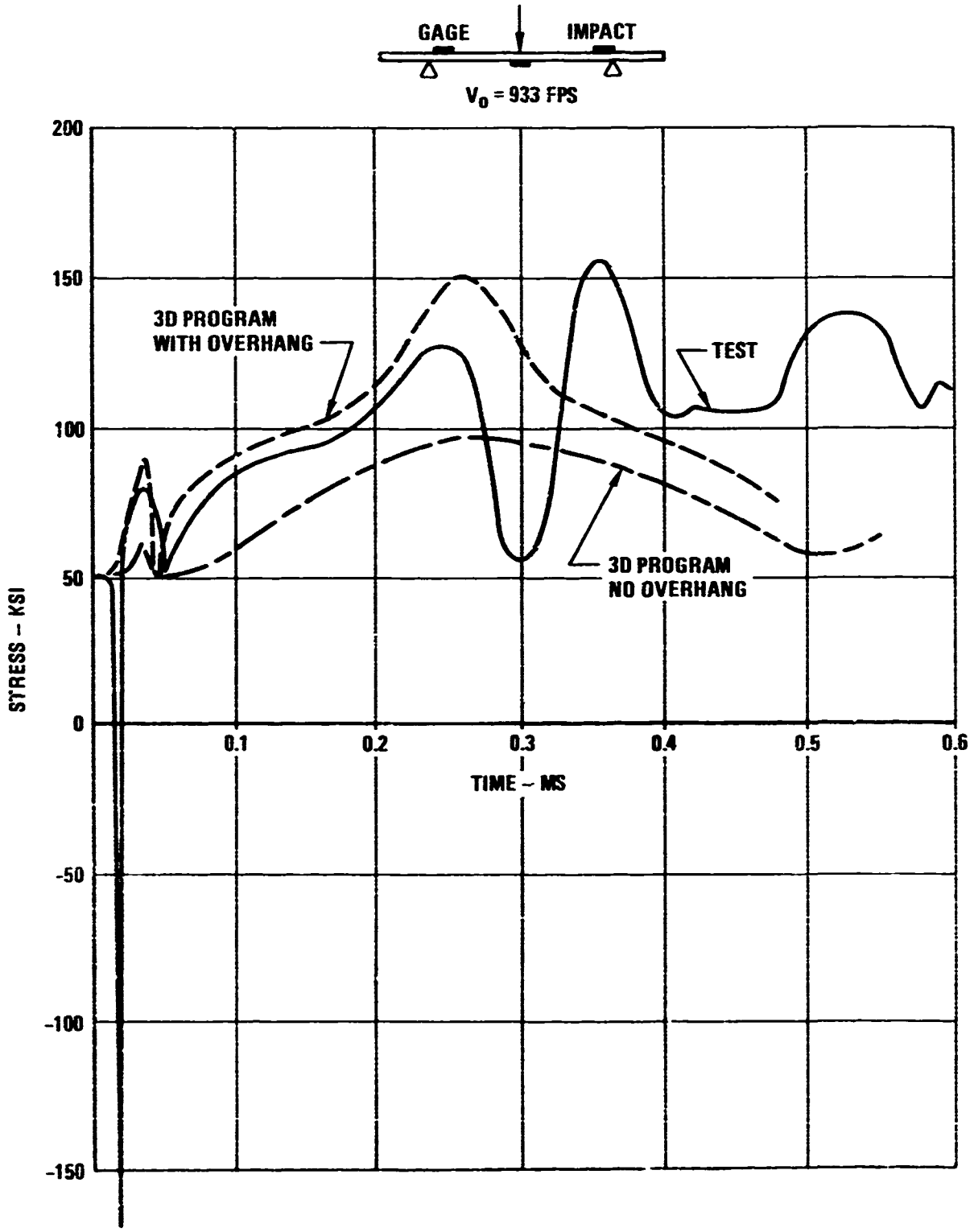

FIGURE 27. STRESSES AT SUPPORT SITE – SIMPLY SUPPORTED SPECIMEN CASE 7611

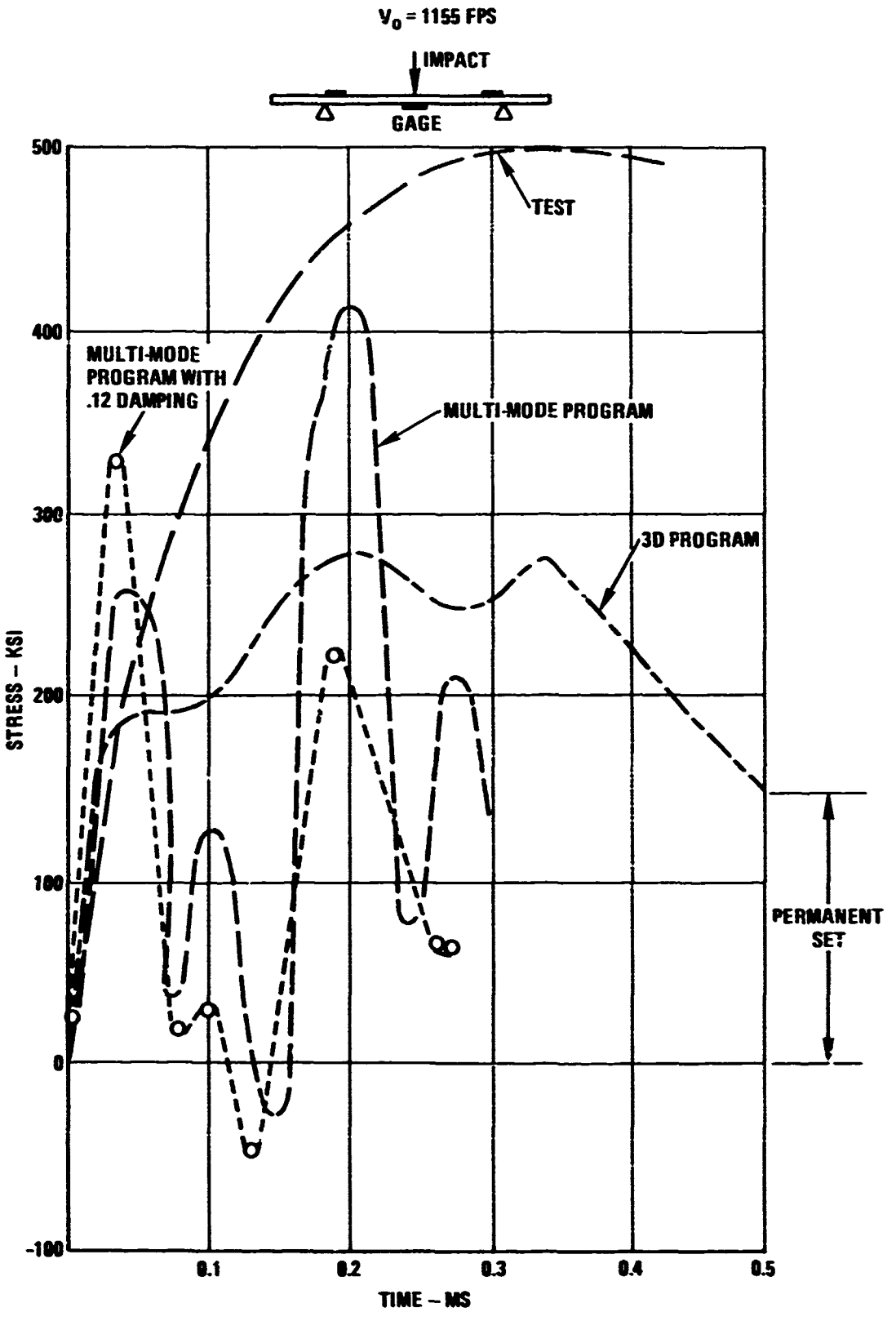

FIGURE 28. STRESSES AT IMPACT SITE – SIMPLY SUPPORTED SPECIMEN CASE 7612

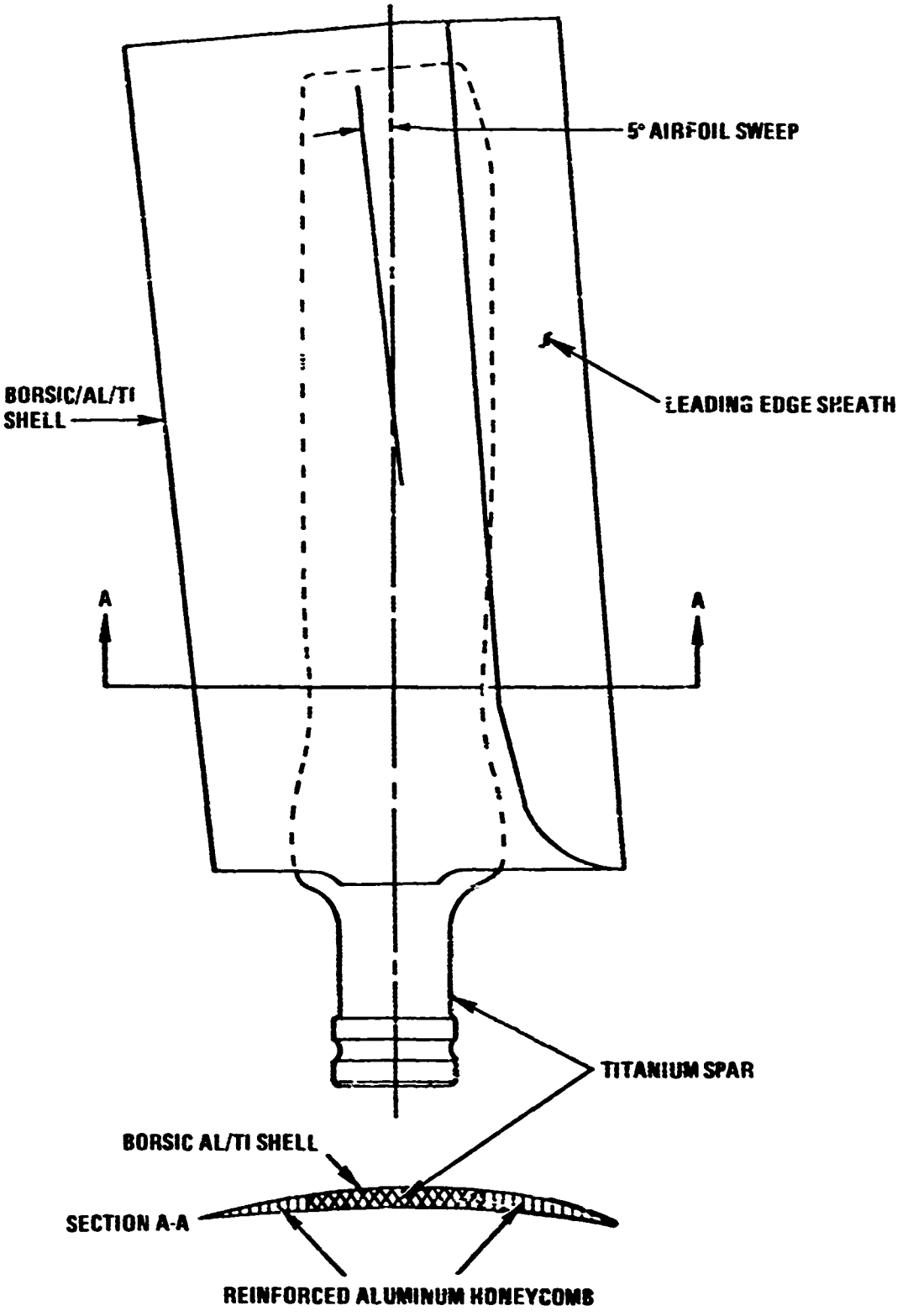

FIGURE 29. HAMILTON STANDARD QCSEE TYPE FOD FAN BLADE DESIGN CONFIGURATION

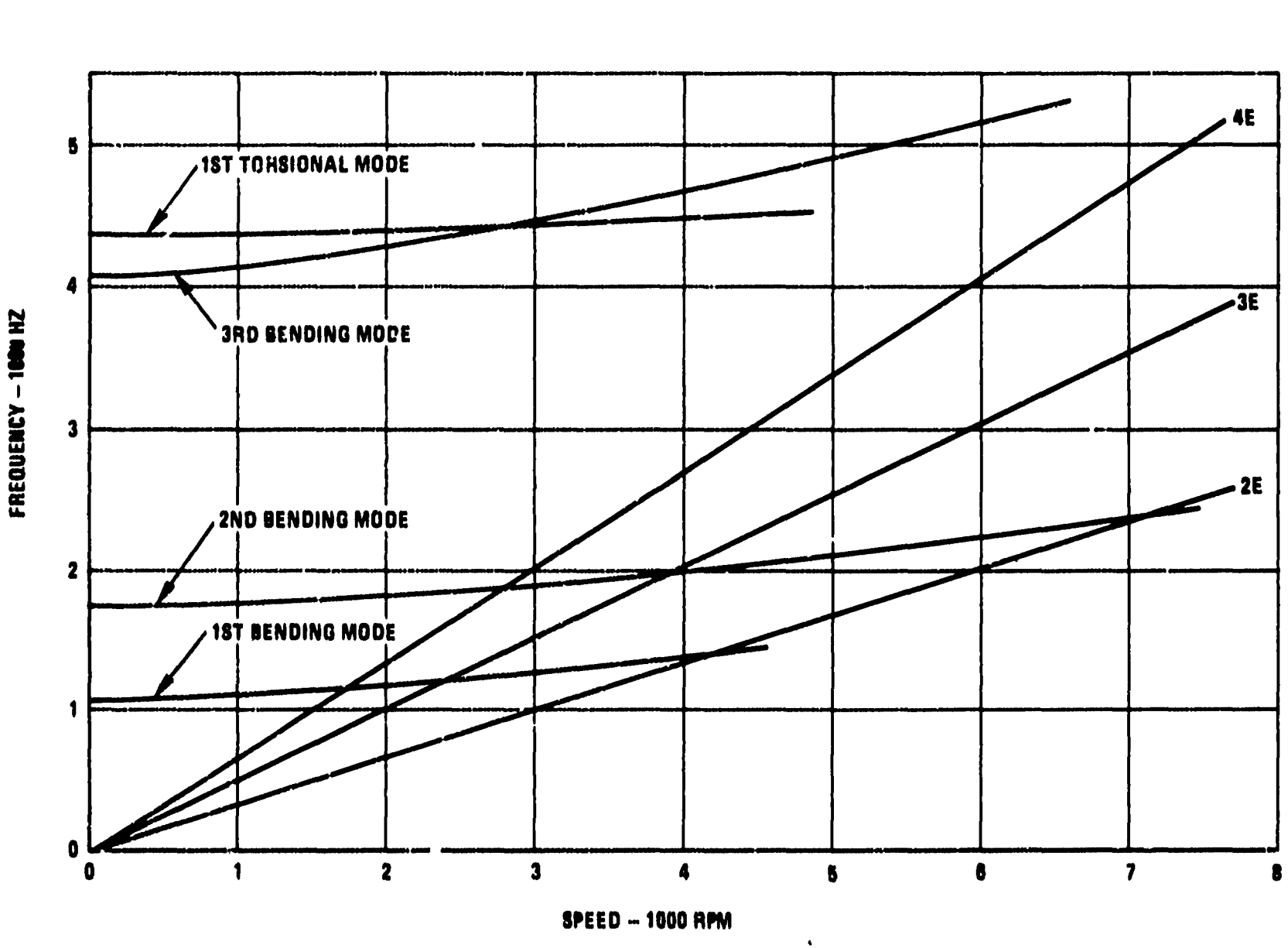

FIGURE 30. QCSEE TYPE FOD FAN BLADE FREQUENCY VS SPEED

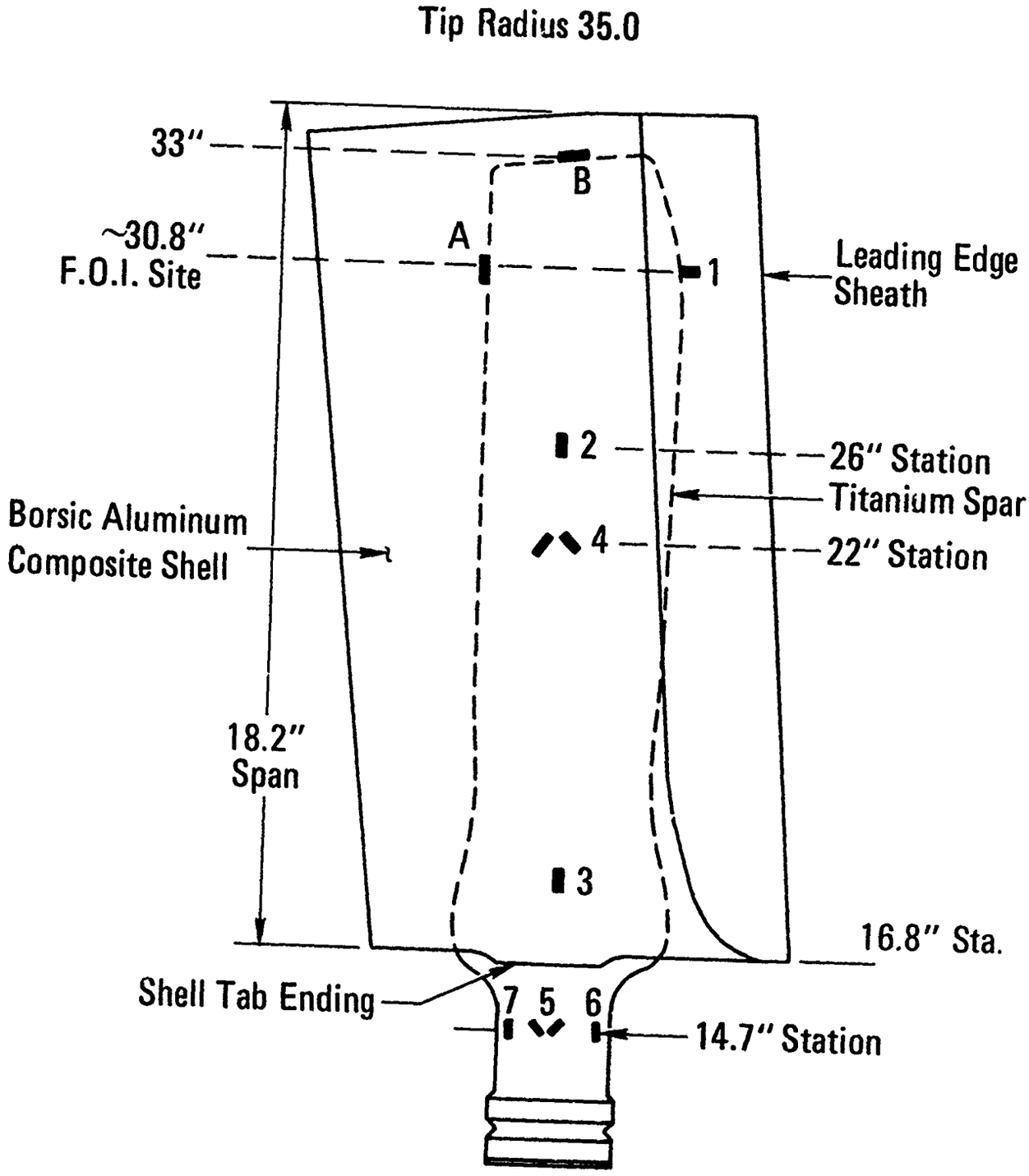

FIGURE 31. FOD FAN BLADE STRAIN GAGE LAYOUT

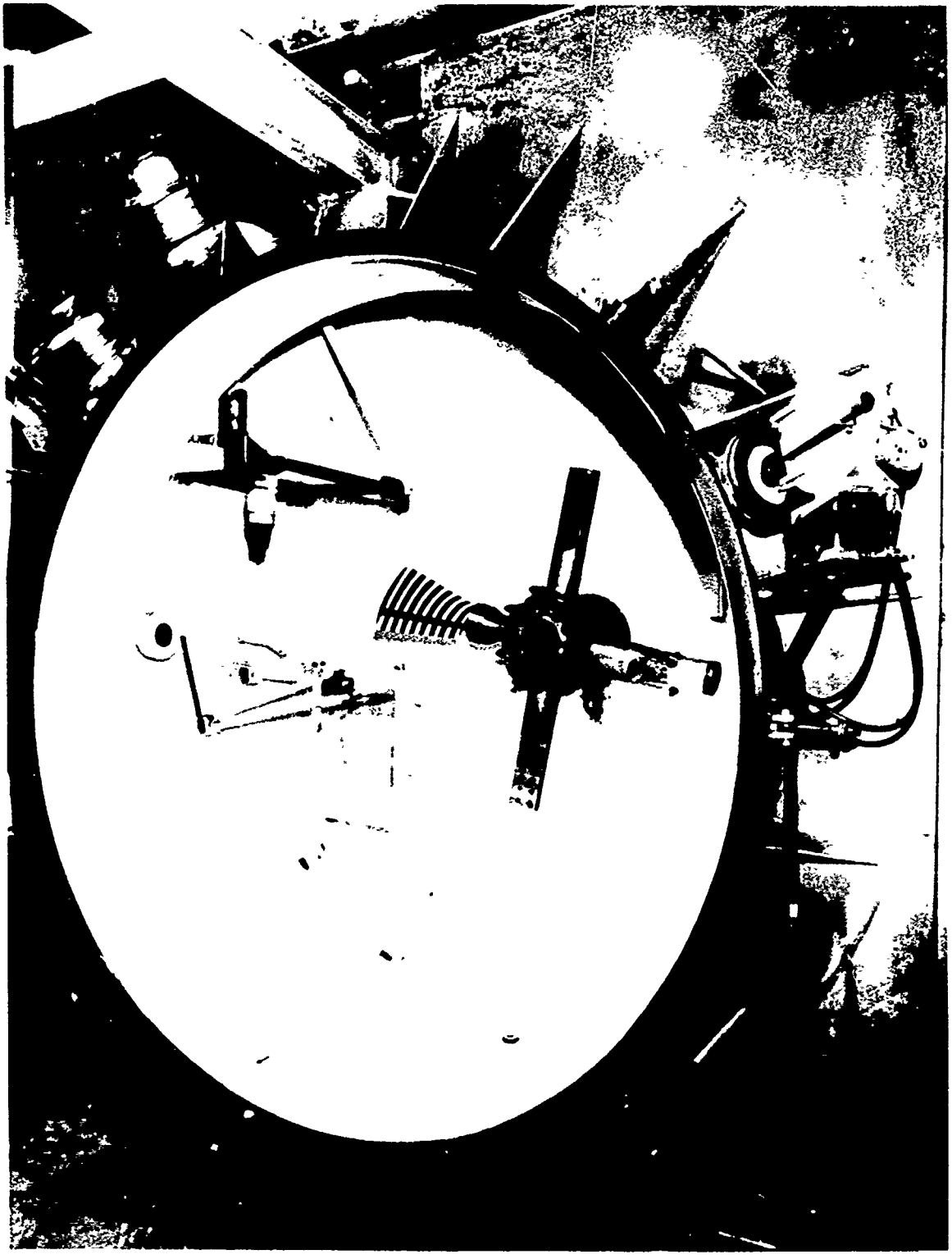

FIGURE 32. WHIRL IMPACT TEST FACILITY SET UP FOR BIRD IMPACT

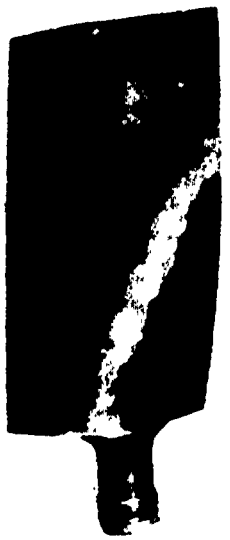

PRETEST

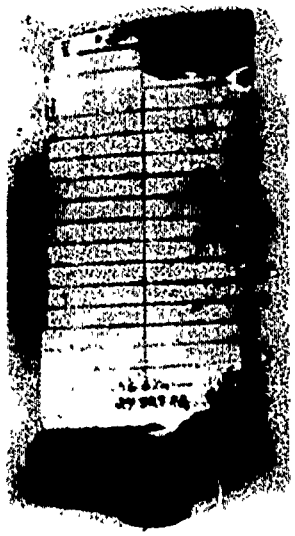

0.36 # SLICE (GELATIN)

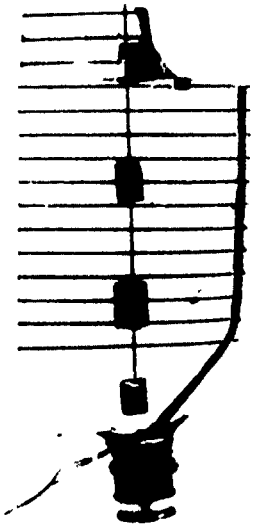

0.97# SLICE (GELATIN)

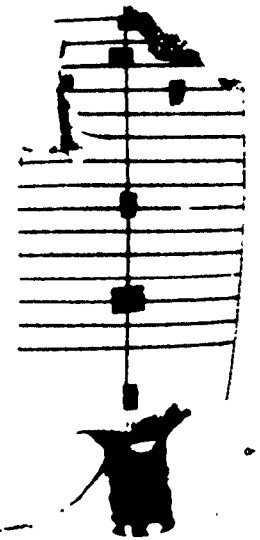

1.68 # SLICE (GELATIN)

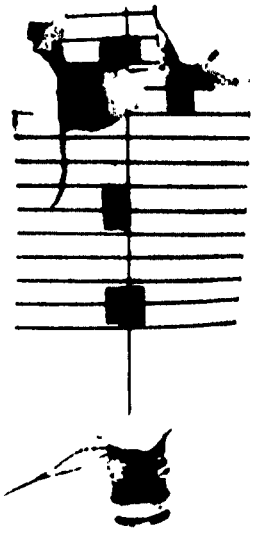

1.74 # SLICE (REAL BIRD)

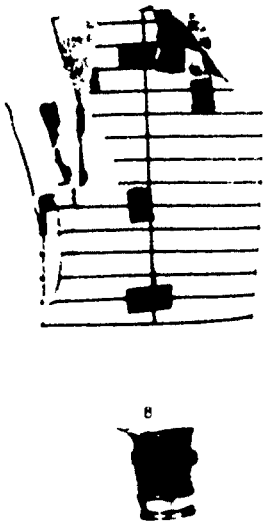

1.43 # SLICE (GELATIN, FIXED ROOT)

FIGURE 33. METAL MATRIX Q-FAN BLADE FOD TEST RESULTS

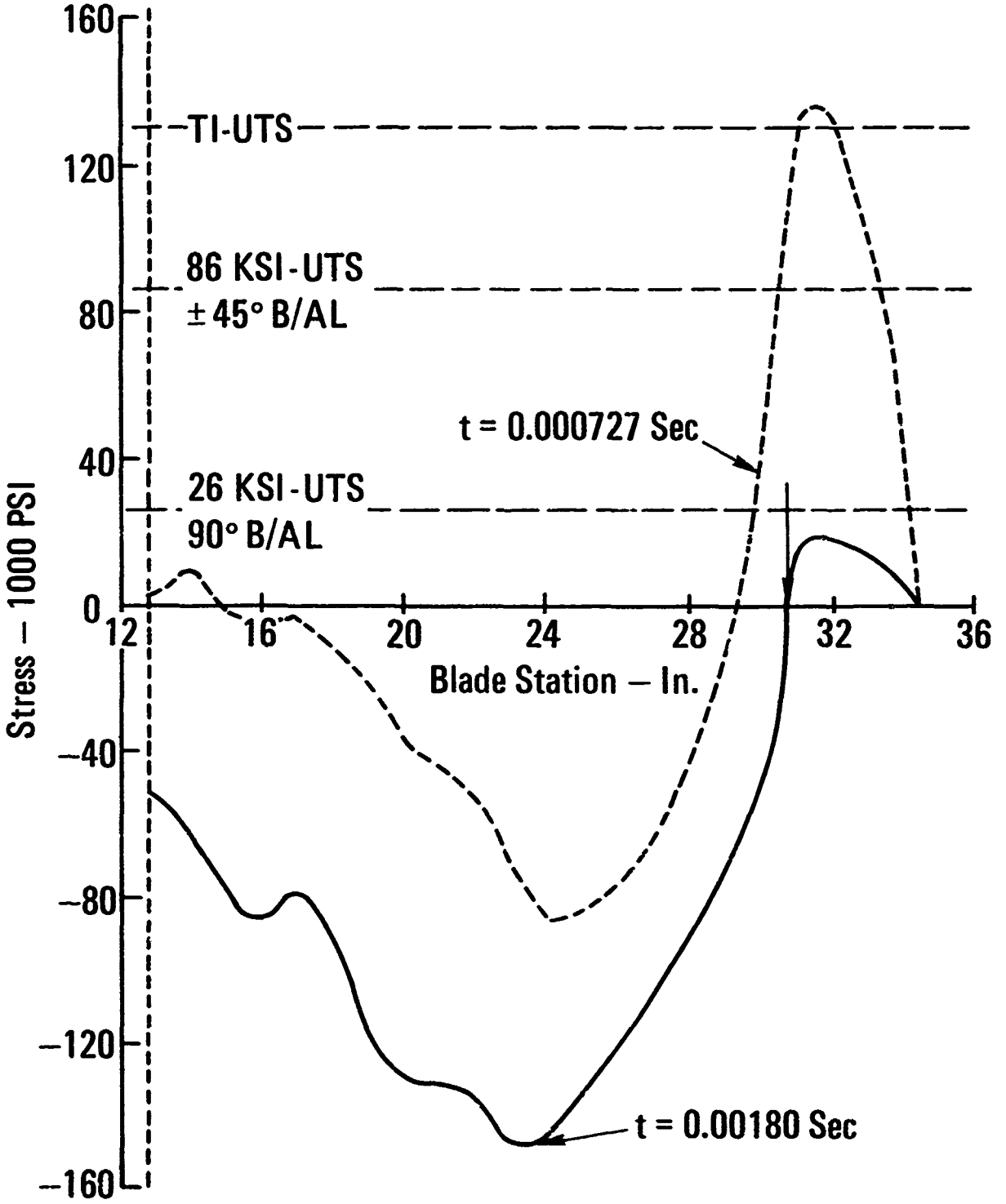

FIGURE 34. Q-FAN DEMO BLADE; 440 GRAM JELLY BIRD; THREE DEGREE IMPACT ANALYSIS

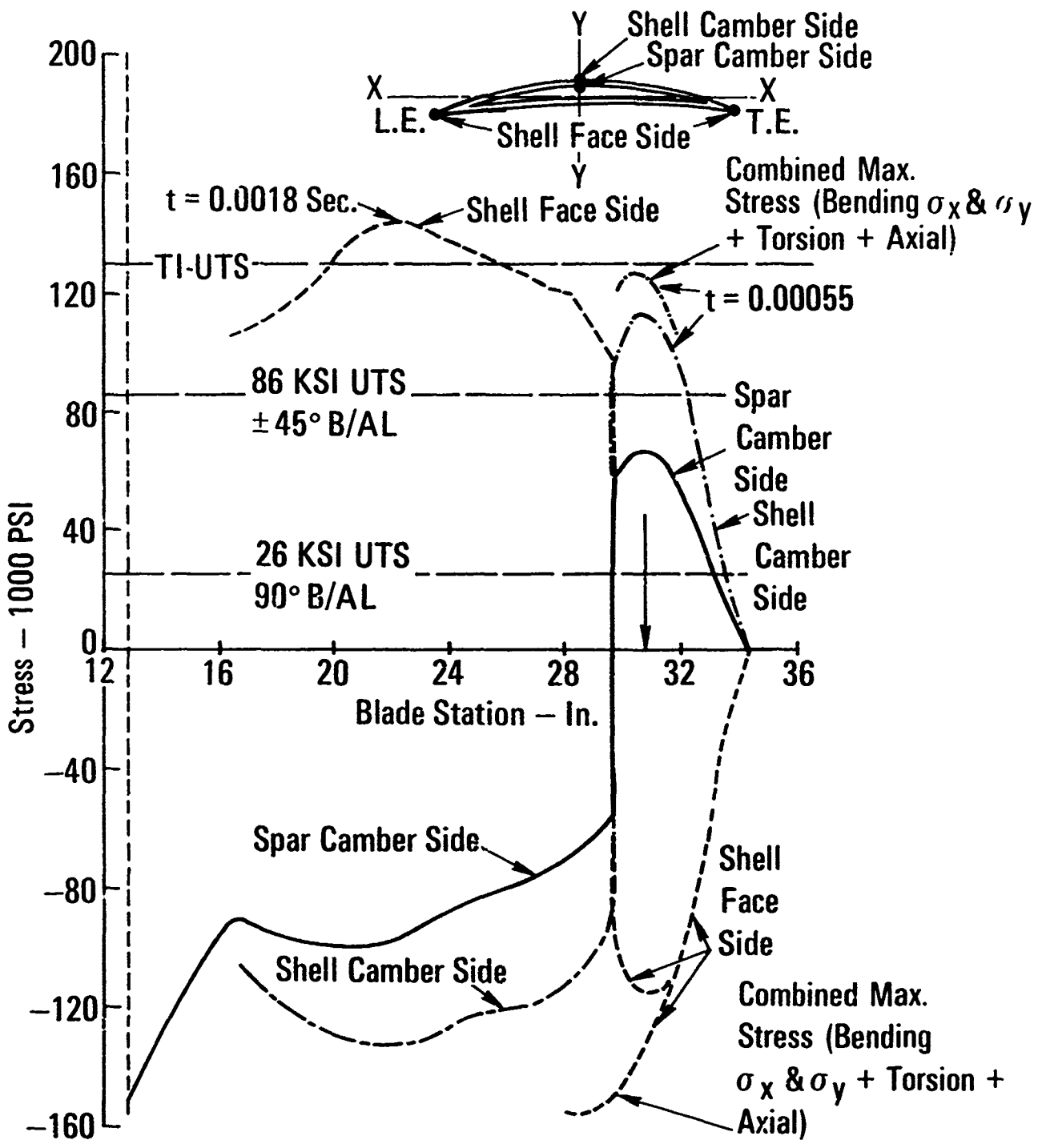

FIGURE 35. PEAK STRESSES VS. RADIUS; Q-FAN DEMO BLADE; 440 GRAM JELLY BIRD MULTIMODE WITH 0.12 DAMPING

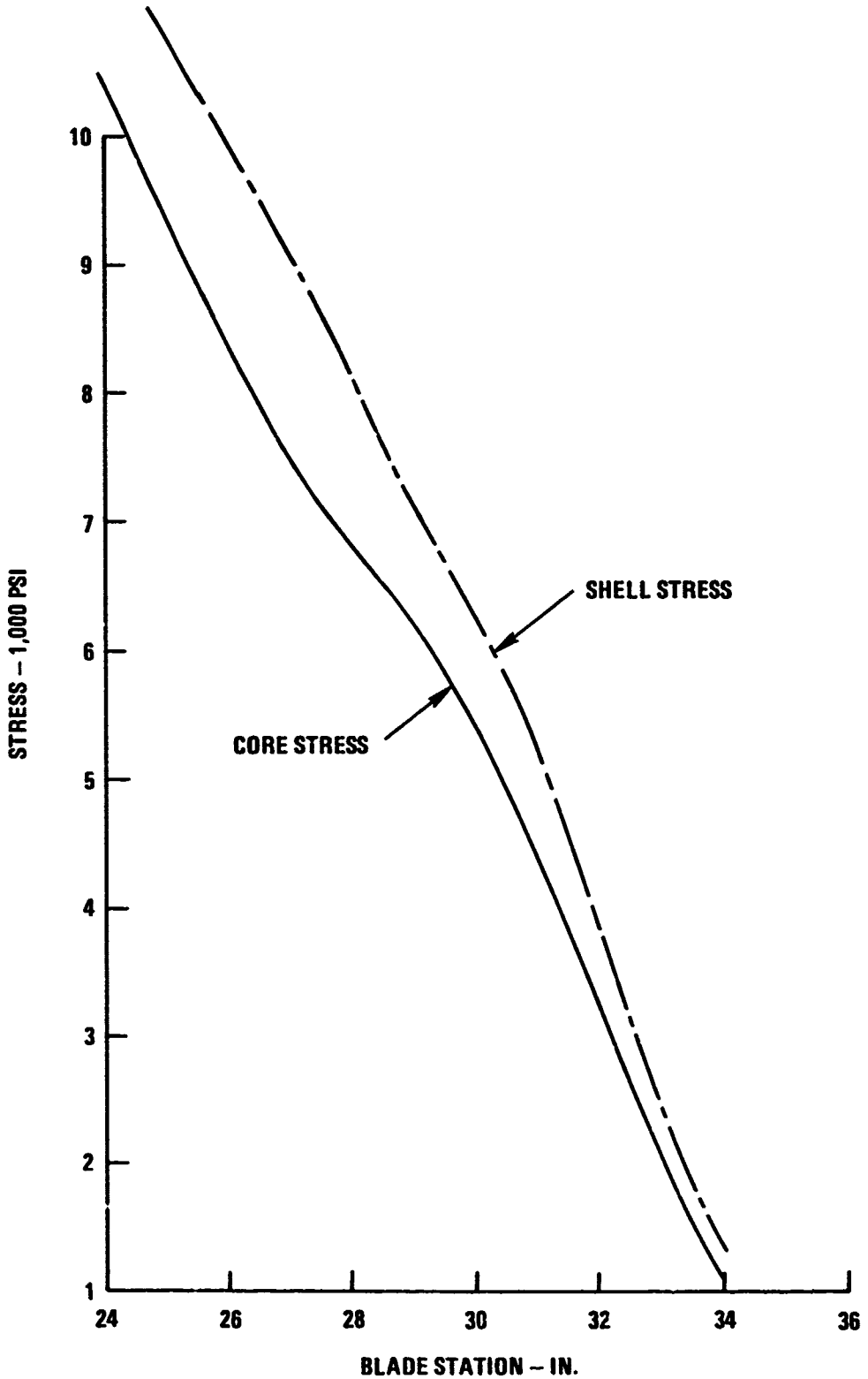

FIGURE 36. CENTRIFUGAL STRESS VS. BLADE STATION FOR CORE AND SHELL FOD Q-FAN DEMO BLADE

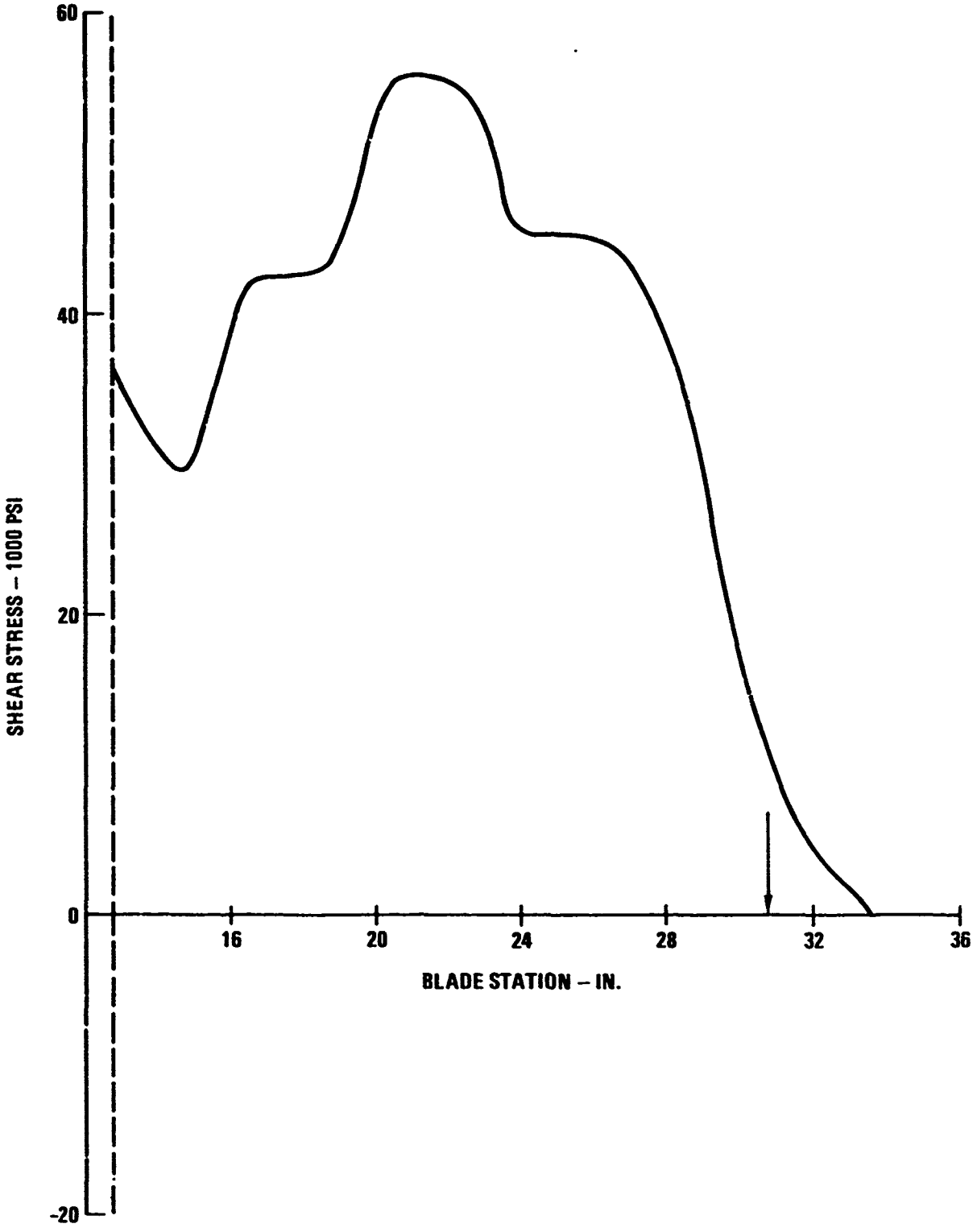

FIGURE 37. CORE SHEAR STRESS VS. BLADE STATION; Q-FAN DEMO BLADE; 440 GRAM JELLY BIRD; MULTI-MODE WITH 0.12 DAMPING

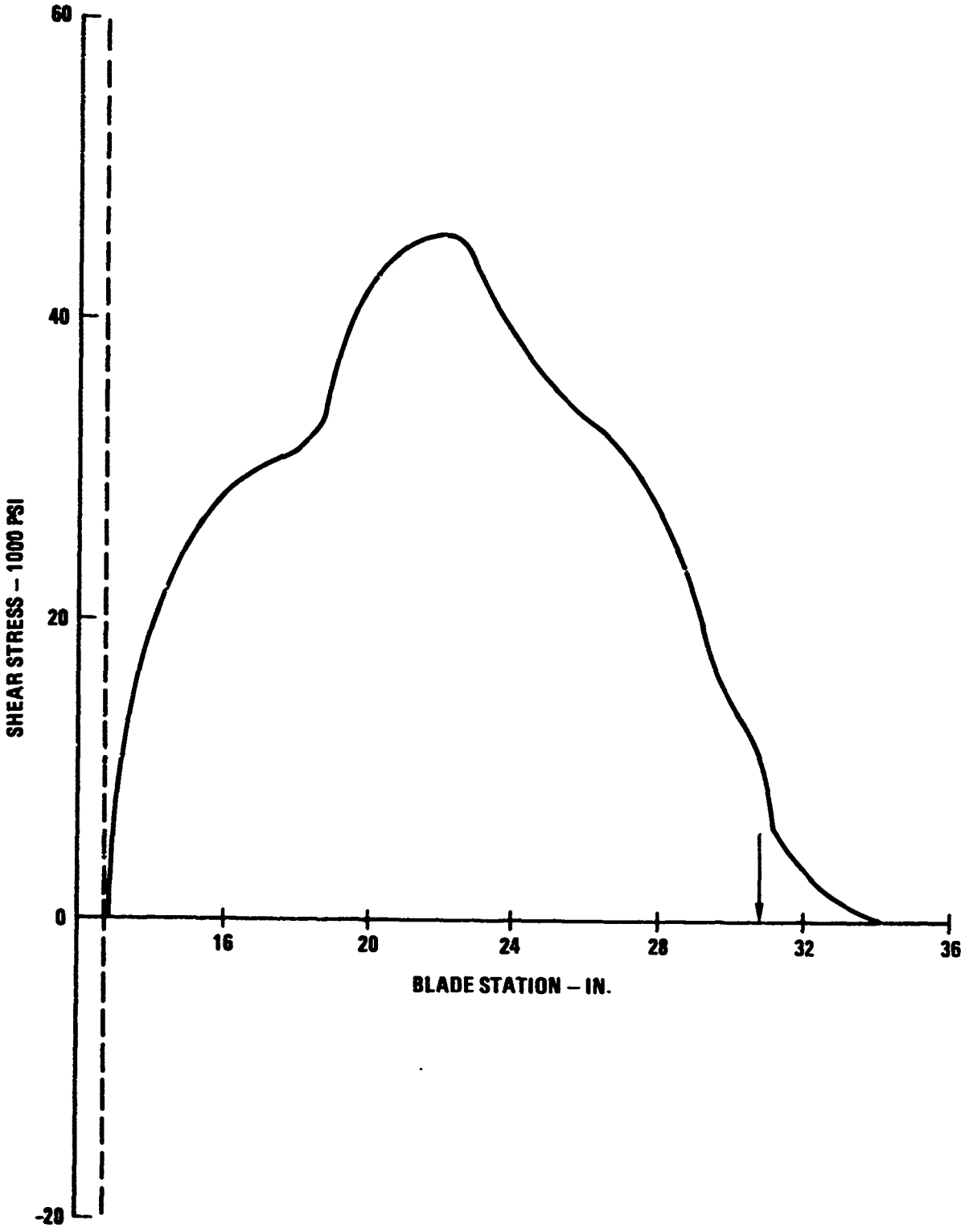

FIGURE 38. SHELL SHEAR STRESS VS. BLADE STATION; Q-FAN DEMO BLADE; 440 GRAM JELLY BIRD; MULTI-MODE WITH 3.12 DAMPING

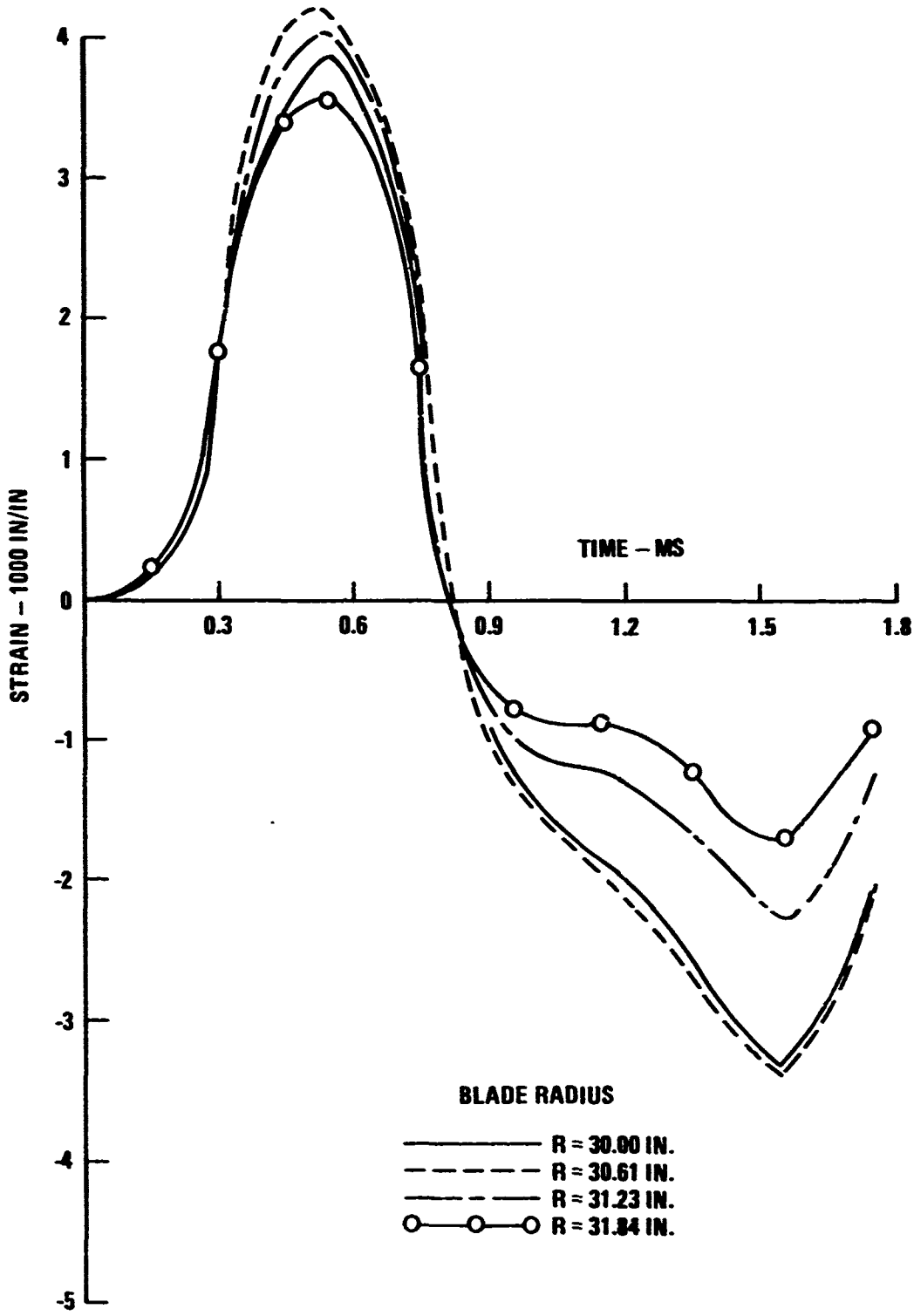

FIGURE 39. STRAIN VS. TIME FOR DIFFERENT RADII OF Q-FAN DEMO BLADE – SPAR

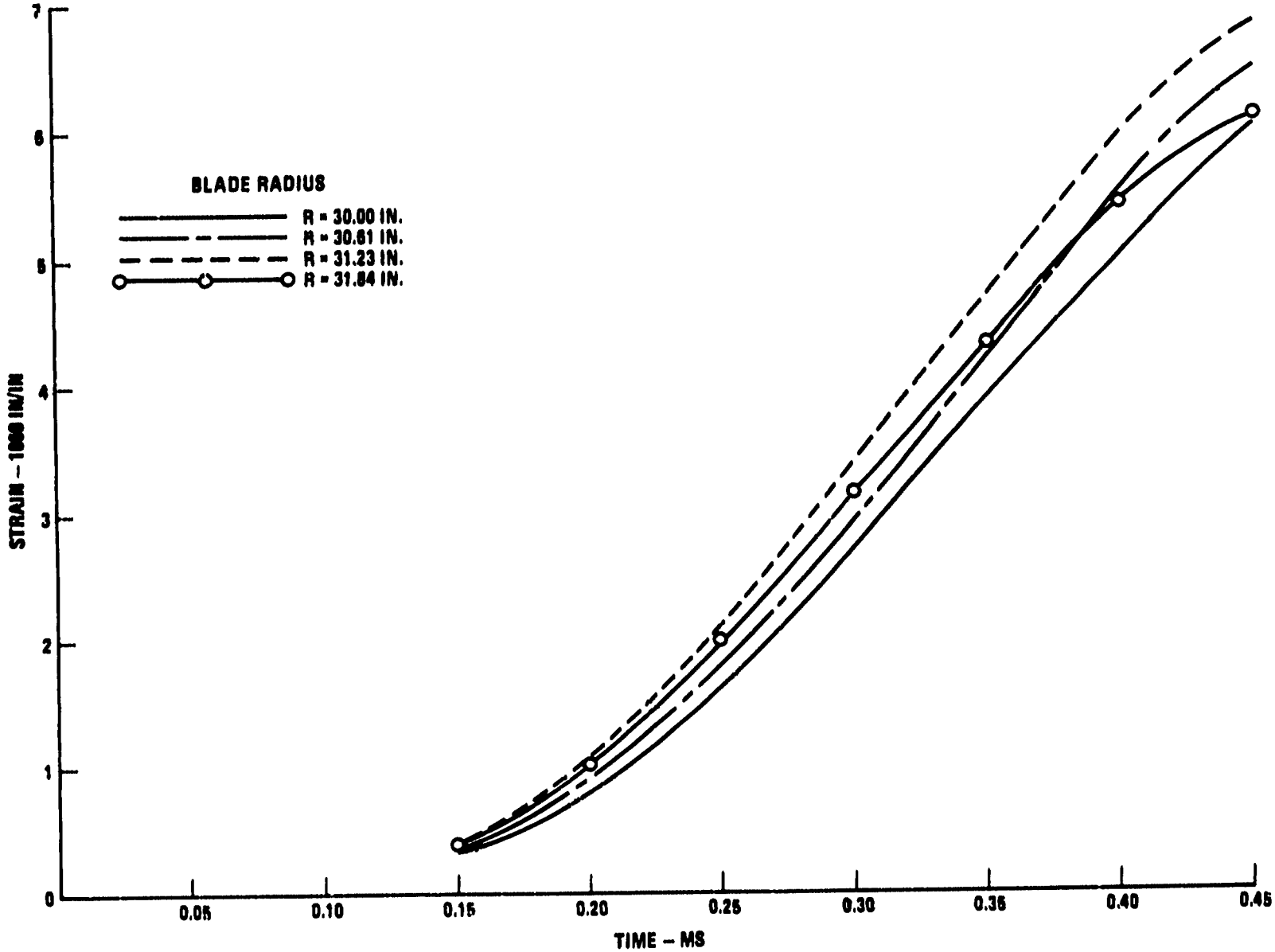

FIGURE 40. STRAIN VS. TIME FOR DIFFERENT RADII OF Q-FAN DEMO BLADE – SHELL

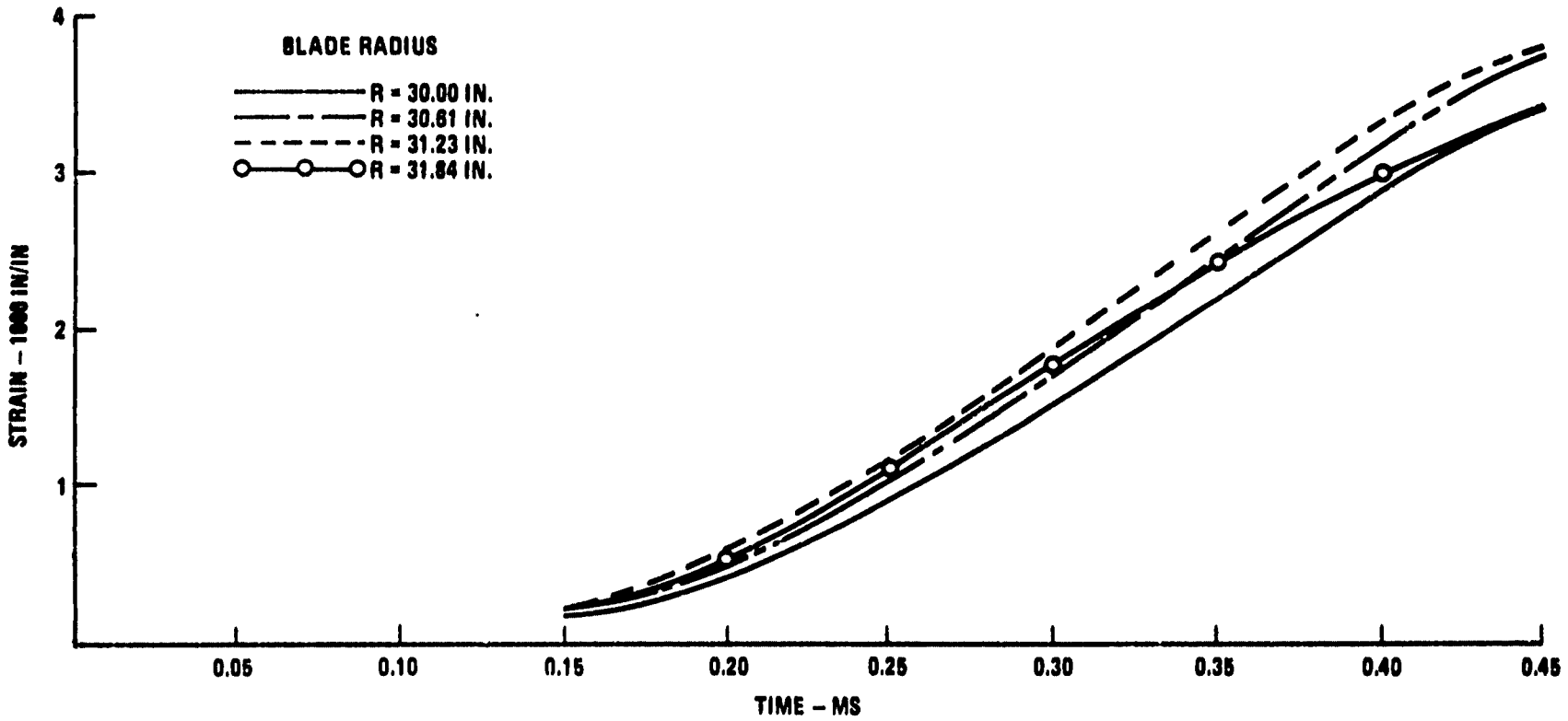

FIGURE 41. STRAIN VS. TIME FOR DIFFERENT RADII OF Q-FAN DEMO BLADE – SPAR

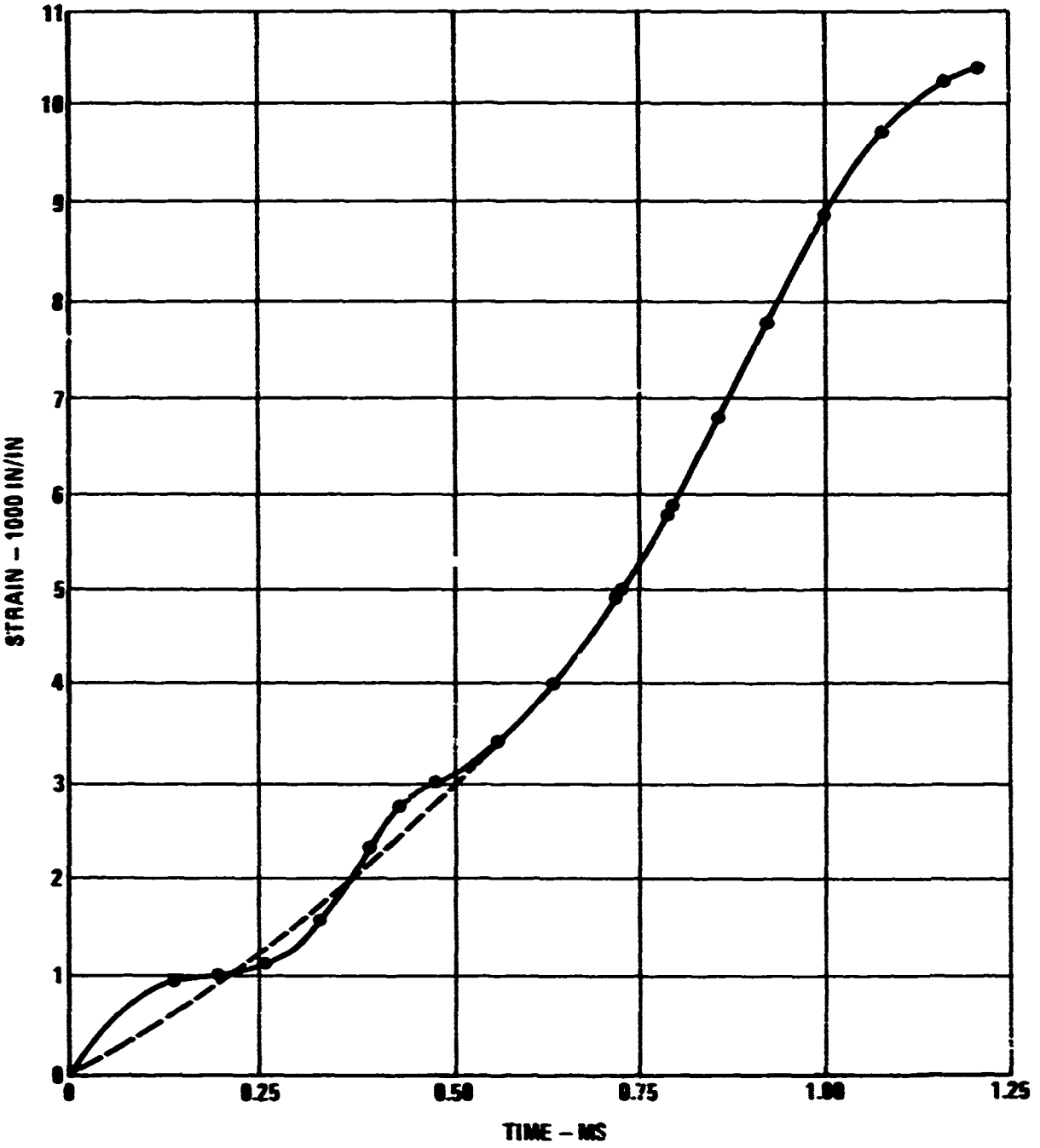

FIGURE 42. STRAIN VS. TIME FOR SHANK REGION OF Q-FAN DEMO BLADE AT R = 12.00 INCHES

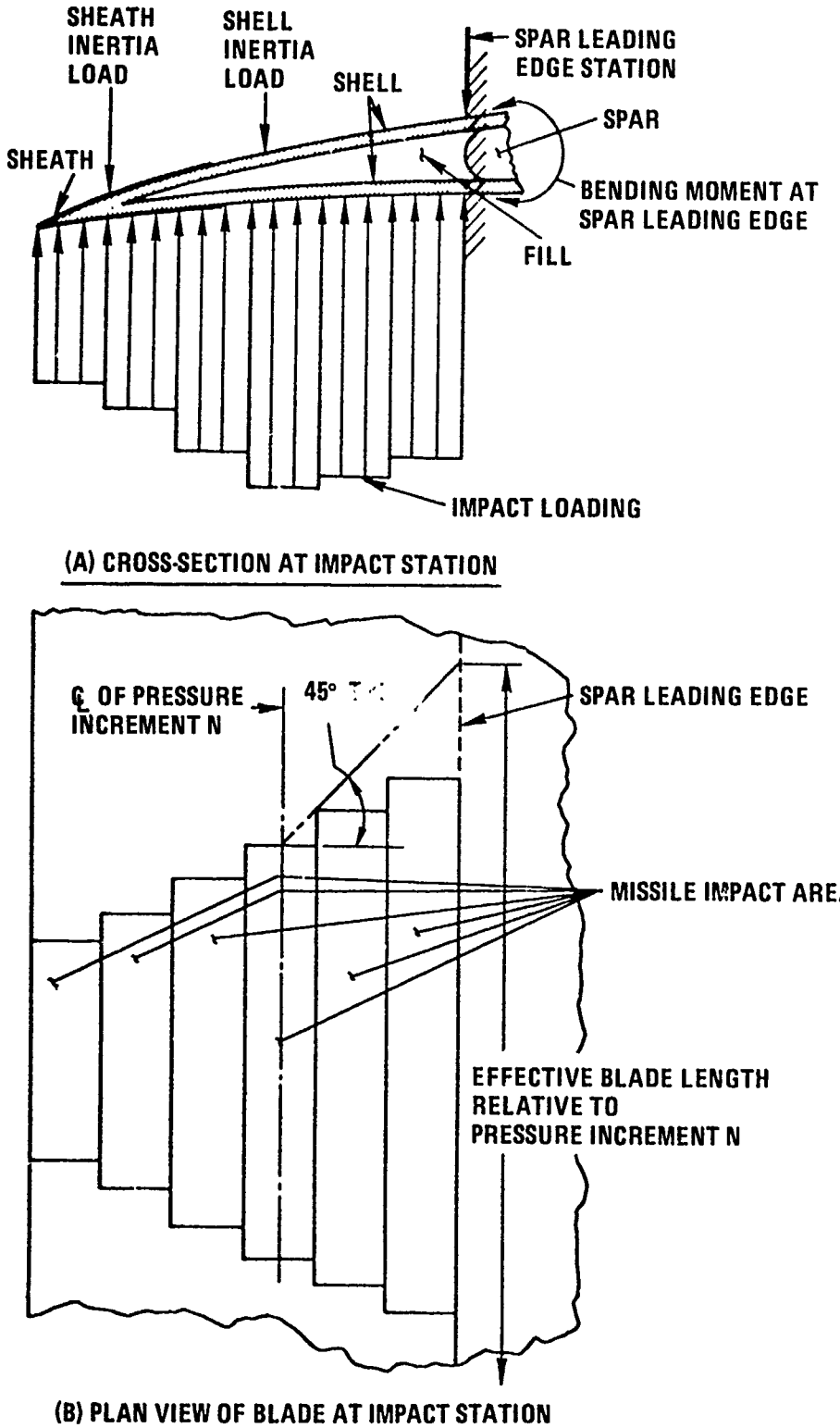

FIGURE 43. LOCAL CHORDWISE BENDING STRESS ANALYSIS MODEL

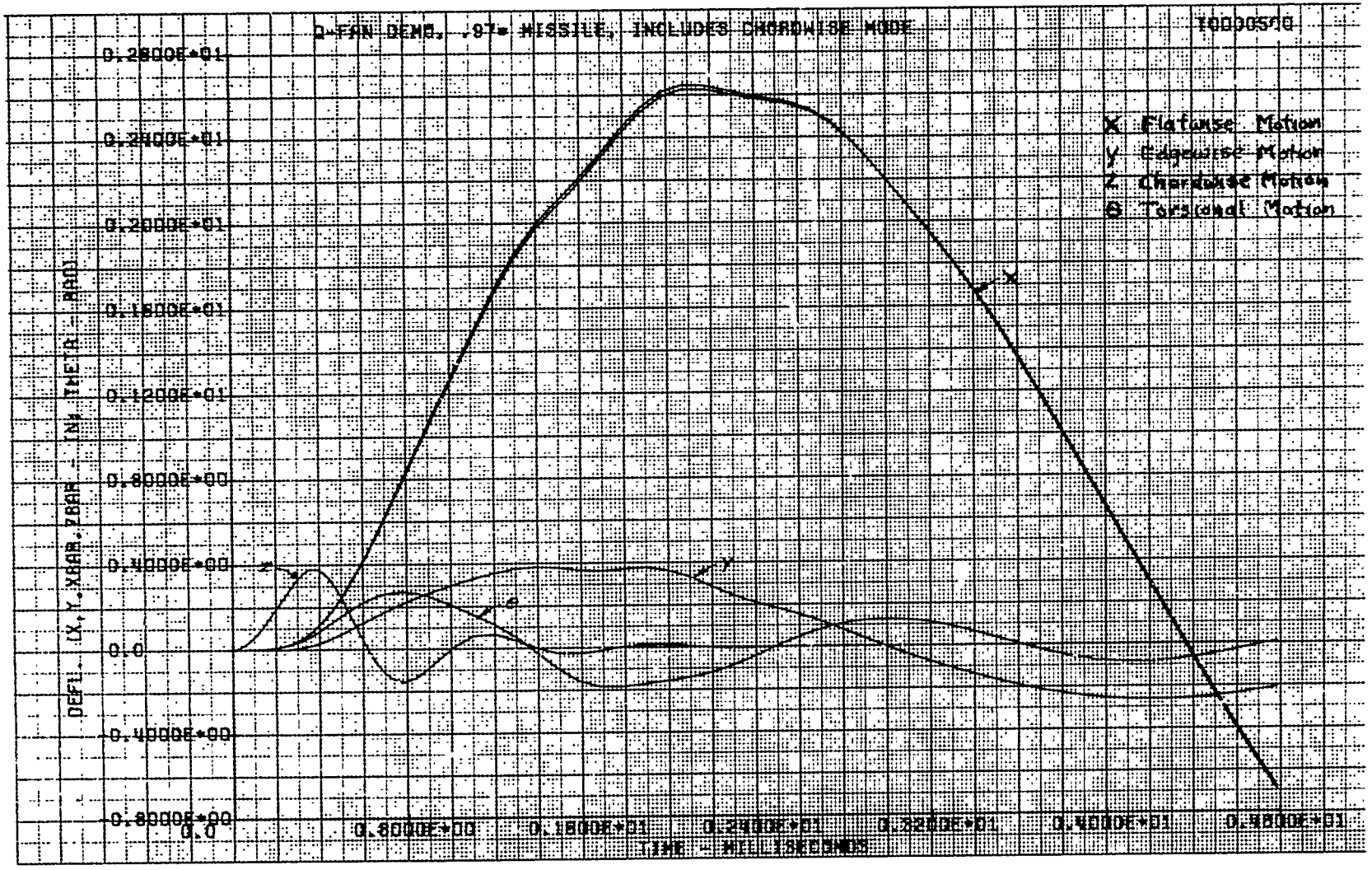

FIGURE 44. RESPONSE OF Q-FAN DEMO BLADE WITH CHORDWISE RESPONSE

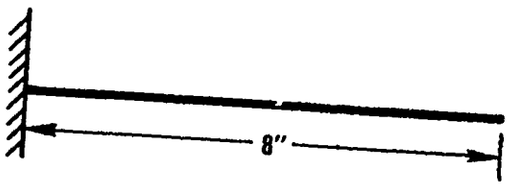

SIDE VIEW

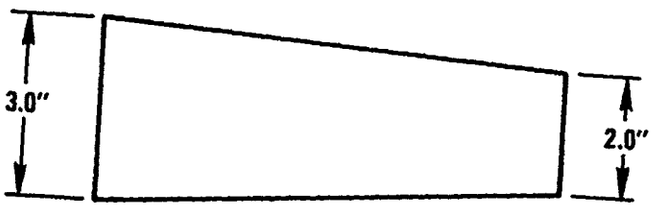

TAPER (b/b_0) = 1.5

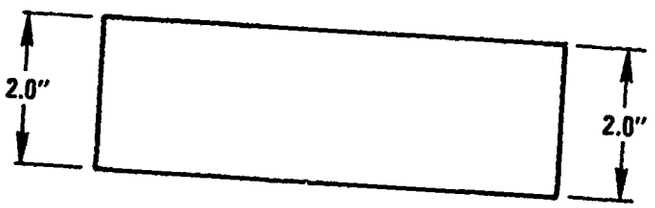

TAPER (b/b_0) = 1.0

TOP VIEW

FIGURE 45. CANTILEVER SPECIMEN FOR MATERIAL IMPACT TEST

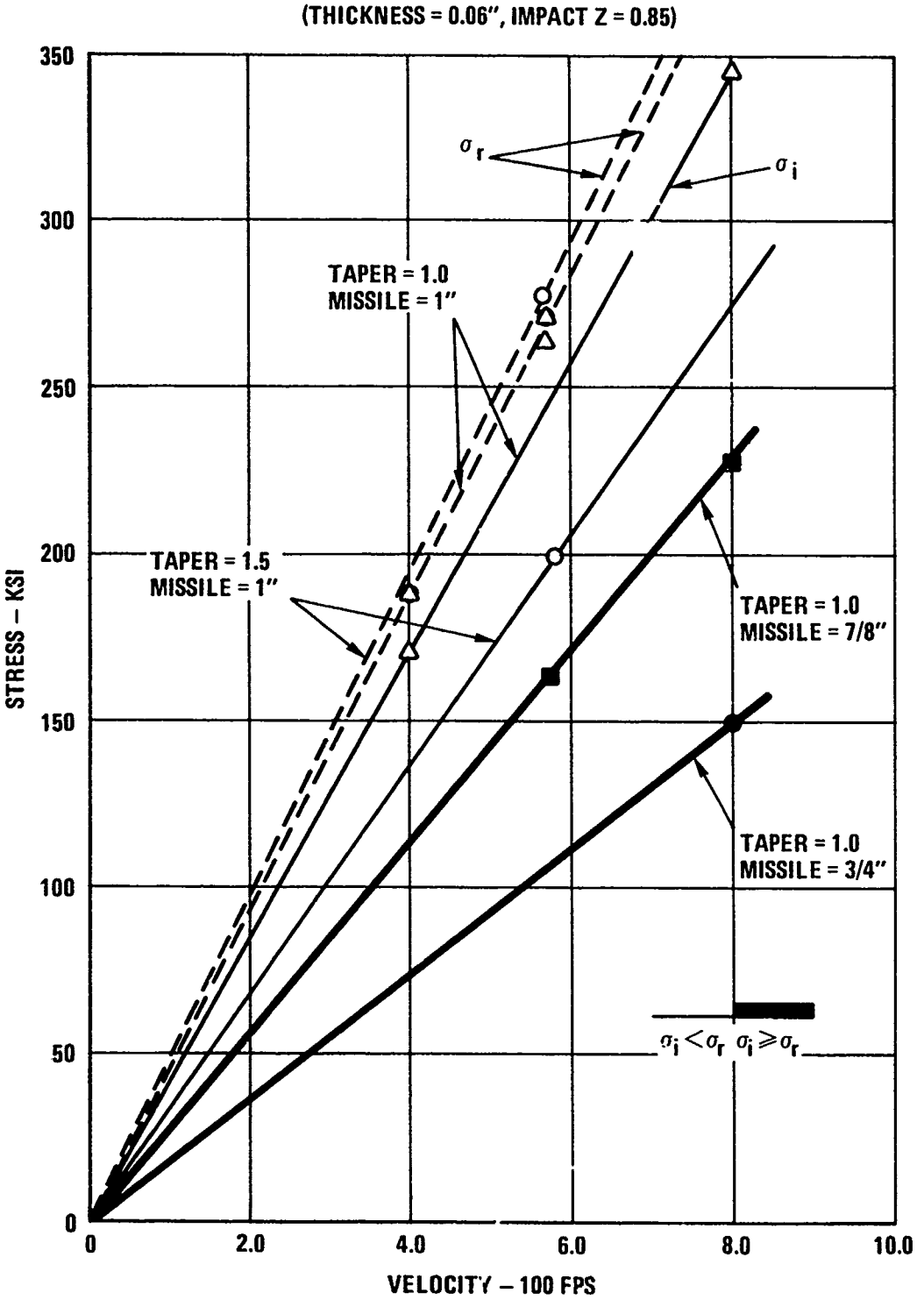

FIGURE 46. CANTILEVER SPECIMEN; MAXIMUM STRESS VS. IMPACT VELOCITY

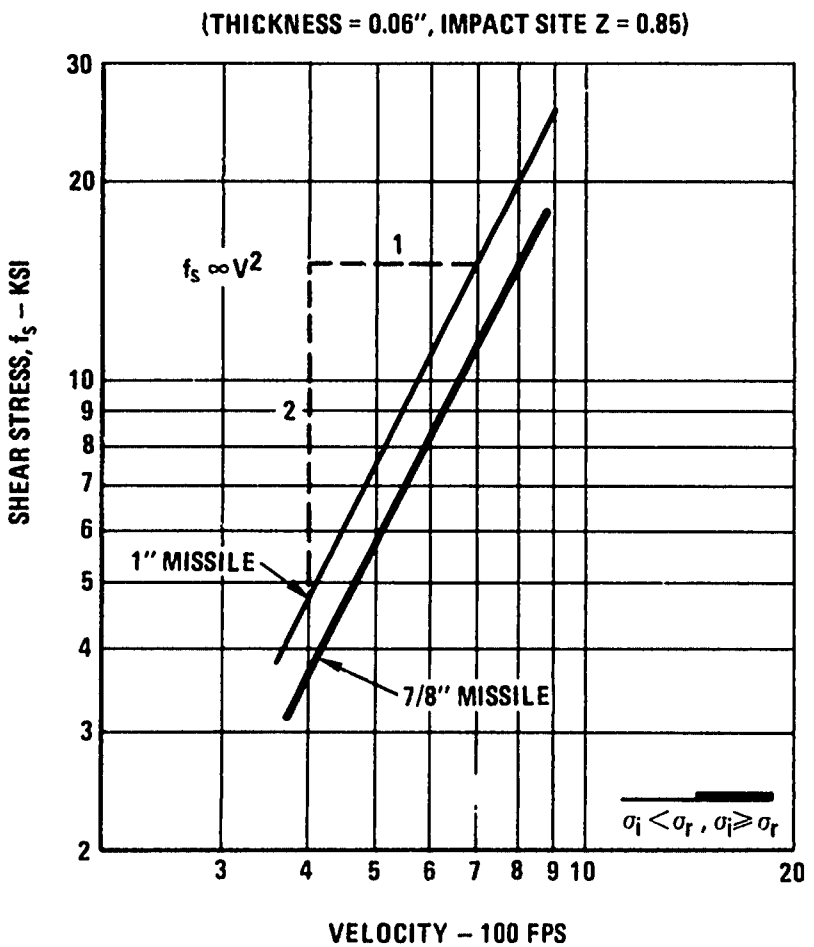

FIGURE 47. CANTILEVER SPECIMEN; MAXIMUM SHEAR STRESS VS. IMPACT VELOCITY

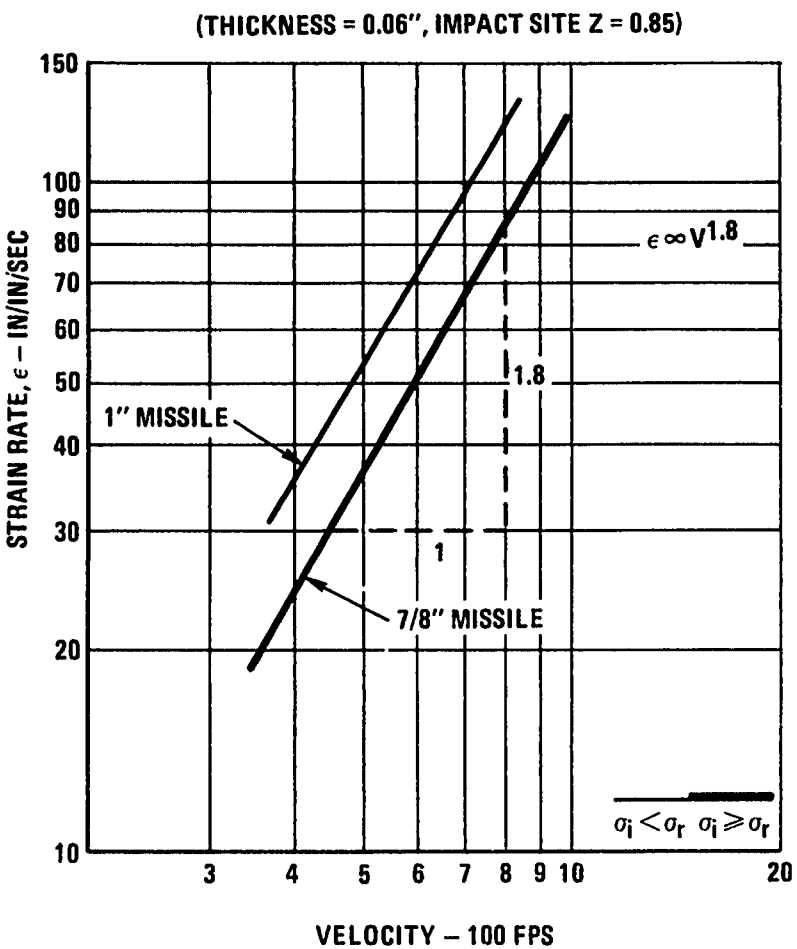

FIGURE 47. CANTILEVER SPECIMEN; MAXIMUM STRAIN RATE VS. IMPACT VELOCITY

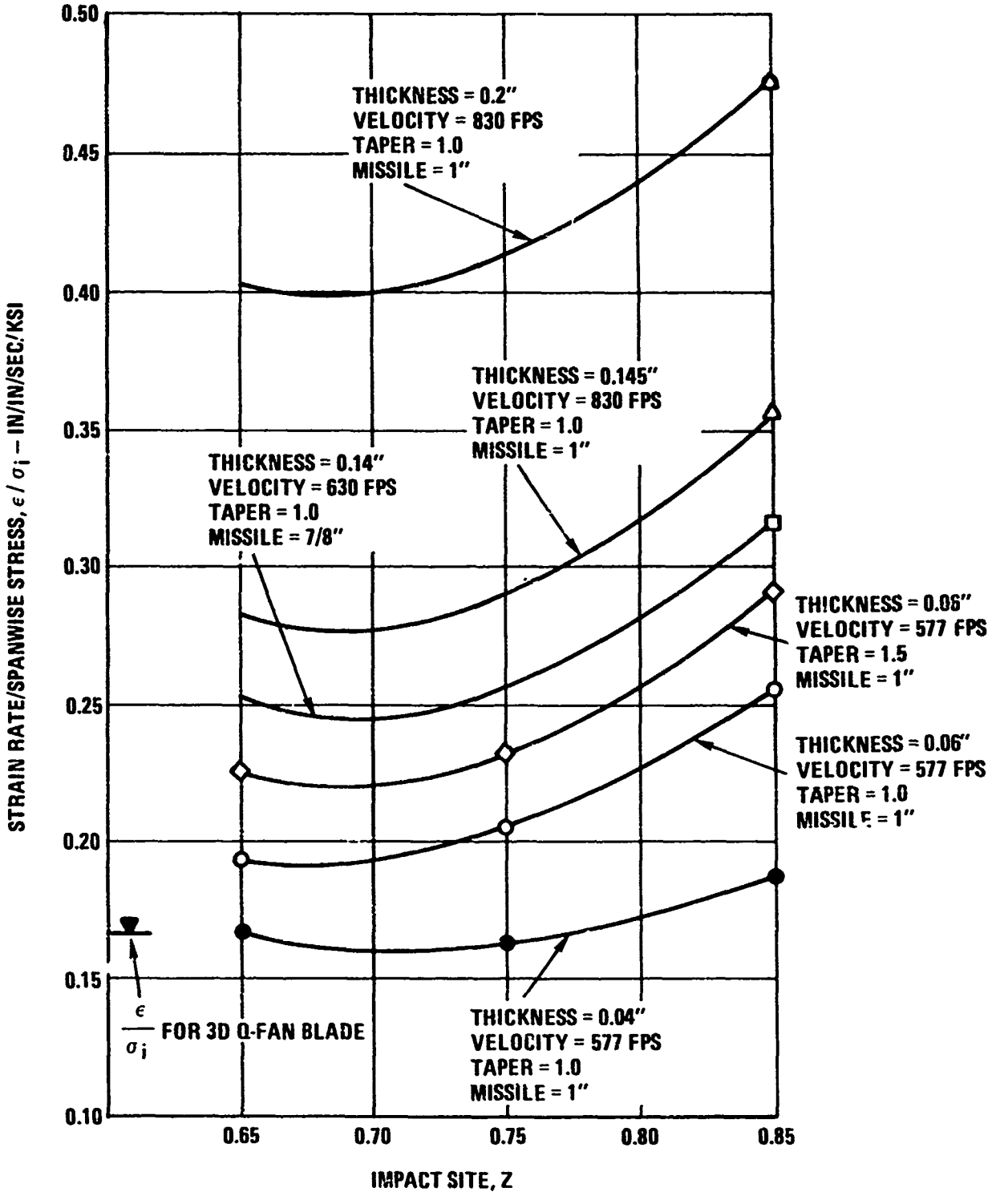

FIGURE 48. CANTILEVER SPECIMEN; MAXIMUM STRAIN RATE/SPANWISE STRESS VS. IMPACT SITE

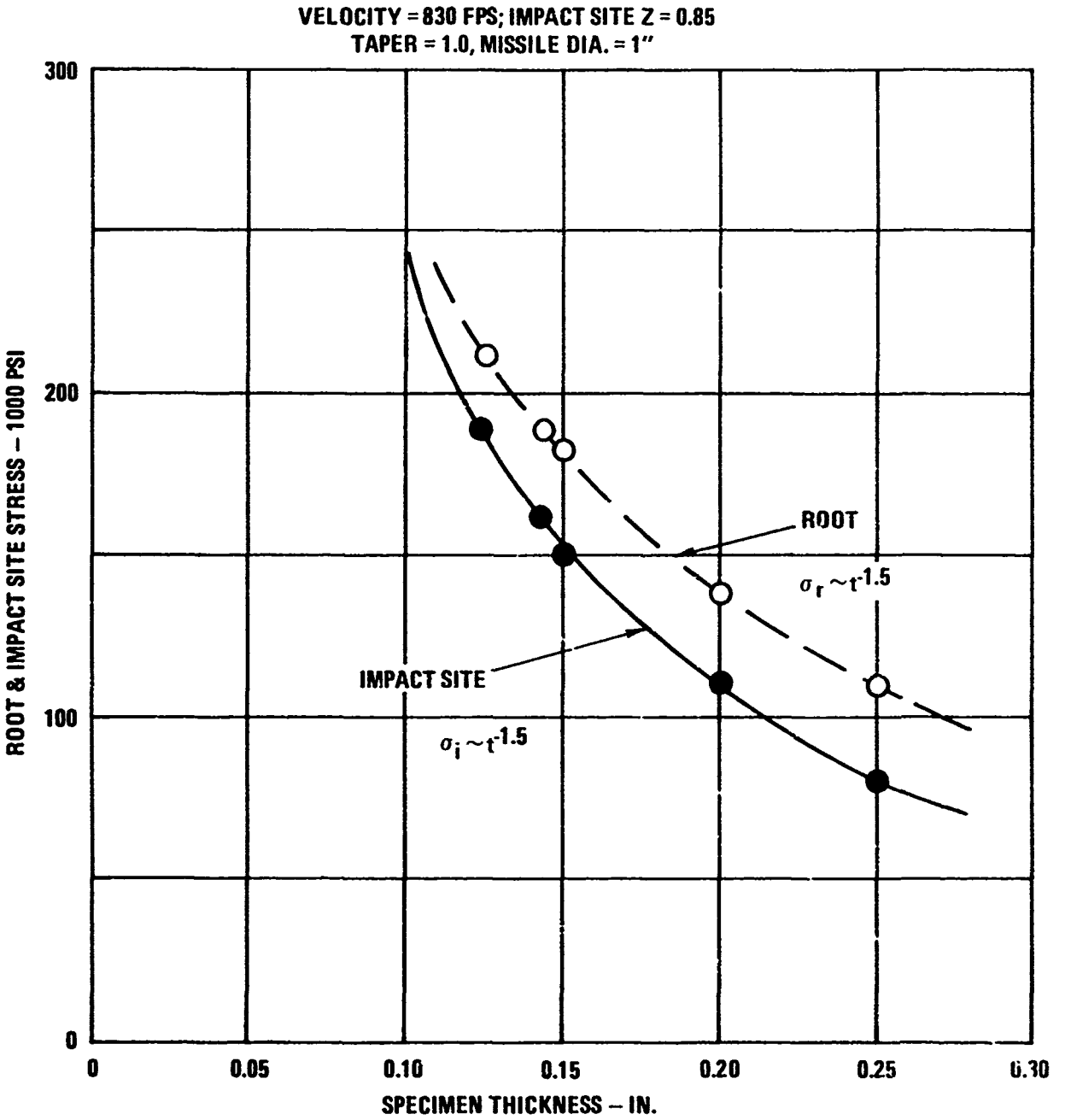

FIGURE 49. CANTILEVER SPECIMENS; VARIATION OF IMPACT STRESS AND ROOT STRESS WITH SPECIMEN THICKNESS

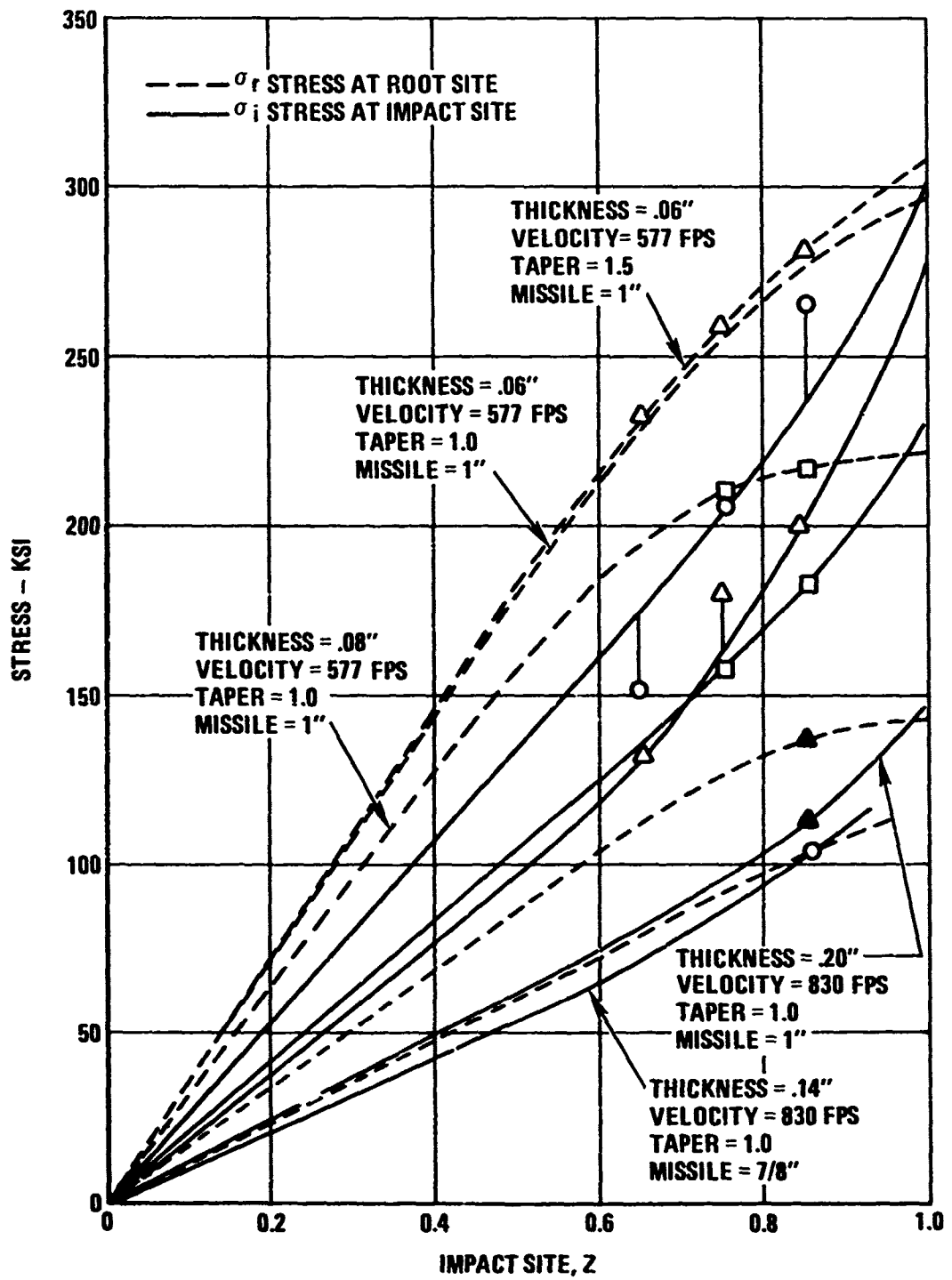

FIGURE 50. CANTILEVER SPECIMEN; MAXIMUM STRESS VS. IMPACT SITE

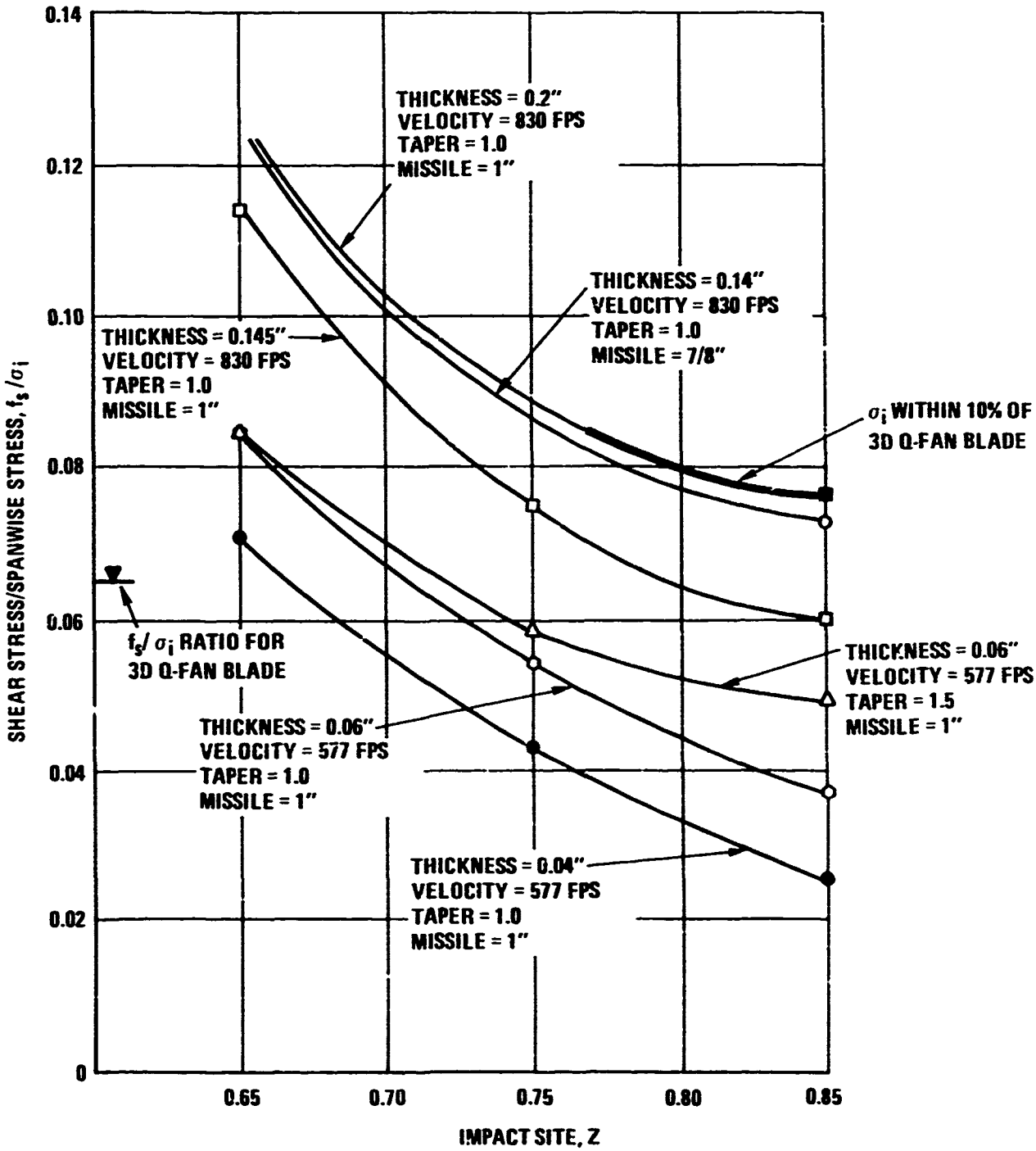

FIGURE 51. CANTILEVER SPECIMEN; MAXIMUM SHEAR STRESS/SPANWISE STRESS VS. IMPACT SITE

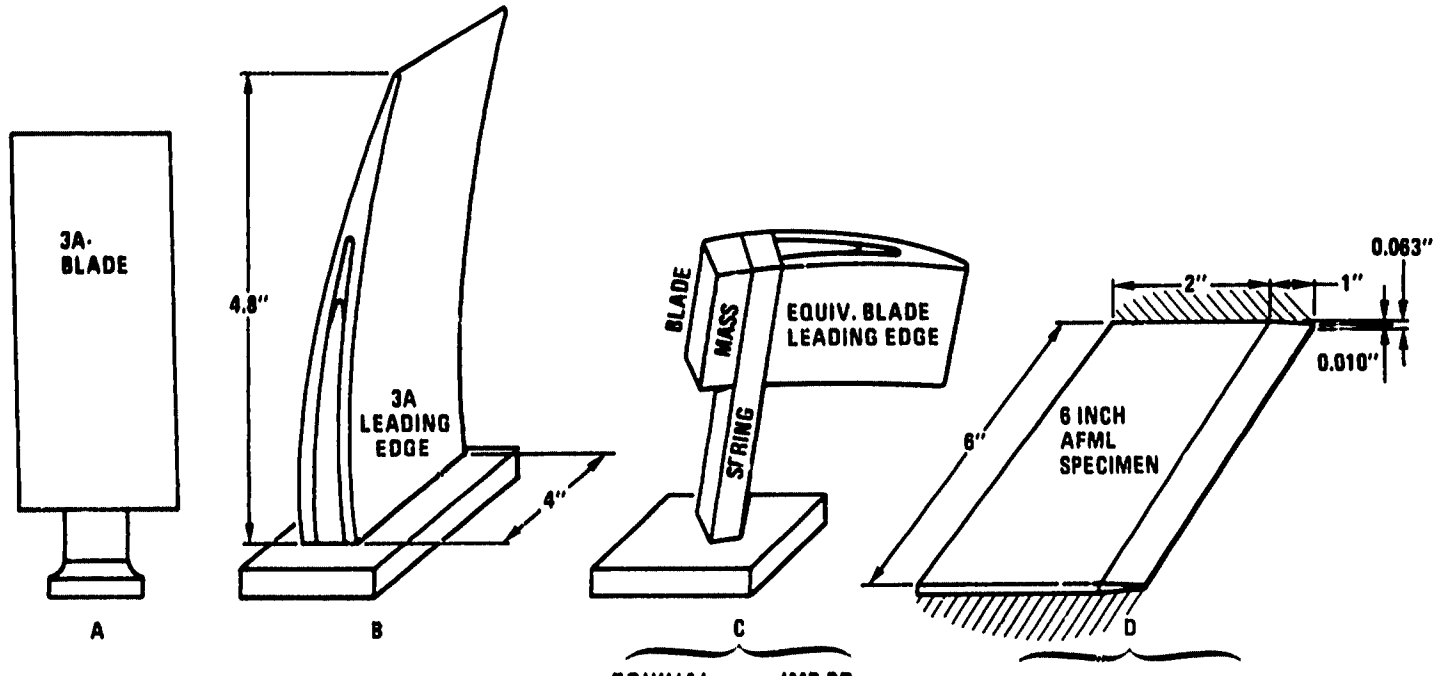

			EQUIVAL.	IMP 3D		
IMPACT VELOCITY	830 FPS	830 FPS	830 FPS	830 FPS	1200 FPS	830 FPS
IMPACT ANGLE	30 DEG	30 DEG	30 DEG	30 DEG	30 DEG	30 DEG
MAX NORMAL IMPACT FORCE	1750 LBS	1700 LBS	1500 LBS	1800 LBS	2900 LBS	7663 LBS
IMPACT TIME	0.209 MS	0.212 MS	0.216 MS	0.209 MS	0.162 MS	0.232 MS
DEFLECT AT MAX FORCE ($X + \alpha\theta$)	0.0035 IN.	0.0099 IN.	0.0163 IN.	0.017 IN.	0.033 IN.	0.030 IN.
DEFLECTION AT END OF IMPACT ($X + \alpha\theta$)	0.0245 IN.	0.0256 IN.	0.0449 IN.	0.032 IN.	0.127 IN.	0.124 IN.
BLADE LOAD AT MAX FORCE	3 LBS	176 LBS	51 LBS	1/93 LBS*	22 LBS	22 LBS
BLADE LOAD AT END OF IMPACT	8 LBS	654 LBS	140 LBS	3/227 LBS*	95 LBS	93 LBS

*GROSS BLADE LOAD/LEADING EDGE LOAD

FIGURE 52. LEADING EDGE TEST SPECIMENS

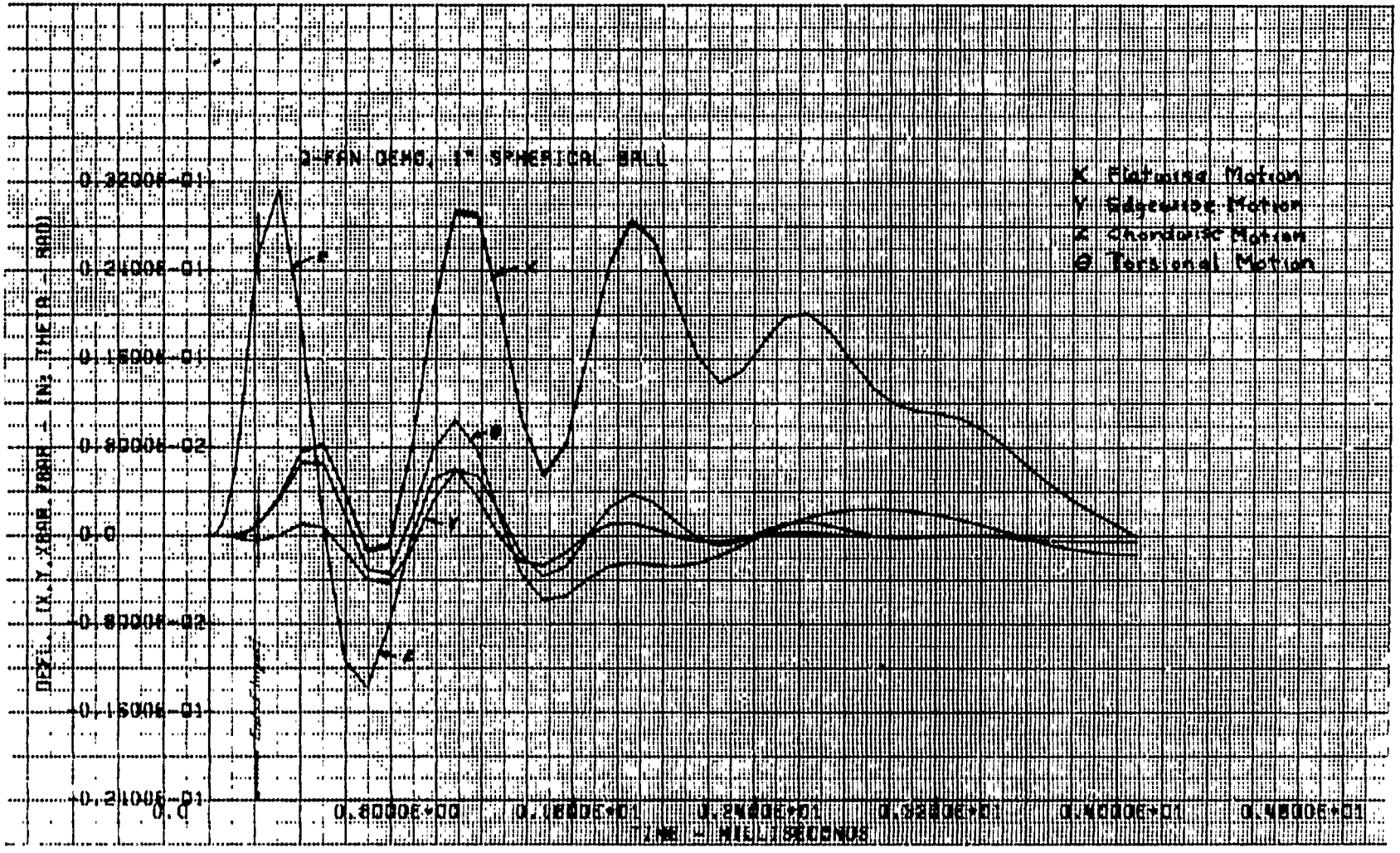

FIGURE 53. ONE-INCH SPHERICAL MISSILE IMPACT OF Q-FAN DEMO BLADE WITH CHORD FLEXIBILITY

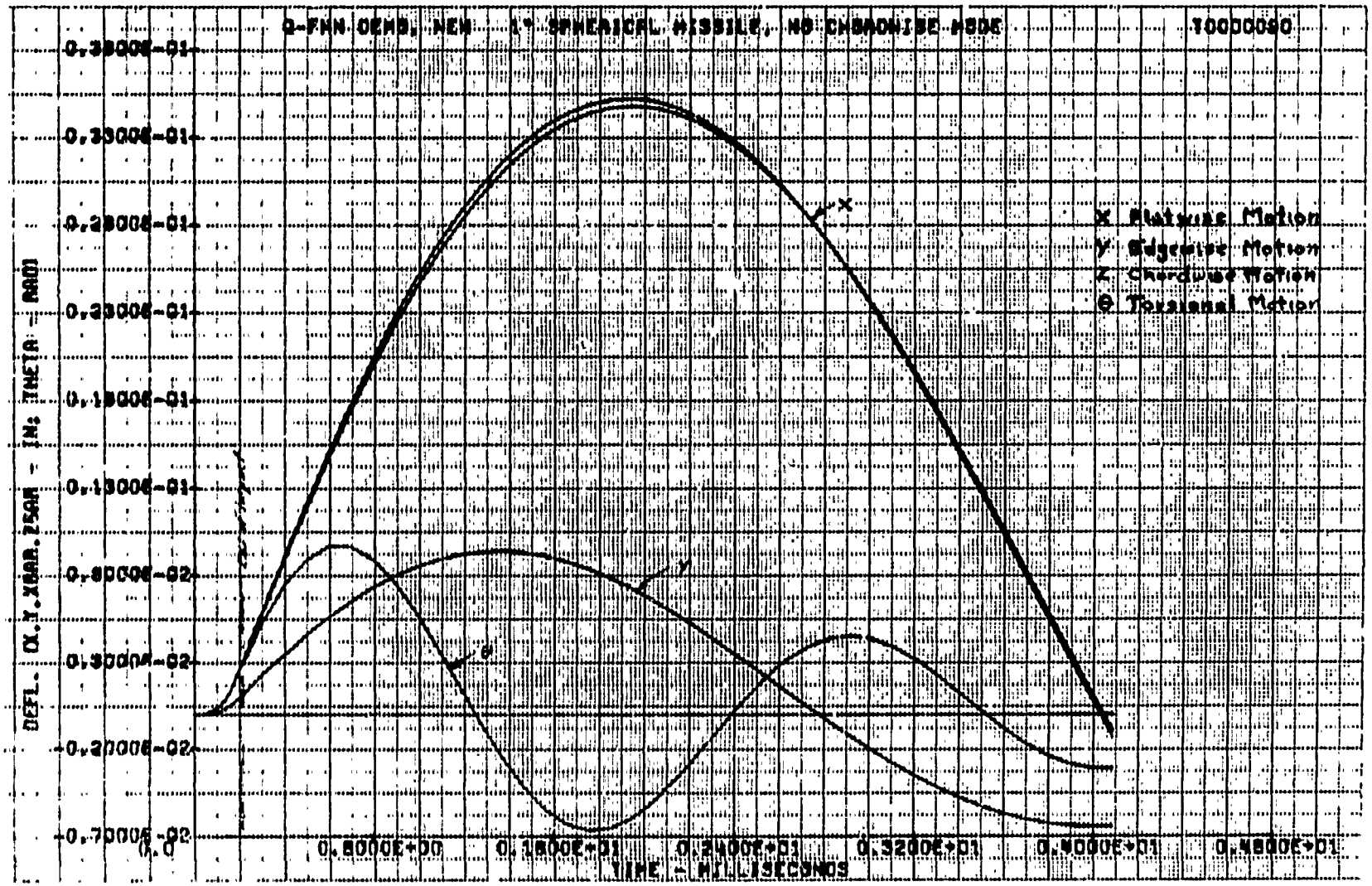

FIGURE 54. ONE-INCH SPHERICAL MISSILE IMPACT OF Q-FAN DEMO BLADE WITH NO CHORD FLEXIBILITY